Antibacterial Porous Polymeric Monolith for On-Chip Cell Lysis

by

Mohamed Aly Saad Aly

A thesis
presented to the University of Waterloo
in fulfillment of the
thesis requirement for the degree of
Doctor of Philosophy
in
Systems Design Engineering

Waterloo, Ontario, Canada, 2015

© Mohamed Aly Saad Aly 2015

Author's Declaration

I hereby declare that I am the sole author of this thesis. This is a true copy of the thesis, including any required final revisions, as accepted by my examiners.

I understand that my thesis may be made electronically available to the public.

Abstract

The application of porous polymeric monolith (PPM) column as an effective tool for bacterial cell lysis is demonstrated in this thesis. By exploiting the expansive surface area and controllable pore size inalienable to PPM, a double mechanism cell lysis technique was developed. The bacterial cell wall is mechanically sheared (mechanical-shear lysis) by flowing through the narrow porous medium of the PPM column, but it is also damaged and disintegrated by physical contact (contact-killing lysis) with the antibacterial polymeric biocide covering the porous surface. This leads to leakage of the intracellular contents. The antibacterial monolithic columns possess the aptitude to constrain the growth, kill and efficiently lyse gram-negative and gram-positive bacterial cells. The developed antibacterial PPM columns can be potentially used in developing commercial macro-columns for cell lysis like the columns commercially available for DNA isolation. Also, they can be used within microfluidic channels for on-chip cell lysis at the heart of integrated sample preparation device.

The developed cell lysis technique efficiently lysed numerous gram-negative and gram-positive bacterial species with no chemical or enzymatic reagents utilized, power consumption required, complicated design and fabrication processes. Also, the cell lysate containing the DNA released from bacterial cells after lysing with the developed antibacterial PPM columns is ready to be used by PCR with no further purification needed. Amplified DNA genes were detected by gel electrophoresis starting from small volume and cells concentration down to 10^2 CFU/ml. This makes it an attractive on-chip lysis device that can be used in sample preparation for bio-genetics and point-of-care diagnostics.

The PPM columns were formed by photo-initiated free radical copolymerization of functional and cross-linker monomers with the assistance of porogenic solvents and

photo-initiator. The porous network was synthesized directly inside a microfluidic channel fabricated in a cross-linked poly(methyl methacrylate) (X-PMMA) substrate by well-controlled, high-throughput, and time and cost effective laser micromachining. The unreacted double bonds at the surface of X-PMMA provide covalent bonding for the formation of the monolith, thus contributing to the mechanical stability of the PPM within the microchannel and eliminating the need for surface treatment.

Two functional monomers belong to two different antibacterial polymers families have been used to form two antibacterial PPM columns. A functional monomer, N-(tert-butyloxycarbonyl)aminoethyl methacrylate, belongs to SMAMPs antibacterial polymer family was used to form antibacterial PPM column, SMAMPs-PPM. To demonstrate that cells were lysed via a dual mechanism, the active (functional) monomer, N-(tert-butyloxycarbonyl)aminoethyl methacrylate (Boc-AEMA), was protected by a Boc group to first demonstrate mechanical shearing lysis alone. Once the protecting group was removed the PPM became antibacterial, leading to improved performance. Both lysis mechanisms were thus validated. Furthermore, the lysis efficiency of the PPM was improved by tuning their hydrophobic-hydrophilic balance and determining the optimal flow rate, at which the bacterial cell walls were sufficiently mechanically sheared through the porous medium of the column to disrupt the cell membrane by physical contact with the antibacterial polymeric biocide covering the pore surface.

To further confirm and validate the dual lysis mechanism with different monomer, an antibacterial PPM, DADMAC-PPM, from a functional monomer that is one of quaternary ammonium compounds, diallyldimethylammonium chloride (DAMMAC), which is intrinsically cationic and antibacterial, was developed. Also the effect of the cross-linking monomer on bacterial growth inhibition, lysis efficiency and the

mechanical stability of the PPM column within the microfluidic channel, using three different cross-linking monomers was studied. Moreover, the bonding efficiency between two layers of X-PMMA substrate at different cross-linker contents was studied. Furthermore, the reusability of the QAC-PPM was investigated and compared with the previously developed SMAMPs-PPM.

The cell lysis efficiency of the biochips were characterized by qualitatively (semi-quantitatively) detecting DNA and quantitatively determining DNA concentration in the crude lysate collected at the outlet of the biochip. By using fluorometry, the ethidium bromide (EtBr) intercalation assay was utilized as an indicator of the presence of DNA in the cell lysate and the DNA concentration was determined by UV-Vis spectrophotometry. Furthermore, lysis was confirmed by off-chip PCR that was further analyzed by gel electrophoresis. The antibacterial PPM columns were reused for 20-30 lysis cycles without any evidence of physical damage to the monolith, significant performance degradation or DNA carryover when they were back-flushed between cycles.

Acknowledgments

Primary, I would like to convey my honest appreciation to my adviser Prof. John T.W. Yeow for his nonstopping supervision during my academic research and graduate study, for his forbearance, inspiration, eagerness, and massive awareness. His wise, generous and knowledgeable guidance enlightened me through research problems that I have faced through my graduate study.

I am pleased to communicate my appreciation to my advisory committee: Prof. Maud Gorbet, Prof. Carolyn Ren and Prof. Juewen Liu for their insight, suggestions, and time in evaluating my work. I should also thank Prof. Axel Guenther from the University of Toronto to accept my invitation to act as the external committee member in my defense. I am also grateful to Prof. Eihab Abdel-Rahman for his encouragement to critically analyzing experimental results and for introducing and encouraging me to use Latex.

I am extremely grateful to Prof. Michel Palmer and Prof. Mario Gauthier from the Chemistry Department for their kindness and generosity to provide access to their lab facilities and their guidance on some of the biological and chemical concepts. I must also thank Mr. Yahya Alzahrany, Olivier Nguon, Mohamed Salah, Eric K. Brefo-Mensah, and Dr. David Donkor for their generous time and support through my experimental work at their labs.

I am extremely thankful to my colleagues who offered me excellent ideas through my experimental and analytical work. Special thanks to Dr. Manu Venkataram, Dr. Said Boybay, Dr. Sarbast Rasheed, Dr. Fred Sun, Dr. Firmin Moingeon, Dr. Ilias Mahmud, and Mr. Mosa Alsehli.

Dedication

To my Lord

To my beloved Parents

To my beloved Daughter

Table of Contents

Author's Declaration ii

Abstract iii

Acknowledgments vi

Dedication vii

List of Tables xiii

List of Figures xv

List of Schemes xxii

List of Abbreviations xxiii

1 Introduction 1

1.1 Background 1

1.2 Cell lysis in microfluidic systems 2

1.2.1 Mechanical cell lysis 3

1.2.2 Thermal cell lysis 3

1.2.3 Electrical cell lysis 4

1.2.4 Chemical cell lysis 4

1.2.5 Antimicrobial cell lysis 9

1.2.5.1 Disinfectants . . . 10
1.2.5.2 Polymeric biocides . . . 12
1.3 Porous monolith . . . 16
1.3.1 Porous polymeric monolith fabrication . . . 17
1.4 Thesis outline . . . 22

2 Boc-Protected Antibacterial PPM **24**

2.1 Experimental . . . 25
2.1.1 Materials . . . 25
2.1.2 Microchip fabrication . . . 26
2.1.3 Network fabrication and deprotection. . . . 27
2.1.4 Monolith formation and characterization . . . 27
2.1.5 Activation of the antibacterial PPM via deprotection . . . 30
2.1.6 Antibacterial activity . . . 30
2.1.6.1 Cell samples. . . . 31
2.1.6.2 Non-porous polymeric network. . . . 31
2.1.7 Cell Lysis efficiency of PPM column. . . . 32
2.1.7.1 PCR reagents experimental setup. . . . 32
2.1.7.2 gel electrophoresis . . . 33
2.2 Results and discussion . . . 33
2.2.1 Monolith formation and bonding to the substrate . . . 33
2.2.2 *t*-Boc group deprotection . . . 36
2.2.3 Antibacterial activity of the non-porous network . . . 36
2.2.4 Cell Lysis efficiency of the PPM column . . . 37
2.2.5 PCR and gel electrophoresis . . . 39
2.3 Conclusions . . . 39

3 Optimized Boc-Protected Antibacterial PPM **41**

3.1 Experimental . . . 42

3.1.1 Materials . . . 42

3.1.2 Microchip fabrication . . . 42

3.1.3 Monolith formation and antibacterial activation . . . 43

3.1.4 Bacterial culture . . . 44

3.1.5 Bacterial cell lysis . . . 45

3.1.5.1 On-chip cell lysis. . . . 45

3.1.5.2 Off-chip cell lysis. . . . 46

3.1.6 Cell lysis efficiency . . . 47

3.1.6.1 DNA detection by fluorometry. . . . 47

3.1.6.2 DNA concentration by UV-Vis spectrophotometry. 47

3.1.6.3 PCR reagents and experimental setup. . . . 48

3.1.6.4 Gel electrophoresis. . . . 48

3.2 Results and discussion . . . 48

3.2.1 Influence of the hydrophobic-hydrophilic balance . . . 48

3.2.2 Influence of flow rate . . . 52

3.2.2.1 Protected PPM. . . . 53

3.2.2.2 Deprotected (antibacterial) PPM. . . . 54

3.2.3 Parameters affect the biochip performance . . . 56

3.2.4 Cell lysis efficiency at different cell concentration . . . 57

3.2.5 Reusability of the biochip . . . 58

3.2.6 Biochip vs. off-chip cell lysis . . . 59

3.2.7 PCR and gel electrophoresis . . . 61

3.3 Conclusions . . . 62

4 QAC Based Antibacterial PPM Column **64**

4.1 Introduction . . . 65

4.2 Experimental 66
4.2.1 Materials 66
4.2.2 Microchip fabrication 67
4.2.3 Off-chip non-porous film 67
4.2.4 PPM formation, characterization and stability 68
4.2.4.1 PPM formation. 68
4.2.4.2 PPM characterization. 68
4.2.4.3 Mechanical stability of PPM columns. 69
4.2.5 Bacterial cultures 69
4.2.6 Antibacterial, leaching, and growth inhibition tests 70
4.2.6.1 Antibacterial activity. 70
4.2.6.2 Leaching property test. 71
4.2.6.3 Bacterial growth inhibition. 71
4.2.7 Cell Lysis efficiency 72
4.2.7.1 DNA detection by fluorometry. 72
4.2.7.2 DNA concentration by UV-Vis spectrophotometry. 72
4.2.7.3 PCR reagents and experimental setup. 73
4.2.7.4 Gel electrophoresis. 73
4.3 Results and discussion 74
4.3.1 Monolith formation, characterization and stability 74
4.3.1.1 Monolith formation. 74
4.3.1.2 Monolith characterization 74
4.3.1.3 Monolith stability. 76
4.3.2 Antibacterial, Leaching and growth inhibition tests 77
4.3.2.1 Antibacterial activity. 77
4.3.2.2 Leaching property test. 79
4.3.2.3 Growth inhibition test. 82

4.3.3 Cell Lysis efficiency of the PPM columns 83
4.3.3.1 DNA detection by fluorometry. 83
4.3.3.2 DNA concentration by UV-Vis spectrophotometry. 85
4.3.3.3 PCR and gel electrophoresis 87
4.3.4 Reusability of the biochip 88
4.4 Conclusions 89

5 Conclusion and Future Work **91**
5.1 Contributions 91
5.2 Advantage, disadvantage and constraints 94
5.3 Conclusion 94
5.4 Publications 96
5.5 Cost breakdown 97
5.6 Future work 97

References **99**

Appendices **111**

List of Tables

2.1 Primers used in PCR experiments 33

2.2 Debonding pressure of the column from the substrate for different cross-linking levels. 36

3.1 Composition of the solutions used to form the eleven PPMs (in wt. %). 43

3.2 Pore size, specific surface area and porosity of the protected PPM 1, 4, 6 and 11, as determined by mercury intrusion porosimetry measurements. 50

3.3 The length and diameter of the used bacterial species 56

3.4 Parameters affect the biochip performance. 57

4.1 Compositions of the monolith solutions used (in wt%). 68

4.2 Pore diameter and porosity of the PPM columns determined by Hg intrusion porosimetry. 76

4.3 The length and diameter of the used bacterial cells 84

5.1 The advantage, disadvantage and constraints of the work presented in this thesis. 95

5.2 Cost breakdown of the developed two antibacterial PPM columns. 98

A1 MMA and EGDMA volumes used in the preparation of the different cross-linked PMMA (X-PMMA) substrates. 112

B1 Channel dimensions and pore information of the optimized PPM column 116
B2 Primers used in PCR experiments 117
B3 DNA carryover after each backwash cycle 119
C1 Primers used in PCR experiments 121
C2 Dimensions of the channel and pore information of the poly(DADMAC-*co*-EGDA) PPM formed in the channel 122
C3 DNA carryover after each backwash cycle 123

List of Figures

1.1 Gram-positive and gram-negative membrane structure. 2

1.2 Red blood cells lysed in a meander channel [12]. 5

1.3 Cell lysis using chemical lysis and sheath flow [17]. 6

1.4 Chemical cell lysis and protein extraction by molecular size and controlled flow rate [14]. 7

1.5 A schematic diagram of the microfluidic system design (left) and a picture of the device (right) [13]. 8

1.6 Single-cell capture and cell lysis in microwells [18]. 9

1.7 Micro-chip before (left) and 1 minute after (right) combining cell suspension with cell lysis reagents [15]. 11

1.8 (a) Schematic diagram of a two layers microfluidic device , (b) top view of the capture champers and (c) Arcella treated with a viability probe [20]. 12

1.9 A schematic diagram of killing mechanism of an antimicrobial polymer to a bacterial cell. 13

1.10 The three classes of antibacterial polymers: polymeric biocides (a), biocidal polymers (b) and biocide-sending polymers (c) [24] 14

1.11 Mass transport within a porous polymer monolith and silica beads [44, 45]. 17

1.12 Yu *et al.*'s [49] PPMs based micro-SPE. 19

1.13 Fabrication process: (A) The mold for the hot embossing procedure where CA is a group of eight silica capillaries, E is epoxy glue and G is glass film, (B) Hot embossing process where Z is thermoplastic substrate, Si is silicon substrate, GP is glass slide and P is the press-pressure, and (C) The micro-fluidic chip, M is the micro-fluidic channels for the PPM, Ci and Co are the inlet and outlet [51]. . . 19

1.14 Kulinski *et al.*'s [52] DNA concentration at different experimental conditions. 20

1.15 Bhattacharyya *et al.*'s [53] (a) hot-embossing and (b) the photografting processes. 21

1.16 Schematic diagrams of (a) LOC, (b) hot-embossing process and (c) packed device [55]. 22

2.1 preliminary fabricated microfluidic chips with and without PPM columns. 29

2.2 Sever cracks on the linear PMMA surface after applying the monolith mixture. 30

2.3 Microfluidic chip fabricated by laser micromachining on a 20% X-PMMA substrate filled with a monolith column (right) and SEM image of the PPM column packing (left). 34

2.4 ATR-FTIR spectra for native and cross-linked PMMA samples with cross-linker contents ranging from 3 to 20 mol%. The vibrational modes at 1637 and 949 cm^{-1} correspond to CH_2 stretching and out-of-plan bending, respectively. Inset: Absorbance at 1637 cm^{-1} for the different X-PMMA samples. 35

2.5 Fluorescence intensities for E. coli suspended in PBS buffer and stained with Live/Dead dye in contact with (A) the deprotected antibacterial non-porous network at time zero and (B) after 300 sec, and in contact with (C) the protected non-porous network at time zero and (D) after 300 sec. 37

2.6 Green (Live) and red (Dead) stain intensities with respect to contact time before and after removing the Boc protecting group. 38

2.7 Fluorescence intensity of EtBr after adding E. coli (blue) and B. subtilis (red) cells suspended in PBS buffer (control), the lysate of E. coli and B. subtilis suspensions flown through the PPM column before (Protected PPM) and after deprotection (Deprotected PPM). 38

2.8 Gel electrophoresis analysis of PCR output for unlysed (column 2) and lysed (through PPM) (column 3) B. subtilis cells, filtered (column 4) and non-filtered (column 5) lysed E. coli and unlysed E. coli (column 6). Column 1 is for a 100 bp DNA ladder. 40

3.1 SEM images for the protected PPMs (A) 1, (B) 4, (C) 6, and (D) 11. 49

3.2 Fluorescence intensity for EtBr before (control sample point at 0) and after intercalation into the DNA released from bacterial cells flowing through the eleven deprotected PPMs at flow rate of 1.5 μL/min. 50

3.3 Absolute concentration of DNA present in the crude cell lysate collected at the outlet of the different deprotected PPMs. 52

3.4 Fluorescence intensity for EtBr intercalated into the DNA released from bacterial cells pumped through protected freshly synthesized PPM 11 at each flow rate ranged from 0.1 to 10 μL/min. The point at 0 μL/min is for the control sample. 54

3.5 Fluorescence intensity for EtBr intercalated into the DNA released from bacterial cells passed through the deprotected PPM (11) at flow rates ranged from 0.1 to 10 μL/min. Point 0 μL/min on the flow rate axis represents the control sample. 55

3.6 Fluorescence intensity for EtBr intercalated into the DNA released from bacterial cells flowing through the deprotected PPM (11) at 4 μL/min at different cell concentration. 58

3.7 Fluorescence intensity for EtBr intercalated into the DNA released from bacterial cells flowing through the deprotected monolith (11) at 4 μL/min over successive runs, for the two different washing protocols (PBS and Acid washes). The first two data points on the horizontal axis (number of uses of the biochip) are for the control samples. . . 59

3.8 Concentration of DNA present in the cell lysate after on-chip cell lysis (deprotected PPM (11) at a flow rate of 4 μL/min) and off-chip mechanical, thermal and chemical cell lysis. 61

3.9 Gel electrophoresis analysis of PCR output. Column (1) is for a 100 bp DNA ladder. Columns (2) and (3): unlysed and lysed E. saccharolyticus. Columns (4) and (5): lysed and unlysed B. subtilis. Columns (6) and (7): lysed and unlysed P. fluorescens. Columns (8) and (9): lysed and unlysed E. coli. 62

4.1 SEM images for the monolithic columns: (A), (B) and (C) are EGDMA, 1,6-HDDMA and EGDA-PPM, respectively; (D), (E) and (F) are EGDMA, 1,6-HDDMA and EGDA-PPM formed in the pre-heated microchip, respectively. 75

4.2 Debonding pressure of the monolithic columns from the substrates for different X-PMMA cross-linking levels and different PPM compositions. 77

4.3 Debonding pressure for the two substrate layers at different X-PMMA cross-linking levels. 78
4.4 Fluorescence intensities for E. coli suspended in PBS buffer and stained with live/dead dye in contact with (A) the three antibacterial networks at time zero, (B) Poly(DADMAC-*co*-EGDA), (C) Poly(DADMAC-*co*-1,6-HDDMA) and (D) Poly(DADMAC-*co*-EGDMA) after 600 second. 79
4.5 Green (live) and red (dead) stain intensity variation with the contact time for poly(DADMAC-*co*-EGDA), poly(DADMAC-*co*-1,6-HDDMA) and poly(DADMAC-*co*-EGDMA) networks. 79
4.6 FT-IR spectra for the N-H stretching absorbance of the unsaturated primary amine groups (right) and C-N stretching vibration in the secondary amine group followed by NH bend (left) of (A, B) poly(DADMAC-*co*-EGDA), (C, D) poly(DADMAC-*co*-1,6-HDDMA), and (E, F) poly(DADMAC-*co*-EGDMA) before (black line), after 1 hour (red line) and after 24 hours (blue line) of washing with PBS. 80
4.7 Colonies produced on agar after the 24 hours leaching tests for (A) control, (B) poly(DADMAC-*co*-EGDA), (C) poly(DADMAC-*co*-EGDMA), and (D) poly(DADMAC-*co*-1,6-HDDMA). 81
4.8 Bacterial growth inhibition for (A and B) positive controls (gram-negative, ATTC 12633 and gram-positive, ATCC 4698 bacteria overnight cultured in nutrient broth (NB) and trypticase soy broth (TSB), respectively), (C) negative control (NB media), (D and E), (F and G), and (H and I) gram-positive and gram-negative bacteria overnight cultured in TSB and NB media, respectively, and $0.5 \times 1\ cm^2$ strip of poly(DADMAC-*co*-EGDMA), poly(DADMAC-*co*-EGDA), and poly(DADMAC-*co*-1,6-HDDMA) monolith films, respectively. 82

4.9 Fluorescence intensity for EtBr before (control) and after intercalation into the DNA released after flowing the bacterial cells through the different PPM columns. 84

4.10 Fluorescence intensity of EtBr before (control) and after intercalating into the DNA released from bacterial cells flowing through the microfluidic channels hosting the poly(DADMAC-*co*-EGDA) PPM column at different cell concentrations. 85

4.11 Absolute concentration of DNA present in unlysed cells (control) and in the crude cell lysates collected at the outlet of the three PPM columns. 86

4.12 Absolute concentration of DNA present in the crude cell lysate collected at the outlet of the outlet of the poly(DADMAC-*co*-EGDA) PPM column at different cell concentrations. 87

4.13 Gel electrophoresis analysis of PCR output. Column 1 (from the left) is for a 100 bp DNA ladder. Columns 2 and 6: lysed and unlysed ATCC 35218. Columns 3 and 7: lysed and unlysed ATCC 186. Columns 4 and 8: lysed and unlysed ATCC 12633. Columns 5 and 9: lysed and unlysed ATCC 4698. 88

4.14 Fluorescence intensity for EtBr intercalated into the DNA released from bacterial cells flowing through the antibacterial poly(DADMAC-*co*-EGDA) PPM at a flow rate of 4 L/min over successive runs . . . 89

A1 FT-IR spectra for the PPM before (blue) and after (red) deprotection of the t-Boc group. Vibrational band assignments: N-CO-O symmetrical stretching at 1518 cm^{-1}, CH_3 bending at 1367 cm^{-1}, and N-CO-O symmetrical stretching at 872 cm^{-1}. 114

B1 PPM column polymerized into cross-linked PMMA microfluidic channel (shown on top left), experimental set up (shown on bottom left) and cell lysis evaluation techniques (shown on right). 116
B2 Absolute concentration of DNA in the crude cell lysate collected at the outlet of protected PPM 11 at flow rates ranged from 0.1 to 10 μL/min. 117
B3 Concentration of the DNA present in the crude cell lysate collected at the outlet of the microfluidic channels hosting deprotected PPM (11) flown at flow rates ranged from 0.1 to 10 μL/min. 118
B4 Florescence intensity of EtBr after intercalating into the DNA released from bacterial cells flowing through the PPM (11) at flow rate of 4μL/min and resulted from mechanical, thermal, and chemical cell lysis. 118
B5 DNA carryover collected in wash cycles after each PPM use. 119
C1 Structure of the cross-linked Poly(DADMAC-*co*-EDGA), Poly(DADMAC-*co*-1,6-HDDMA), and Poly(DADMAC-*co*-EGDMA) networks. . . . 122
C2 ATR-FTIR spectra for DADMAC (powder), poly(DADMAC-*co*-EDGA), poly(DADMAC-*co*-1,6-HDDMA), and poly(DADMAC-*co*-EGDMA) cross-linked networks. 122
C3 DNA carryover collected after each PPM use and control sample. . 123

List of Schemes

2.1 Reactions for the formation of the monolith column on 20% X-PMMA surface, and removal of the Boc protecting group with 85% phosphoric acid. 28
A1 Synthesis of X-PMMA. 112
A2 Synthesis of Boc-EA. 113
A3 Synthesis of Boc-EAMA. 114

List of Abbreviations

The following notations are used throughout the text; other notations are used at their relevant positions:

ATP	Adenosine triphosphate
ETA	Aminoethanol
$AEMA - HCl$	2-Aminoethyl methacrylate hydrochloride
NH_4Cl	Ammonium chloride
$ATRP$	Atom transfer radical polymerization
ATR	Attenuated total reflectance
$B.\ subtilis$	Bacillus subtilis
$B - PER$	Bacterial protein extraction reagent
BAC	Benzalkonium Chloride
BPO	Benzoyl peroxide
BMA	n-butyl methacrylate
BSA	Bovine serum albumin
$Boc - EA$	N-(tert-Butoxycarbonyl)ethanolamine
$Boc - AEMA$	N-(tert-butyloxycarbonyl)aminoethyl methacrylate
$BHIB$	brain-heart infusion broth
ClO_2	Chlorine dioxide
$CDCl_3$	Chloroform-d
CFU	Colony forming unit
T_c	Contact time
$X - PMMA$	Cross-lined Poly(methyl methacrylate)
K_d	decomposition rate
DNA	Deoxyribonucleic acid
DI	Deionized
BOC_2O	Di-tert-butyl dicarbonate
$DATP$	Deoxyadenosine triphosphate
$DCTP$	Deoxycytidine triphosphate
$DGTP$	Deoxyguanosine triphosphate
$DTTP$	Deoxythymidine triphosphate
$DADMAC$	Diallyldimethylammonium chloride
DCM	Dichloromethane
$DEAE$	Diethylaminoethyl
$DIPEA$	N,N-Diisopropylethylamine
$E.\ faecalis$	Enterococcus faecalis
$E.\ coli$	Escherichia coli
$E.\ saccharolyticus$	Enterococcus saccharolyticus
$EGDA$	Ethylene glycol acrylate
$EDTA$	ethylenediaminetetraacetic acid
$EGDMA$	Ethylene glycol dimethacrylate
$EtBr$	Ethidium Bromide

$FTIR$	Fourier transform infrared
GFP	Green fluorescent protein
GTC	Guanidinium Thiocyanate
$t^{1/2}$	Half-life time
$1,6-HDDMA$	1,6-hexanediol dimethacrylate
HDP	Host defense peptides
Hg	Mercury
KGM	konjac glucomannan
LOC	Lab on a Chip
LPS	Lipopolysaccharides
LB	lysogeny broth
$MgCl_2$	Magnesium chloride
$MACl$	Methacryloyl chloride
MMA	Methyl methacrylate
MIC	minimal inhibitory concentration
$MW-CNTs$	Multi-walled carbon nanotubes
NB	nutrient broth
OD	Optical density
ppm	Parts Per Million
PBS	Phosphate buffer saline
Pt	Platinum
K_2CO_3	Potassium carbonate
PVP	Polyvinylpyrrolidone
PCR	Polymerase chain reaction
$PDMS$	Polydimethylsiloxane
$PMMA$	Poly(methyl methacrylate)
$Poly(MMA-EGDMA)$	Poly(MMA-*co*-EGDMA)
PPM	Porous polymeric monolith
KBr	potassium bromide
PSI	Pounds per square inch
PI	Propidium iodide
$P.\ fluorescens$	Pseudomonas fluorescens
$P.\ putida$	Pseudomonas putida
RCF	Relative centrifugal force
$16SrRNA$	16S ribosomal RNA
RNA	Ribonucleic acid
$NaHCO_3$	Sodium bicarbonate
$NaCl$	Sodium chloride
Na_2SO_4	Sodium sulfate
SPE	Solid phase extraction
SDS	Sodium dodecyl sulfate
$SMAMPs$	synthetic mimics of antimicrobial peptides
TEA	triethylamine
TFA	trifluoroacetic acid
THF	tetrahydrofuran

Chapter 1

Introduction

1.1 Background

Sample preparation for bacteria detection is a time consuming and labor-intensive procedure in DNA analysis. It also introduces one of the greatest variables in subsequent analysis due to its complexity. Sample preparation steps conventionally include cell categorizing and separation, cell lysis, deoxyribonucleic acid (DNA) isolation and refining, amplifying regions in DNA genes using polymerase chain reaction (PCR) and finally detection. Cell lysis, DNA isolation/purification and PCR are at the heart of the biological sample preparation process for bacteria detection. Cell disruption is a process used to release the biological materials within a cell. Cell lysis falls under the cell disruption category in which the cell membrane is dissolved or disrupted. DNA extraction and purification is the process that involves extracting and separating the DNA from the cell lysate. In most cases the concentration of the sample is very low, therefore PCR is needed to amplify the DNA molecules extracted from bacteria cells and generate a number of duplicates of the gene of interest to reach a detectable value.

Micro-total analysis systems, μTAS, scale down and integrate laboratory functions and processes on miniaturized chips. Manz *et al.* [1] proposed the concept of lab-on-a-chip (LOC) system through micro-chip analyzers. The introduced chip was made of silicon and included sample pretreatment, sorting, and detection. Lab-

on-a-chip devices have a few potential superiorities over the macro-conventional laboratory devices. Replacing massive, time consuming and expensive laboratory processes by μTAS in performing complex analytical chemistry operations promises enhanced reproducibility and reliability, simplified handling, shorter analysis time, lower sample and chemical consumption as miniscule amounts of both samples being tested and reagents are needed for the process, and lower contamination risk. Therefore, it can reduce the time taken to synthesize and analyze samples, lower costs of testing and reduce the amount of chemical waste. Further, miniaturization has the potential for integrating various functional components in one device, thus allowing portability and carrying out of multiple analyses simultaneously.

1.2 Cell lysis in microfluidic systems

Both gram-negative and gram-positive bacterium share many characteristics; they both have cytoplasmic membranes, a peptidoglycan film, which is much thicker in gram-positive compared to gram negative bacteria, as proteins exist in the outer membrane which act like pores for particular molecules to enter and depart to and from the cell. The greatest difference between gram-positive and gram-negative bacterium is cell membrane. Fig. 1.1 shows the cell membrane comparison between gram-positive and gram-negative bacterium. As a result, gram-positive bacteria are harder to lyse compared to gram-negative bacteria.

Cell lysis refers to a process in which the cells are broken down by disrupting their membrane and results in the liberation of their cytoplasmic content, namely

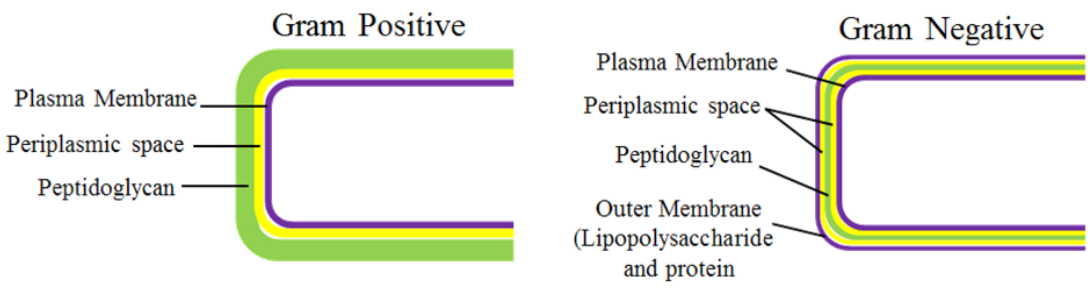

Figure 1.1: Gram-positive and gram-negative membrane structure.

the DNA, RNA, and proteins essential for molecular genetic analysis and clinical diagnostics. Developments in LOC techniques have opened up various possibilities to scale down bio-genetics and molecular diagnostic machines into miniaturized devices with numerous advantages such as higher sensitivity and accuracy, and a reduction in the reaction volumes, which in return, minimizes the material cost and the waste produced. Cell lysis, as a primary step in sample preparation, has been achieved through fundamentally different techniques; according to the lysis mechanism, five lysis methods are well established for LOC applications.

1.2.1 Mechanical cell lysis

Mechanical cell lysis is conceptually the simplest method to achieve lysis, as it uses mechanical forces to disintegrate the membrane. There are numerous techniques to disrupt the cell membrane by contact between the cells and lysing objects. One method is to force the cells through narrow gaps or pores with sharp edges that are smaller than the cells [2], thereby shearing the cell membrane and rupturing it to release its intracellular content. Burke *et al.* thus formed a narrow porous polymeric monolith (PPM) within a poly(dimethylsiloxane) (PDMS) microfluidic channel and used it to lyse white blood cells (B lymphocytes), by shearing the cell membrane through the small pores of the monolith [3]. Mahalanabis *et al.* introduced a microfluidic chip to lyse bacterial species and extract genomic DNA by mechanical shearing through a PPM column within a microfluidic channel, but with the assistance of chemical reagents [4]. Blockage generally is a major drawback in such minute microfluidic devices.

1.2.2 Thermal cell lysis

Thermal cell lysis is accomplished by thermal shock consisting of freezing and thawing cycles, or otherwise by heating the cell suspension [5]. This causes the proteins within the cell membrane to be denatured, which leads to irreparable damage and release of the intracellular components. Thermal cell lysis is useful to avoid contam-

ination in downstream processes, because it is a reagentless lysis technique. The fact that accurate temperature administration is necessary to prevent damaging the DNA is a noteworthy downside of thermal cell lysis [6]. The high power requirements for heating also make thermal cell lysis undesirable for portable systems.

1.2.3 Electrical cell lysis

It can be achieved by exposing the cells to a high-intensity pulsed electric field (PEF) [7] that destabilizes and disintegrates the membranes, by producing nanopores leading to their dielectric breakdown [8]. The lysis efficiency and time both depend on the electric field strength. Shahini *et al.* investigated the electric field improvement by carbon nanotubes (CNTs) to develop low voltage electrical cell lysis biochip to lyse Chinese hamster ovary (CHO) cells [9]. Electrical cell lysis is reagentless, quicker and cost less than chemical lysis; thus it is widely integrated in micro-electromechanical system (MEMS) devices. Unfortunately, it requires a high power consumption which is an unfavorable parameter within miniaturized systems. Electrical cell lysis also often demands complicated designs to accommodate the electrodes, which results in difficult fabrication.

1.2.4 Chemical cell lysis

It is often called chemical permeabilization that uses chemical means to permeabilize the outer cell membrane. Enzymes are sometimes used to permeabilize cell walls as a prerequisite to chemical cell lysis. Lysing agents can be used to target the cells either through continuous flow in microfluidic channels [10] or by incubation in micro-chambers [11].

Buffers such as ammonium chloride which is often used to lyse red blood cells [12], detergents (disrupting the membrane by dissolving the fat and protein layers on the cell wall, thus forming pores and membrane become permeable) including Triton X-100 [13] and sodium dodecyl sulfate (SDS) [14], chaotropic agents like guanidinium thiocyanate (GITC) [14], ethanol and magnesium chloride (interfering

with intermolecular forces in proteins) and enzymes, for example, lysozyme [15, 16], lysostaphin and proteinase-k [16] (digesting the peptidoglycans in the cell walls, ultimately compromising their integrity) are the most common chemical agents used.

Sethu *et al.* chemically lysed red blood cells in a three-inlet, one-outlet, two hexagonal phosphate buffer saline (PBS) and lysis buffer channels and a long meander channel microfluidic device, shown in Fig. 1.2, fabricated using conventional soft lithography techniques [12]. A cell lysis solution containing ammonium chloride is pumped through one inlet that splits into two branches of a hexagonal channel. The whole blood sample is simultaneously injected at a lower flow rate into the second inlet. It is focused in a small flow edged on the two sides by the cell lysis reagent as shown in the inset of Fig. 1.2, thereby creating a sheath flow that increases the contact between the lysis reagent and the cell membrane enhancing the efficiency of lysis.

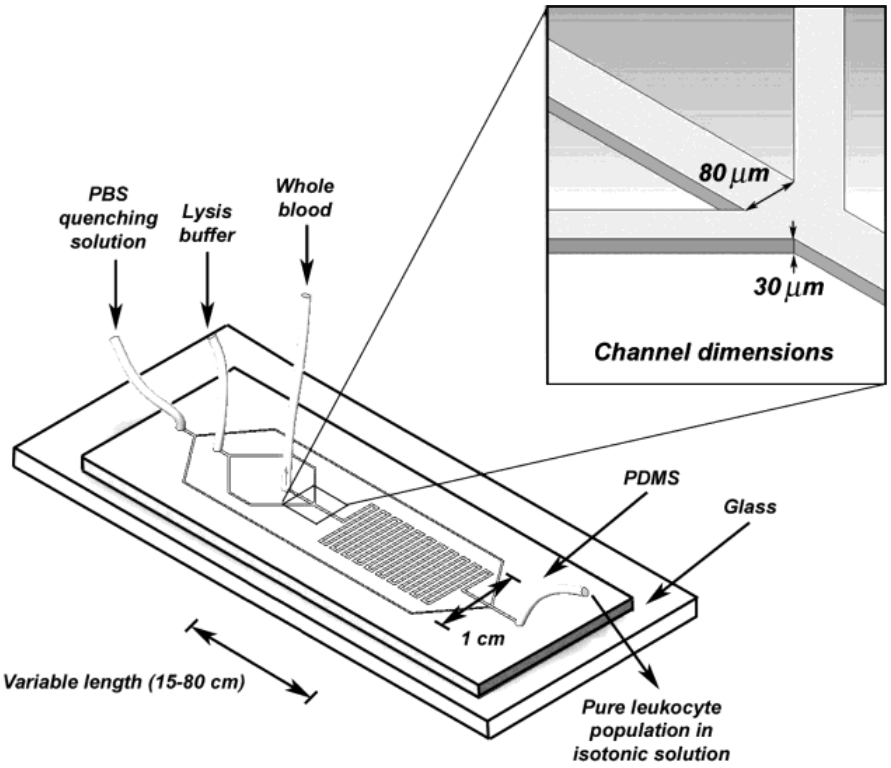

Figure 1.2: Red blood cells lysed in a meander channel [12].

The mixture fluid then flows in a long planer meander channel to enrich the mixing. PBS solution is introduced into the third inlet to meet with the mixture at the outlet of the meander channel to dilute the lysis reagent. It is then collected from the outlet. Radoslaw *et al.* developed a microfluidic device that coupled cell lysis of two cell lines with fluorescence-based enzyme assay [17]. The micro-device, shown in Fig. 1.3, employs an identical cell lysis approach and similar micro-device geometry to that introduced by Sethu *et al.*

Shilling *et al.* introduced a three-inlet, two-outlet and two-microchannel microchip that chemically lysed E. coli bacterial cells as well as extracted and detected proteins of a certain size using different microfluidic flow rates at the inlets and the outlets and as illustrated in Fig. 1.4 [14]. A cell sample and a chemical lysing reagent (SDS or bacterial protein extraction reagent (B-PER)) are pumped into a lysis channel through separate inlets and with different flow rates. As the bacterial sample and lysing reagent meet, they flow down a long microchannel mixing only by lateral diffusion which causes the lysing reagent to laterally diffuse into the cell sample as it is molecularly smaller (higher diffusion coefficient) than the

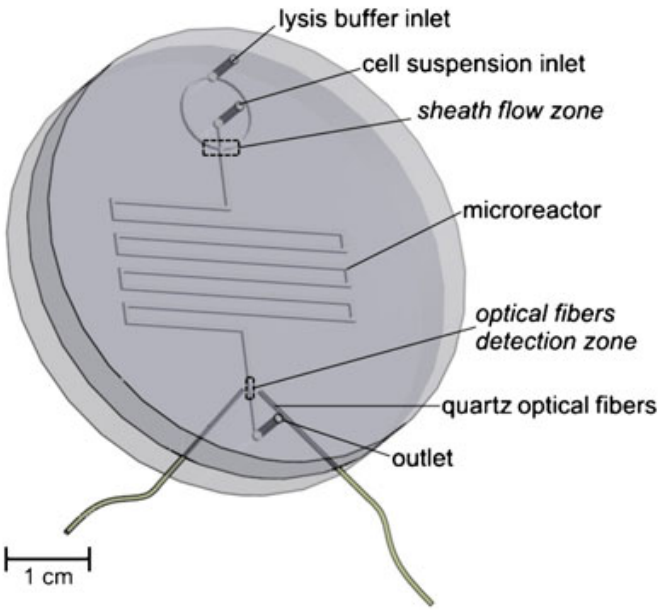

Figure 1.3: Cell lysis using chemical lysis and sheath flow [17].

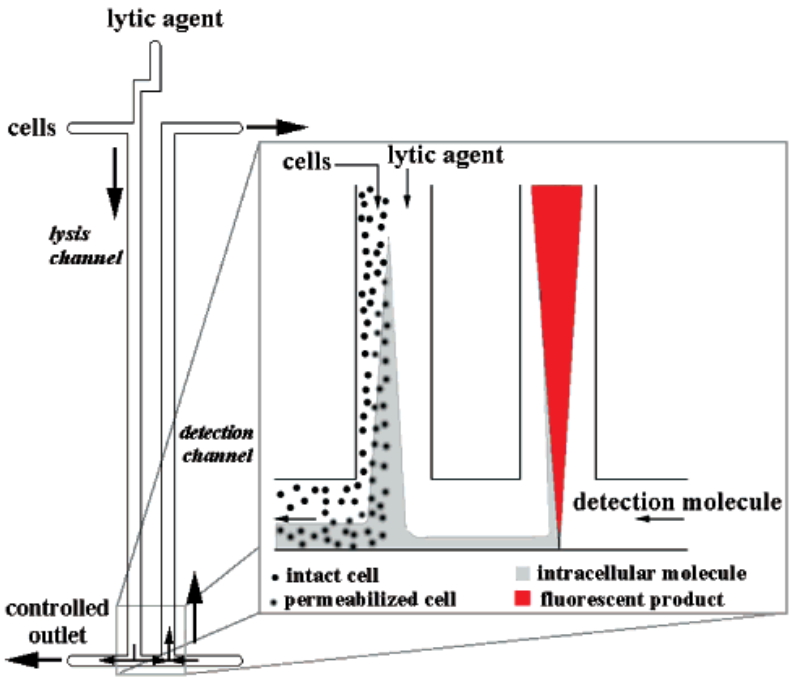

Figure 1.4: Chemical cell lysis and protein extraction by molecular size and controlled flow rate [14].

cell sample. This diffusion causes the disintegration of the membrane and leakage of intercellular compounds. The protein diffuses out of the lysed cell into the channel. Cell lysis channel ends at a T-junction where the fluid splits according to the molecular size of the fluid contents which is controlled by the different flow rates at the outlets. This device could be generalized for several bacterial species and for extracting any molecular component such as DNA or RNA. It can also be integrated with other biological processes such as PCR.

El-Ali *et al.* described a lab-on-a-chip that performs controlled chemical cell lysis of mammalian cells using detergents such as Triton X-100 as lysin [13]. The device uses gas-liquid flow to improve combining between cells and lysis reagent to increase the lysis efficiency in contrast with using sheath flow or controlled flow rates. The microfluidic device, made of glass substrate chemically/thermally bonded to polymeric layer, consists of four inlets (gas, stimulus, cells sample and cell lysis buffer inlet), six serpentine microfluidic channels (gas, stimulus, sample cells, cell lysis buffer channels, cell lysis and stimulus zones), thermo-electric heaters

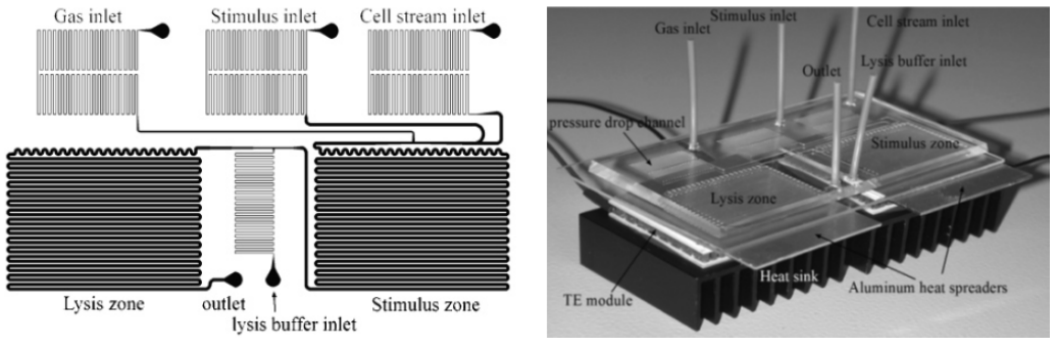

Figure 1.5: A schematic diagram of the microfluidic system design (left) and a picture of the device (right) [13].

and coolers to manage the heat through cell stimulus and cell lysis as illustrated in Fig. 1.5.

Irimia *et al.* investigated the intracellular contents of single cells by demonstrating a microfluidic bio-chip for chemical cell lysis for extremely low cell suspension volume down to a 1 $\times 10^{-12}$L [10]. A cell specimen holding a solitary cell and a 1×10^{-12} L of cell lysis reagent (PBS, SDS or guanidinium thiocyanate) are joined together in a polymeric 10^{-12} L repository where lysis take place and lysed cell is imaged with a marker. Once lysis is done, cytoplasmic contents are diluted to be ready for succeeding processes. Sasuga *et al.* demonstrated a less complicated single-cell chemical cell lysis microchip using an array of Pico-liter microwells [18]. An aliquot of the bacterial suspension is dropped onto a group of microchannels formed in a polymeric layer allowing cells to settle in the channels and afterward the abundant cells are evacuated. The polymeric layer hosting the cells is reversed to create a stream cell with a cover glass and afterward a CelLytic-M (detergent) is connected to the stream cell. The polymeric layer is then bonded to the bottom coverslip to form enclosed channels. The cells are progressively lysed in the enclosed micro-channels as shown in Fig. 1.6.

The expansive number of miniaturized devices that utilize chemical substances to lyse cells shows the adaptability of this technique, which make it an attractive technique to be integrated into sample preparation systems. But, the high price of the chemical and enzymatic agents used and their possible interference of the

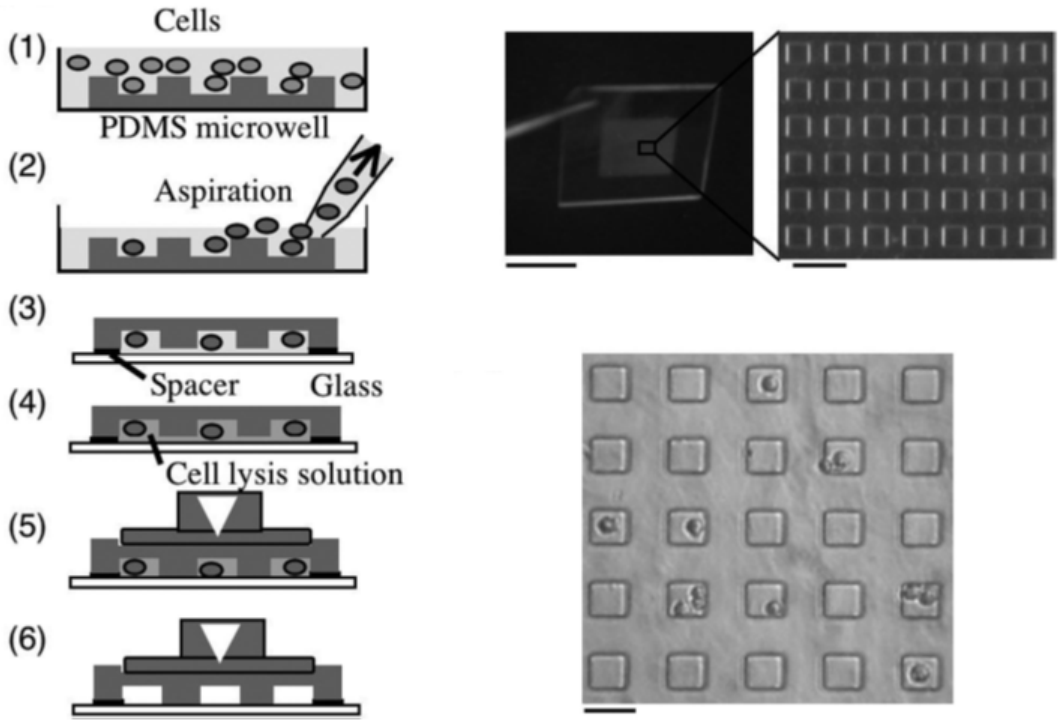

Figure 1.6: Single-cell capture and cell lysis in microwells [18].

chemical and enzymatic agents used with the subsequent analysis processes is the major downside of chemical lysis.

1.2.5 Antimicrobial cell lysis

It uses variety of agents such as disinfectant, biocides, antibiotics and antiseptics. In this lysis category, the lysin first is attracted to the bacterial surface changing the permeability of the bacterial wall, slowly damages and disintegrates the cell membrane, leading to the release of the intracellular substances. Two antimicrobial agents will be covered:

1. Disinfectants such as quaternary ammonium compounds (QACs) such as benzalkonium chloride (BAC).

2. Polymeric biocides, also known as antimicrobial polymers, are a class of polymers with antimicrobial activity. These polymers are effective in one of two forms:

a. aqueous solution

b. coating on the surface of nanoparticles or on the wall of a microchannel/microchamber

to lyse bacteria on contact.

1.2.5.1 Disinfectants

Quaternary ammonium compounds are permanently positively charged independent of the pH of their solution. Quaternary ammonium compounds (QACs) are produced by alkylation of tertiary amines in a procedure known as 'quaternization'. Quaternary ammonium compounds possess antimicrobial property and used as antimicrobials and disinfectants such as benzalkonium chloride (BAC) [19].

Kim *et al.* evaluated the cell lysis efficiency of several cell lysis agents through statistically designed experiments that carried out and observed by a microscope in PDMS based microfluidic device [15]. Six lysins: alpha olefin sulfonate, BAC, Triton X-100, lysozyme, Ethylenediaminetetraacetic acid (EDTA) and SDS were evaluated on E. coli and B. subtilis, and adenosine triphosphate (ATP) was extracted in proportion to the cell lysis efficiency. Bioluminescence detection kit was used for a rapid and quantitative detection of ATP that contains luciferin-luciferase reagent which yields light in the presence of ATP. The strength of the produced light is corresponding to ATP volume and was measured by a luminometer. A 0.1mL of each of the bacteria samples was treated with 0.1 mL of each of the six surfactants for 1 minute at room temperature, and afterward a 0.1 mL aliquot of the bioluminescence detection reagent was added. A concentration of 202 and 99 parts per million (ppm) for lysozyme and BAC, respectively, were shown to enhance the quality of lysis. BAC and lysozyme disintegrate cell membrane and wall by, respectively, dissociation of the cellular membrane lipid bilayers and interruption of the β-1,4-glycosidic linkages in the cell wall. Thus, a synergistic interface between BAC and lysozyme might improve the extraction value of adenosine triphosphate [15]. To confirm the optimized cell lysis reagents, a two-inlet, two-outlet and a 90 μm $\times$ 300 μm $\times$ 28 mm central microchannel microfluidic device was used. An optimal flow rate of 0.1 μL per min achieved by micro-syringe pumps contributed to cell lysis [15]. Fig. 1.7 illustrates a micrograph of the used microchannel.

Santillo *et al.* introduced a lab-on-a-chip to study the cell lysis efficiency at

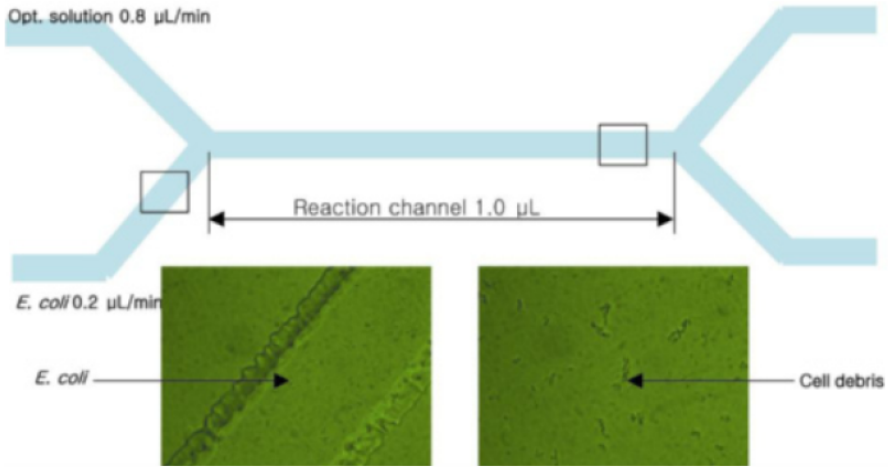

Figure 1.7: Micro-chip before (left) and 1 minute after (right) combining cell suspension with cell lysis reagents [15].

various flow rates and volumes of several lysins agents against single cells and populations of Arcella vulgaris [20]. The efficacy of BAC, SDS, chlorhexidine digluconate, Triton X-100 and phenol were evaluated. The device captures cells, allows well managed excess to chemical reagents, and visually captures a single cell lysis. Fig. 1.8a shows the developed microfluidic device which composed of two layers bonded to form an enclosed device. The 50 μm high, lower channel has a 1mm inlet that separates to 2 mm width and divides into eight different chambers, as shown in Fig. 1.8b. Cells are captured in the chambers, when cell suspension flows into the system, as shown in Fig. 1.8c. Flow continues through the 10 μm high channel located above the chambers where cells are captured, so it can exit the device. Experiments revealed that lysis efficiency depends on lysis reagent concentration and flow rate of the cell suspension. More cell lysis occurred at higher concentrations and lower flow rates. At low concentrations, cells were exposed to less cell lysis agents, which yield significantly longer cell lysis time. At a constant cell concentration of 1 mM and flow rate of 5 μL per minute, the cell lysis efficiency of all five biocidal agents were compared. BAC and Triton X-100 show a fast and strong cell lysis effect which agrees with Kim *et al.* results [15], but chlorhexidine digluconate, phenol and SDS show a slow and weak cell lysis effect.

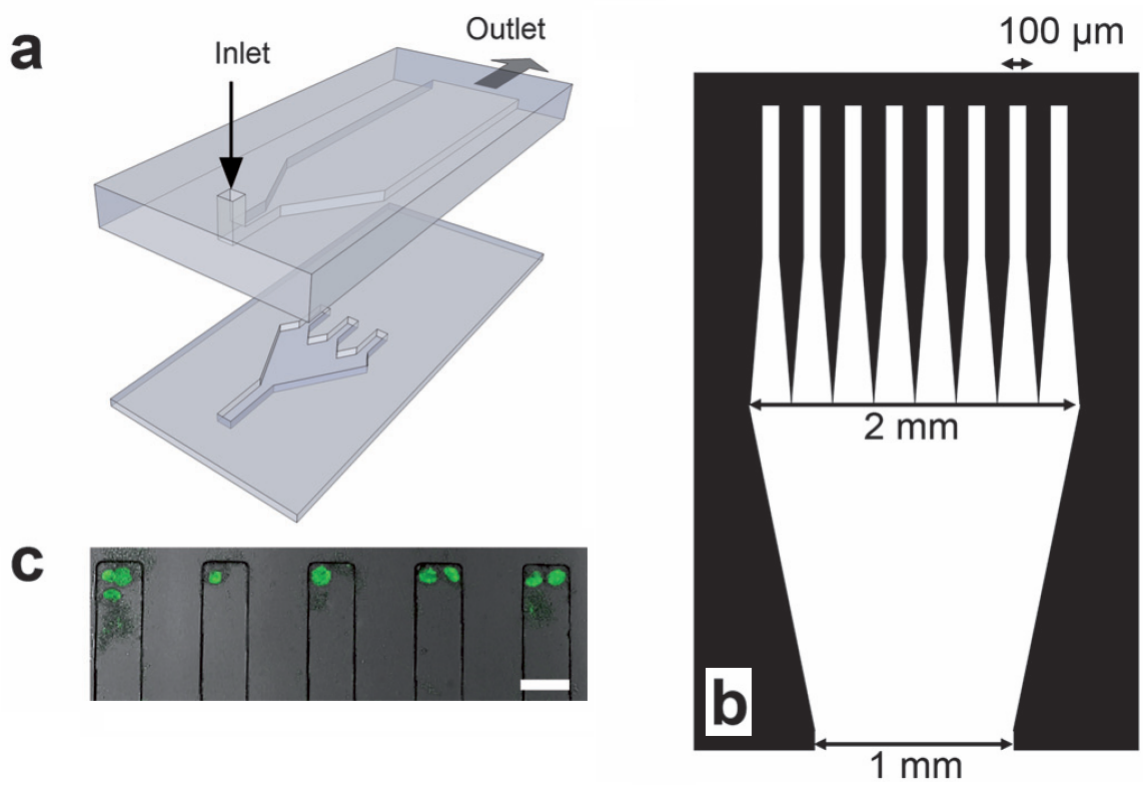

Figure 1.8: (a) Schematic diagram of a two layers microfluidic device , (b) top view of the capture champers and (c) Arcella treated with a viability probe [20].

1.2.5.2 Polymeric biocides

Antimicrobial polymers are polymers possessing antimicrobial activity that is the aptitude to constrain the growth, lyse and eventually kill microorganisms for instance bacteria, fungi and often viruses. Development is progressing to engineer these polymers in order to copy the characteristic of natural host defense peptides (HDPs) utilized by the immune system in living life forms to fight microscopic organisms. That rising family of antimicrobial polymers, called 'synthetic mimics of antimicrobial peptides' (SMAMPs), [21] are formed to emulate the principle elements of HDPs: cationic charge and amphiphilic character, which prompt the imbuing and afterward the breakdown of the bacterial membrane.

Antimicrobial polymers commonly kill bacteria by diminishing the nutrition sources for bacteria, thereby stopping bacteria from recreation in a process called 'bacterial conjugation' [19] as illustrated in Fig. 1.9. Most bacterial surfaces are

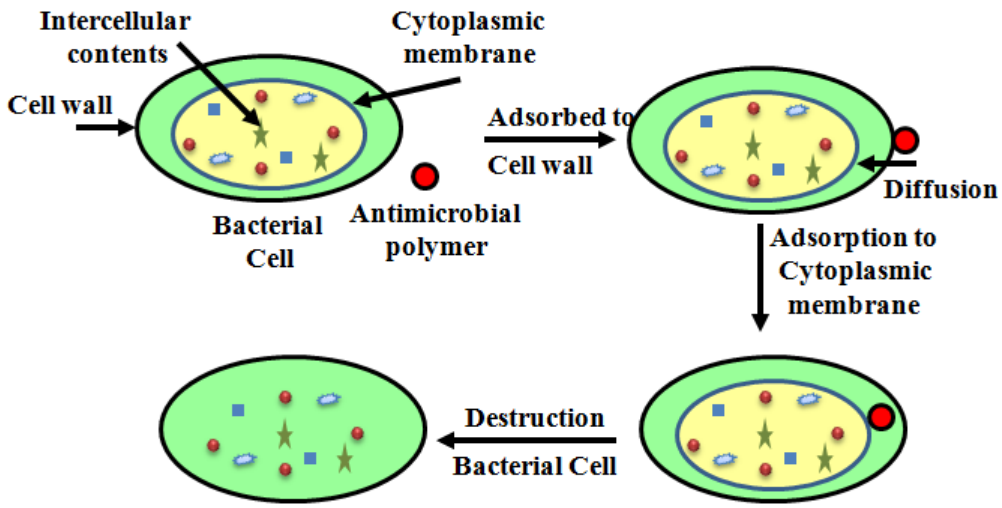

Figure 1.9: A schematic diagram of killing mechanism of an antimicrobial polymer to a bacterial cell.

composed of peptidoglycan, phospholipids, lipoproteins and lipopolysaccharides (LPS) and have a negative net charge. The polymer is first attracted toward the anionic outer cell membrane surface. The integrity of the cell wall is compromised. The antimicrobial polymer then diffuses through the outer cell membrane and adsorbs onto the plasma membrane. Binding of the polymer to phospholipids occurs with an increase in inner membrane permeability accompanied by bacteriostasis which is the inhibition of growth, but not the killing, of bacteria. The disintegration of the membrane and the following release of cellular contents causes the killing of the cell [22].

Antimicrobial polymers were first introduced by Cornell *et al.* in 1965, when they presented polymers that kill bacteria on contact [23]. Antibacterial polymers often come in aqueous solution and surface coating forms. Antimicrobial polymers in aqueous solutions are first reviewed. Antimicrobial polymer surface modified nanoparticles in aqueous solution are reviewed next. Finally, antibacterial polymeric surface coatings and their potential application in microfluidic devices are reviewed.

Three types of antimicrobial polymers are available in solution form: polymeric biocides, biocidal polymers and biocide-releasing polymers [24]. Their working prin-

ciples are illustrated in Fig. 1.10. Polymeric biocides are composed of antibacterial monomers, so the repeating units are biocides as shown in Fig. 1.10a. A drawback of this class of polymers is that biocidal monomers do not often produce antibacterial polymers [24]. On the other hand, biocidal polymers do not necessarily require antimicrobial monomers, but the active biocidal property is embodied within the entire polymer as illustrated in Fig. 1.10b. Kawabata *et al.* introduced a soluble pyridinium type (polycationic) polymer that exhibits stronger antibacterial activity (99.9% of bacteria killed upon 5 min. of contact time) against gram-positive bacteria than that of corresponding monomeric compounds and conventional disinfectants, such as benzalkonium chloride and chlorhexidine [25]. Zuo *et al.* demonstrated similar results by comparing the antibacterial activity of quaternary ammonium acrylic monomer and the corresponding homopolymer to gram-positive bacteria, S. aureus and gram-negative bacteria, E. coli [26].

Biocide releasing polymers are polymers with functional groups that are biologically active (biocides). The polymeric backbone functions as a carrier for biocides (functional groups) that travel to bacterial cells. These polymers send the biocidal unites near by the cytoplasmic membrane in high concentrations as shown in Fig. 1.10c. Vogl *et al.* first introduced this class of polymers in 1979 by polymerizing salicylic acid [27]. A plethora of biocide releasing polymers has been synthesized in the last decade [28–30].

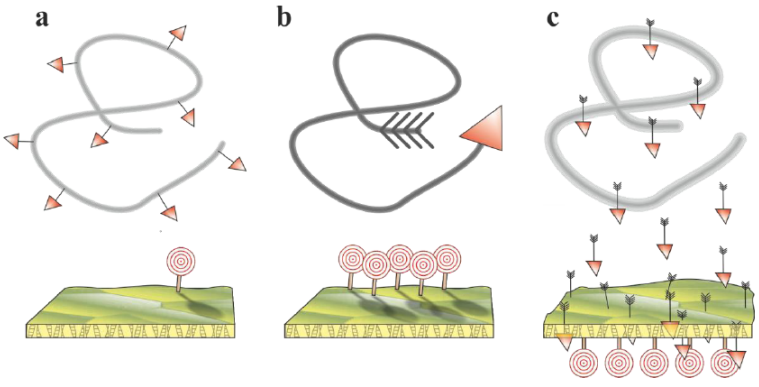

Figure 1.10: The three classes of antibacterial polymers: polymeric biocides (a), biocidal polymers (b) and biocide-sending polymers (c) [24]

.

Antibacterial surfaces are form of antimicrobial polymers killing cells by physical contact. Tiller *et al.* developed in 2001 surfaces that killed bacteria upon physical contact, and termed this phenomenon 'contact-killing' [31]. Antibacterial polymers have been attached to numerous surfaces by several techniques including chemical grafting [32, 34], layer-by-layer deposition [35, 36], plasma polymerization [37] and grafting from [38]. Madkour *et al.* thus used surface-initiated atom transfer radical polymerization (ATRP) to form an antibacterial co-polymer, poly(butyl methacrylate-*co*-aminoethyl methacrylate), from surfaces [38]. These showed high antibacterial properties that killed 100% of S. aureus and E. coli in less than 5 min.

Antimicrobial polymeric surface coatings have shown very promising results that could be adapted in LOC, as they were coated, grafted and functionalized over a variety of surfaces with fast response against a large number of bacterial species and also viruses. Madkour *et al.* functionalized silicon substrates and glass surfaces with surface coating of antibacterial polymers utilizing the 'grafting from' attachment method [38]. These surfaces showed high antibacterial property that lysed 100% of S. aureus and E. coli in approximately 4 min. Li *et al.* introduced a multi-level antibacterial films with release-killing, contact-killing and anti-adhesion properties that was prepared from polymer-chlorine dioxide ClO_2 mixed with Zinc chloride to produce "contact-killing" activities [39]. The coating exhibited contact-killing property by killing B. subtilis, S. aureus and E. coli after a physical contact time of 10 minutes. Lee *et al.* grew non-leaching antibacterial polymeric surfaces on the surfaces of glass and paper using atom transfer radical polymerization (ATRP) [40]. Following polymerization, the polymer-modified surfaces were populated with quaternary ammonium groups. The coating was tested against E. coli or B. subtilis demonstrating a substantial antibacterial capacity that killed 95% of the bacteria cells within 15 minutes of contact.

Coating or surface modifying nanoparticles is one approach for the antibacterial polymeric surface coatings. Wan *et al.* described a polymeric micro-chip integrating cell lysis and PCR in one micro-chamber [41]. Poly(quaternary ammonium) compound surface functionalized gold nanoparticles, $Au_{(+)}$NPs, were utilized for

cell lysis. The biocidal activity of the QAC and the high surface area to volume ratio that AuNPs offer were utilized to enhance cell lysis efficacy. It was also reported that $Au_{(+)}$NPs caused PCR inhibition which was overcome by PCR additives such as bovine serum albumin (BSA).

Cell lysis reagents such as detergent, disinfectants and biocides often inhibit succeeding processes such as PCR [42, 43]. Therefore, reducing or eliminating the use of these agents will reduce the cost and complexity of the LOCs. Thus designing a non-leaching antimicrobial surface with large surface area will avoid the use of cell lysis reagents that is a hurdle to filter without affecting the subsequent processes.

1.3 Porous monolith

Polymeric and silica porous monolith have drawn much attention recently for extracting the three major biological macromolecules: DNA, RNA and proteins. Porous polymeric monoliths (PPMs) were introduced during the last ten years. In contrast with silica beads, a monolith is a solitary, continuous polymeric structure formed using *in situ* polymerization. For microfluidic systems, channels serve as the molds for PPMs. The mass transport within a microchannel or capillary filled or partially filled with porous monolith material is a convective transport as the mass is pushed to pass through the entire isolation medium compared to a diffusion mass transport within microchannel filled with beads as illustrated in Fig. 1.11. As a result, many properties of the PPMs do not depend on flow rate [45]. Monoliths have no interstitial voids, have very short diffusion distances and multiple pathways for the flow as shown in Fig. 1.11. Within a monolith, a group of joined pores creates a constant matrix, occupied with unified pores that create stream paths of a constant size and lead to a more efficient interaction with the component of interest and the pores as shown in Fig. 1.11. PPM within microchannels develops an array of paths in the constant part of a porous material that displays high permeability in the axial direction, a high pore surface area of the internal path and lower backpressure than that of traditional beads [45]. The versatility of their prepara-

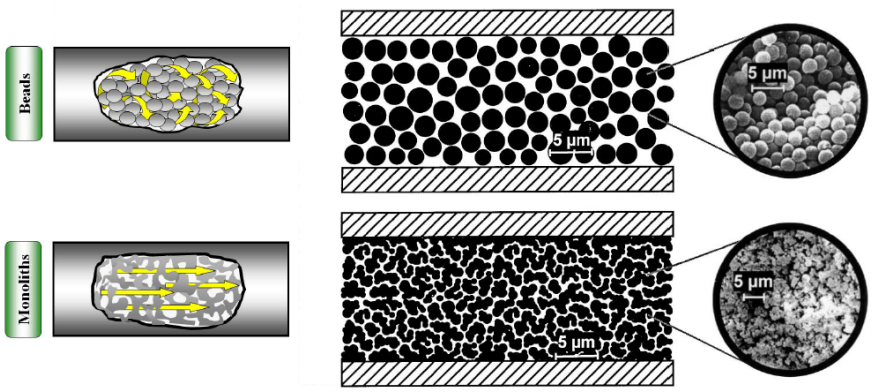

Figure 1.11: Mass transport within a porous polymer monolith and silica beads [44, 45].

tion techniques leads to the ease of modifying their surface by grafting the pore surfaces with chosen polymers yielding constituents with hydrophobic, hydrophilic, ionizable, and zwitterionic surface chemistries that broaden the extraction scope for PPMs. Also, the characteristic properties of the porous of the monolith can be easily tuned and managed.

1.3.1 Porous polymeric monolith fabrication

The fabrication of PPMs is mainly done in two steps: microchannel surface modification and PPMs formation. As reported by Stachowiak *et al.*, the first step creates a thin polymeric film with a plethora of unreacted double bonds that are used to covalently bond the PPM to the substrate and avoid the creation of any gaps between the PPM and the micro-channel wall [46]. Functionalizing the surface of the micro-channel is usually done by grafting via surface photo-initiated free radical polymerization. That is the channel surface is pretreated via UV initiated grafting to covalently bond the monolithic column to the substrate.

The second step involves the fabrication of the PPM column within the microfluidic channel or chamber. The polymerization process of the PPMs is usually done by free radical polymerization that is initiated either by thermal energy or by ultraviolet radiation of a mixture composed of functional and cross-linker monomers and porogenic solvents in the presence of an initiator. Monomers are the repeated

units of the polymer that works as the backbone of the PPMs. In free radical polymerization, a polymer is formed by consecutively adding of free radical units. Radical units are produced in two main mechanisms using either thermal energy or UV radiation with the assistance of thermal or photo initiators, respectively. Initiation happens in two processes starting by creating radicals and then these radicals moves to the monomer blocks present in the polymerization mixture [47]. Succeeding the free radicals production, monomer blocks are added by the initiated free radicals, thus polymer branches are growing leading to full polymerization.

Thermal and photo initiation are the main initiation mechanism used in forming PPM columns and they vary in the way a bond is cleaved to produce radicals [48]. Porogenic solvents are important components in forming PPM columns and they help in dissolving functional and cross-linker monomers to create a uniform mixture and also control the structure porosity. The final stage in the second step is defining the location of the PPM column within the micro-fluidic cavity [48].

PPM was first used within microfluidic channels by Yu *et al.*, when they prepared hydrophobic PPMs with ionizable surface using UV-initiated co-polymerization, to work as anion exchange micro-solid phase extraction (μSPE) preconcentrator [49]. A porogenic mixture composed of hexane and methanol was used to define the desired porous properties and consequently flow resistance. They achieved low flow resistance within the microchannel filled with PPM enabled high flow rates of 10 μL/min exceeding flow velocities in typical analytical microchips. The device consisted of 100 μm $\times$ 40 μm $\times$ 6 cm rectangle microchannel as shown in Fig. 1.12. The microfluidic device was tested against low molecular weight probe, Coumarin 519, Coumarin 519-peptide conjugate and green fluorescent protein (GFP). Hua *et al.* evaluated the compatibility and performance of hydrophobic butyl methacrylate (BMA) based PPM solid phase extraction beds copolymerized with a cationic monomer and poly-cationic surface coating utilized to lower protein and peptide adsorption on capillary walls which was fabricated within micro-fluidic glass chips [50]. They concluded that polymeric coating with cationic surface charges and the PPM are well matched, yielding high efficiency isolation and a vigorous function-

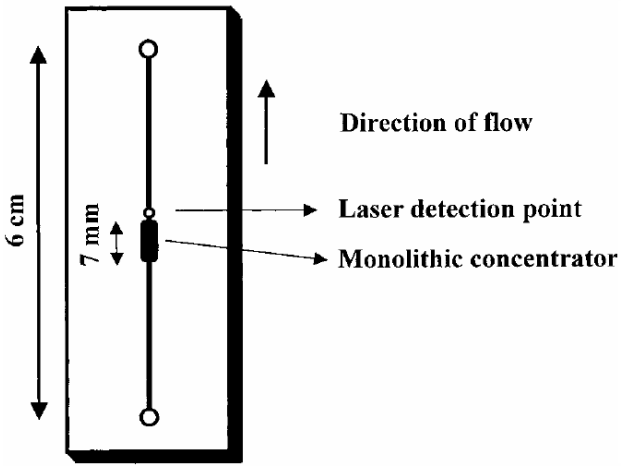

Figure 1.12: Yu *et al.*'s [49] PPMs based micro-SPE.

alization to minimize protein adsorption.

Tan *et al.* developed a group of PPM-SPE in a thermoplastic micro-fluidic chip by UV initiated co-polymerization of BMA and EGMA for sample cleanup and pre-concentration [51]. The microchip was formed by hot embossing the micro-fluidic channel and thermally bonding the two polymeric substrates to create an enclosed micro-fluidic chip. The micro-chip was composed of eight micro-fluidic channels joined via silica capillaries as illustrated in Fig. 1.13. The monolith solution was pumped into the channels and polymerization was triggered by UV irradiation. The micro-fluidic chip filled with PPM was evaluated with two samples to demonstrate its analytical potential.

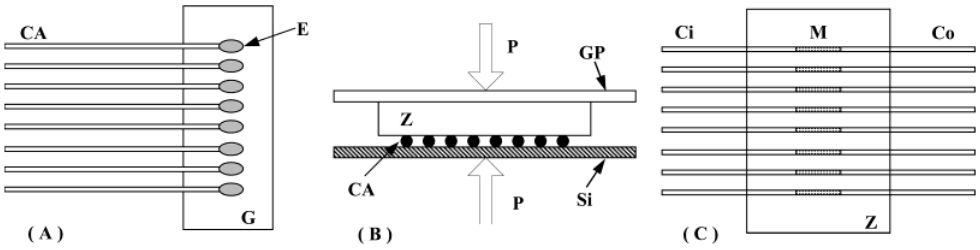

Figure 1.13: Fabrication process: (A) The mold for the hot embossing procedure where CA is a group of eight silica capillaries, E is epoxy glue and G is glass film, (B) Hot embossing process where Z is thermoplastic substrate, Si is silicon substrate, GP is glass slide and P is the press-pressure, and (C) The micro-fluidic chip, M is the micro-fluidic channels for the PPM, Ci and Co are the inlet and outlet [51].

Kulinski *et al.* developed a polymer micro-fluidic module that lyse E. coli bacterial cells mixed with human hematuric urine by mechanically shearing the bacterial cell membrane by pumping through the narrow pores of PPM column with the assistance of lysis buffer (guanidine thiocyanate (GuSCN) containing lysis buffer (buffer RLT)) and then isolate the DNA by solid phase extraction [52]. The solid phase extraction used in this work was composed of PPM column impregnated with silica beats taking advantage of the intrinsic affinity of the DNA molecules to silica beats. They demonstrated the cell lysis and the DNA extraction by off-chip real-time PCR. They quantitatively determine the DNA isolation efficiency of the developed module by determining the concentration of the liberated DNA using a commercial kit, Quant-IT PicoGreen Assay. Fig. 1.14 shows the values of the DNA concentration after the isolation process done by the developed module.

Mahalanabis *et al.* introduced a micro-fluidic sample preparation system to lyse bacterial species and then extract genomic DNA from human blood [4]. The micro-channels were fabricated by hot embossing and the channels were bonded with thermoplastic substrate. The bacteria were lysed by mechanically shearing the bacterial cell membrane by flowing into a PPM-μSPE formed into a micro-fluidic channel in the presence of detergent lytic reagents. The genomic DNA was extracted using a PPM impregnated with silica particles in a μSPE column formed within a micro-channel using UV-initiated co-polymerization of functional and cross-linker

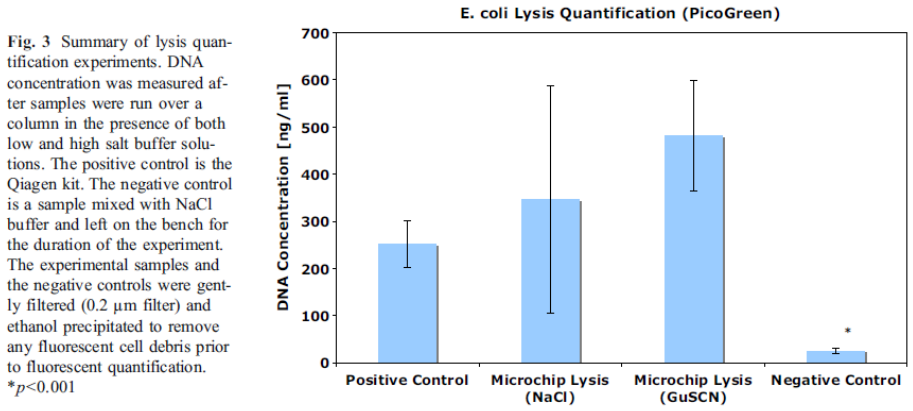

Figure 1.14: Kulinski *et al.*'s [52] DNA concentration at different experimental conditions.

monomers. Chaotropic buffer (3M GuSCN) and 0.8 mg/ml proteinase K were added in the extraction process. Genomic DNA released from lysed E. coli, B. subtilis and E. faecalis bacteria were isolated.

Bhattacharyya *et al.* introduced a polymeric micro-fluidic chip for SPE based isolation of DNA for various applications [53]. Fig. 1.15 shows the fabrication process of the developed polymeric micro-fluidic biochip . The solid phase within the microchannel was composed of a PPM with infused silica particles. DNA isolation was done by binding the DNA molecules to the silica particles impregnated into the PPM. The PPM column was fabricated by UV-triggered co-polymerization of methacrylate and dimethacrylate monomers with assistance of UV initiator and porogenic solvents [53]. The channel was functionalized via UV grafting to enhance the attachment of the PPM to the channel surface. The same group has also used PPMs in both cell lysis and DNA extraction microchannels in the same cyclic polyolefin microfluidic device [54]. They formed a PPM column infused with multi-walled carbon nanotubes (MW-CNTs) within the cell lysis microchannel and PPM infused with silica particles SPE column within the extraction microchannel. DNA was successfully isolated using the introduced microfluidic device.

Klapperich *et al.* upgraded the PPM/MW-CNTs lysis and PPMs/silica DNA isolation microchip introduced by Bhattacharyya *et al.* by integrating the PCR stage within the same polymeric microfluidic device as shown in Fig. 1.16 [55].

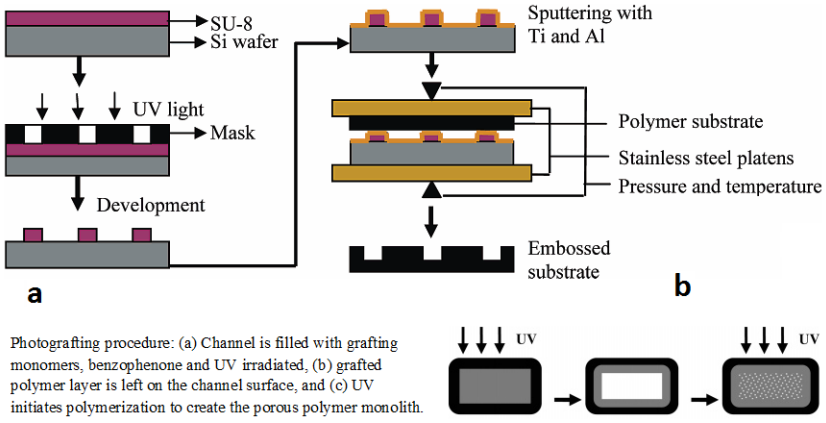

Figure 1.15: Bhattacharyya *et al.*'s [53] (a) hot-embossing and (b) the photografting processes.

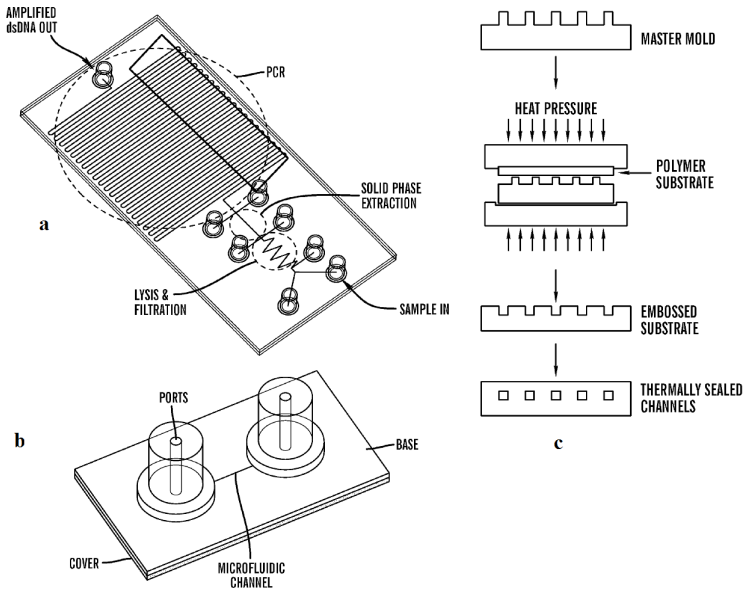

Figure 1.16: Schematic diagrams of (a) LOC, (b) hot-embossing process and (c) packed device [55].

1.4 Thesis outline

This document is organized into five chapters list of references cited in the thesis and appendices. A background and a literature review of the work done in the area of research relevant to the work introduced in this thesis are presented in Chapter 1.

In Chapter 2, a novel dual mechanisms cell lysis technique based on a Boc-protected antibacterial porous polymeric monolith column polymerized directly in a microfluidic channel fabricated from 20% cross-linked PMMA substrate by well-controlled, high-throughput laser micromachining is demonstrated. The antibacterial property and the cell lysis efficiency of the developed PPM against B. subtilis and E. coli bacteria were validated and confirmed. The usefulness of using X-PMMA as an attractive substrate material and the bonding between the substrate and the PPM is investigated.

In Chapter 3, the cell lysis efficiency of the bio-chip presented in Chapter 1 is optimized; the usefulness of the lysis technique presented in Chapter 1 is further

confirmed in terms of reusability of the PPM columns, by demonstrating that the PPM columns show no evidence of physical damage, DNA carryover, and suffer from no significant performance loss when they are used in 20 successive lysis cycles after they were back-flushed between cycles; the ability of the optimized bio-chip to lyse two gram-positive and two gram-negative bacteria at low cell concentration down to 10^2 CFM/ml and yield a DNA that is detectable after performing off-chip PCR. The optimized Boc-PPM based bio-chip showed better lysis efficiency when compared to off-chip traditional mechanical, thermal and chemical cell lysis.

In Chapter 4, an on-chip cell lysis based on a quaternary ammonium compound (QAC) antibacterial PPM column is presented. The influence of the cross-linker monomer on leaching property, mechanical stability, morphology, porosity, bacterial growth inhibition and cell lysis efficiency of the PPM is investigated. The ability of the developed antibacterial PPM to constrain the growth and lyse Micrococcus luteus (Schroeter) (ATCC 4698), Kocuria rosea (ATCC 186), Pseudomonas putida (ATCC 12633) and Escherichia coli (ATCC 35218)) bacterial cells are demonstrated. The bio-chip was reused 30 consecutive cycles with no evidence of physical damage, DNA carryover, and suffers from no significant performance loss.

In Chapter 5, conclusions were drawn from the findings of this work and recommendations for future work on on-chip cell lysis based on antibacterial PPM column were provided.

References section lists the references cited in Chapter 1 through Chapter 4.

Appendices section contains three appendices: Appendix A, B and C which cover additional experimental details, figures and tables of Chapter 3, 4 and 5, respectively.

Chapter 2

Boc-Protected Antibacterial PPM

In this chapter, a porous polymeric monoliths with antibacterial surfaces within a microfluidic chip was prepared to form an antibacterial porous structure belonging to the SMAMPs family. The antimicrobial PPM columns are fabricated by *in situ* photoinitiated free radical copolymerization of n-butyl methacrylate (BuMA) and N-(tert-butyloxycarbonyl)aminoethyl methacrylate (Boc-AEMA), cross-linked with ethylene glycol dimethacrylate (EGDMA) in the presence of photoinitiator, 2,2-dimethoxy-2-phenylacetophenone (DMPAP), and porogenic solvents, 1-dodecanol and cyclohexanol. In the PPM developed, bacterial cells undergo lysis through a dual mechanism: mechanical-shear lysis, by forcing bacterial cells to flow into the porous medium of the PPM column, and antibacterial contact-killing, when the cells come in contact with the antibacterial surface of the monolithic column. The non-leaching nature of the antibacterial structure yields a lysate ready to use for PCR. The use of cross-linked poly(methyl methacrylate) X-PMMA as a substrate for the microfluidic channel that covalently bonds with the monolithic column through the unreacted C=C double bonds present on the surface of poly(methyl methacrylate-*co*-ethylene glycol dimethacrylate),poly(EGDMA-*co*-MMA), is demonstrated. This approach contributes to the mechanical stability of the biochip and eliminates the need of surface functionalization to create a bonding intermediate layer between the substrate and the PPM column.

The porous network was synthesized directly inside a microfluidic channel fabricated in a X-PMMA substrate by well-controlled, high-throughput laser micromachining. To validate both the mechanical-shear and contact-killing lysis (unprotected PPM column), a functional monomer contains a Boc protecting group was used. Thus, Bacterial cell suspension was flown into the protected PPM and the observed lysis was due to the mechanical-shear lysis. After removing the Boc protecting group with %85 phosphoric acid, an amphiphilic and cationic network structure reminiscent of 'synthetic mimics of antimicrobial peptides' (SMAMPs) was obtained and the cell lysis observed was due to both mechanical-shear and antibacterial contact-kill mechanisms. The antibacterial activity of the PPM columns was tested against Bacillus subtilis (B. subtilis) and Escherichia coli (E. coli) cells. Cell lysis was evidenced by DNA release, which was then amplified by off-chip PCR and confirmed by gel electrophoresis, to verify that the antibacterial monolithic columns did not interfere with the PCR process. The developed on-chip cell lysis does not require chemical and/or enzymatic reagents, power consumption, or complicated design and fabrication processes, which makes it an attractive on-chip lysis device that can be used in sample preparation for bio-genetics and point-of-care diagnostics.

2.1 Experimental

2.1.1 Materials

The chemical and biological materials used in this chapter are mentioned below:

Methyl methacrylate (MMA, 99%), butyl methacrylate (BuMA, 99 %), and ethylene glycol dimethacrylate (EGDMA, 98%) were purchased from Sigma-Aldrich (Oakville, ON Canada), and filtered over alumina prior to use to remove polymerization inhibitors. Dichloromethane (DCM, 99.9%, Chromasolv Plus), tetrahydrofuran (THF, 99.9%, Chromasolv Plus), and triethylamine (TEA, 99.5%) were also purchased from Sigma-Aldrich and were distilled prior to use. Di-tert-butyl dicarbonate (BOC_2O, $\geqslant$99%, reagent grade), ammonium chloride (NH_4Cl, $\geqslant$99.5%),

2-aminoethanol (ETA, ⩾99.5%), sodium sulfate (Na_2SO_4, ⩾99.0%, ACS reagent), chloroform-d ($CDCl_3$, 99.8 atom % D), citric acid (ACS reagent,⩾ 99.5%), potassium carbonate (K_2CO_3, 99.995%), sodium bicarbonate ($NaHCO_3$, ACS reagent, 99.7-100.3%), sodium chloride (NaCl, BioXtra, ⩾99.5% (AT)), aluminum oxide (Al_2O_3, type CG-20), benzoyl peroxide (BPO, 97%), N,N-diisopropylethylamine (DIPEA, 99% Reagent Plus), methacryloyl chloride (MACl, ⩾97% purum), 1-dodecanol (98%, reagent grade), cyclohexanol (99% Reagent Plus), 2,2-dimethoxy-2-phenylacetophenone (DMPAP, 99%) and methanol (⩾99.9% Chromasolv) were purchased from Sigma-Aldrich and used without further purification. 2-Aminoethyl methacrylate hydrochloride (AEMA-HCl, 95%) was purchased from Polysciences Inc. (Warrington, PA) and was used without further purification. Fumed silica (powder, 0.2-0.3 μm avg. part size), phosphoric acid (85%), 1,4-dioxane (anhydrous, 99.8%), trifluoroacetic acid (TFA, 99%) and potassium bromide (KBr, ACS reagent, ⩾99.0%) were purchased from Sigma-Aldrich and used as received. iTaq polymerase, 10X PCR buffer, and magnesium chloride were obtained from Bio-Rad. Primers, and dNTP mix (dATP, dCTP, dGTP and dTTP) were obtained from Sigma-Aldrich. Ethidium bromide (EtBr, UltraPure 10 mg/ml) was purchased from Life Technologies Inc. (Burlington, ON Canada). 100 bp DNA ladder was purchased from BioLabs (Ipswich, MA).

2.1.2 Microchip fabrication

The synthetic procedure of X-PMMA substrate is provided in Appendix A. Microfluidic channels were micromachined on the X-PMMA substrates with a 10.6 μm CO_2 laser engraving system (Universal Laser Systems, VLS2.30, Mississauga, ON Canada). In order to obtain an enclosed channel, another piece of the X-PMMA substrate in which two holes were drilled for the inlet and outlet was chemically bonded with the substrate hosting the microchannel. A thin layer of BuMA was applied between the two X-PMMA layers to enhance bonding between the two networks. Thermal bonding was achieved by placing the top and bottom substrates under pressure in a vise press and in a pre-heated oven at 130 °C for 30 min. Two

30G syringe needles were trimmed and placed over the inlet and outlet holes. They were set with epoxy glue mixed with fine fumed silica powder, to achieve a hard and stable adhesive layer.

2.1.3 Network fabrication and deprotection.

The composition used to prepare the antibacterial network was first investigated off-chip, by mixing 0.3 g of N-(tert-butoxycarbonyl)aminoethyl methacrylate (Boc-AEMA, 30 wt %), 0.025 g of BuMA (2.5 wt %), 0.175 g of EGDMA (17.5 wt %), 0.5 g of distilled THF (50 wt %), and 5 mg of DMPAP (1 wt % with respect to the monomers). The synthetic procedures of N-(tert-butoxycarbonyl)aminoethyl methacrylate (Boc-EAMA) and N-(tert-Butoxycarbonyl)ethanolamine (Boc-EA) are provided in Appendix A. The mixture was sonicated for 45 min., to help dissolve the crystallized Boc-AEMA, and then stirred for 30 min. to achieve complete dissolution. The mixture was used to form a thin network on a flat 20% X-PMMA substrate by photoinitiated polymerization under UV irradiation. The substrate with the grafted film was then washed with ethanol and dried under nitrogen for 5 min., immersed in a beaker containing 25 mL of phosphoric acid with stirring for 3 h for deprotection, washed with ethanol, and dried for 10 min.

2.1.4 Monolith formation and characterization

A mixture consisting of Boc-AEMA (15.6 wt %), BuMA (1.3 wt %), EGDMA (9.1 wt %), 1-dodecanol (52.4 wt %), cyclohexanol (21.6 wt %), and DMPAP (1 wt % with respect to the monomers) was introduced into the microchannel, and polymerization was triggered by irradiation for 15 min The microchannel was then flipped 180 degrees and left under the UV source for 15 min. at 365 nm UV wavelength and 200 mJ/cm^2 energy in a cabinet containing a UV lamp (ENF-260C, Spectronics Corp. Westbury, NY) as shown in Sch. 2.1. Fig. 2.1 A and B show preliminary fabricated microfluidic chips with and without PPM columns, respectively. Two 30G syringe needles were trimmed and placed over the inlet and

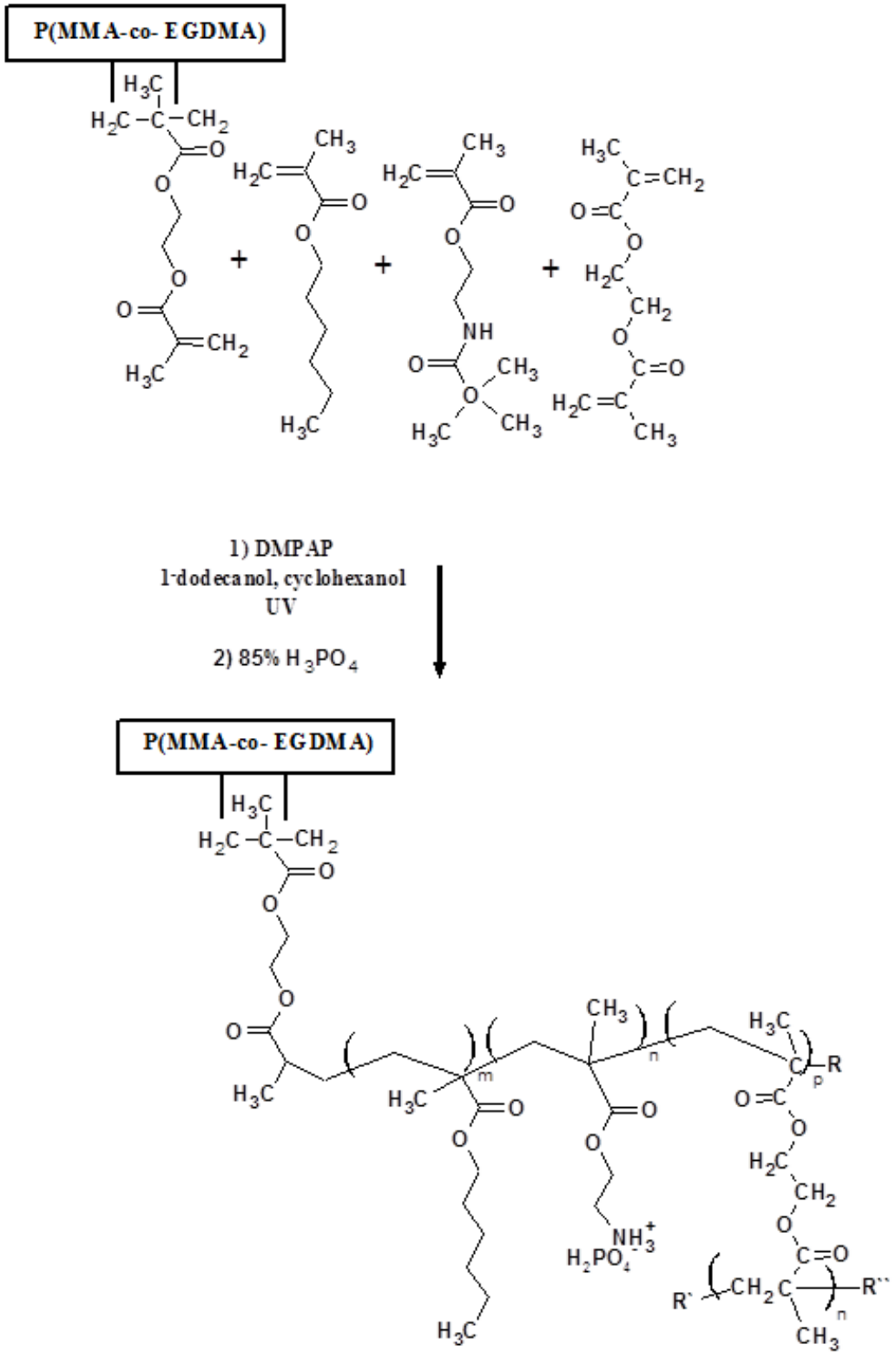

Scheme 2.1: Reactions for the formation of the monolith column on 20% X-PMMA surface, and removal of the Boc protecting group with 85% phosphoric acid.

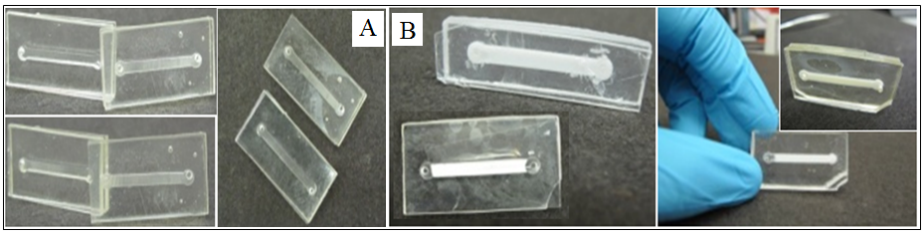

Figure 2.1: preliminary fabricated microfluidic chips with and without PPM columns.

outlet holes. They were set with epoxy glue mixed with fine fumed silica powder, to achieve a hard and stable adhesive layer. Using a 'Pico Plus Syringe Pump' (Harvard apparatus, Holliston, MA) the microchannel was flushed with ethanol to remove the unreacted monomers and the porogens.

Linear PMMA was first considered as a substrate for the microfluidic channels, but it cracked and gradually dissolved when exposed to the monomers and solvents as shown in Fig. 2.2. To overcome this obstacle cross-linked PMMA was synthesized and used instead of linear PMMA. This approach also ensures that unreacted double bonds on the cross-linked surface improve adhesion between the PPM column and the substrate. Attenuated total reflectance-Fourier transform infrared spectroscopy (ATR-FTIR) was used to confirm the presence of dangling C=C double bonds on the surface of the cross-linked PMMA. Monolith pressure tests were conducted to evaluate the bonding strength between the monolith column and the substrate. To that end the microfluidic chip containing the PPM column was connected to a compressed N_2 cylinder that was used to pump ethanol through the monolithic column. The pressure was increased in 10 psi increments every 5 min. to determine the pressure at which the monolithic column started to debond from the substrate.

Images of the monoliths were obtained with a Hitachi SU-70 scanning electron microscope (SEM) (Hitachi High-Technologies Corporation, Tokyo, Japan) at an acceleration voltage of 10 kV. The SEM samples were prepared by immersing the microchannel hosting the PPM column into liquid nitrogen, and then cutting perpendicularly to the monolith-filled X-PMMA channel. Gold was sputtered onto the samples prior to SEM imaging.

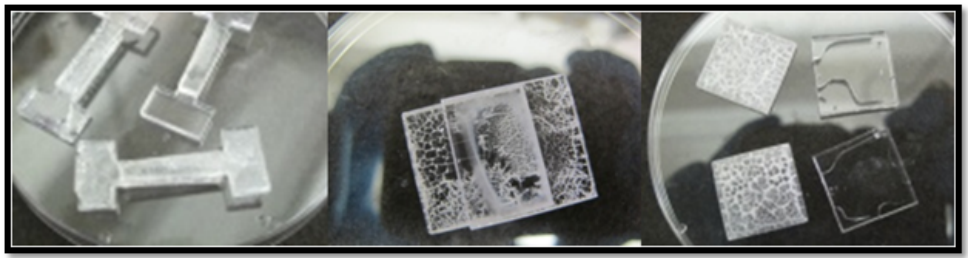

Figure 2.2: Sever cracks on the linear PMMA surface after applying the monolith mixture.

2.1.5 Activation of the antibacterial PPM via deprotection

Deprotection of the Boc-AEMA units was achieved by flowing 250 μL of 85% phosphoric acid through the PPM column before flushing with ethanol and deionized (DI) water to remove acid residues. After purging, the PPM column was opened by cutting vertically through the monolith-filled X-PMMA channel with an electrical saw. The column material was then removed by scraping and ground into a fine powder, mixed with KBr in a 1:30 weight ratio, and dried in a vacuum oven at 60°C overnight. KBr pellets were prepared for analysis by pressing the powder in a dye at 10 kpsi for 3 min. on a Carver 3851 Press (Thomas Scientific, Swedesboro, NJ). To validate the deprotection process, Fourier transform infrared (FT-IR) spectra were acquired at room temperature on a Bruker Tensor 27 spectrometer (Bruker Optics, Milton, ON Canada) by averaging 64 scans recorded at a rate of 1 scan/s. The wavenumber region scanned was between 400 and 4000 cm^{-1}.

2.1.6 Antibacterial activity

The antibacterial properties of the non-porous network and the micro-porous monolithic column were investigated by several techniques. The same composition of the functional and cross-linking monomers was used in both the nonporous network and the porous column. E. coli and B. subtilis bacterial cells were selected to evaluate the cell lysis ability of the antibacterial PPM column on gram-negative and gram-positive bacterial cells, respectively.

2.1.6.1 Cell samples.

E. coli and B. subtilis cells were grown in lysogeny broth (LB) in an incubator at 37°C, shaking at 180 RPM and left overnight. The bacterial cells were then washed twice with DI water and then re-suspended in phosphate buffered saline (PBS) before the experiments. The stock cell concentration was adjusted with an Ultrospec 2100 pro UV/Visible spectrophotometer (Biochrom Ltd., Cambridge, UK), to prove an optical density (OD) value of 0.6 at 600 nm ($OD_{600} = 0.6$) for the bacteria sample. The cell solutions were then diluted as needed in different experiments.

2.1.6.2 Non-porous polymeric network.

The antibacterial property of the deprotected network were evaluated by the LIVE/DEAD Cell Viability Assay (L7012, Molecular Probe, Burlington, ON Canada), used to directly monitor cell viability. The assay uses two fluorescent nucleic acid stains, SYTO 9 (green) and propidium iodide (PI; red). The SYTO 9 stain penetrates both healthy bacterial cells (with intact membranes) and non-healthy cells (with disintegrated cell membrane); it therefore labels both live and dead bacteria. Conversely PI infiltrates only cells with disintegrated membranes, thus decreasing the SYTO 9 fluorescence intensity. Consequently, cells with healthy membranes fluoresce green while cells with disintegrated membranes fluoresce red, while the background remains virtually non-fluorescent. Images were captured on a fluorescence microscope (Nikon Eclipse E600FN upright, Nikon Canada Inc., Mississauga, ON Canada) with a digital camera (Nikon Photometrics Coolsnap EZ 12-Bit Monochrome Cooled CCD and NIS-ELEMENTS IMAGING Software) through a dual-band filter, so that bacteria with healthy and disintegrated cell membranes could be visualized simultaneously. SYTO 9 and PI (0.15 μL of each) were mixed on a vortex mixer, 100 μL of bacteria suspension were added and mixed, and the stock mixture was incubated for 15 min. at 37 °C. A 10 μL of bacterial suspension-stains mixture was dropped over the non-porous network and covered with a thin microscope slide.

The sandwiched layers were left in contact under the microscope, and fluorescent microscopic images were recorded at zero and after 300 sec of contact time.

2.1.7 Cell Lysis efficiency of PPM column.

Cell lysis was confirmed via the Ethidium Bromide (EtBr) Intercalation Assay as an indicator of DNA presence in the cell lysate. When EtBr is exposed to ultraviolet light, it fluoresces with an orange color which intensifies after intercalation in DNA. This assay thus relates the intensity of EtBr fluorescence to the DNA concentration in the cell lysate. The fluorescence intensity of EtBr after intercalation in the DNA released from the microchannel hosting the porous and antibacterial monolithic column was quantified with a Quanta-Master 4 spectrofluorometer (Photon Technology International, London, ON). A 0.1 mL aliquot of bacterial cells was suspended in PBS buffer (E. coli and B. subtilis at OD_{600} = 0.25) and pumped through the PPM column before and after deprotection at a flow rate of 1 μL/min, and the cell lysate was collected at the outlet. In this assay 0.02 mL aliquots of E. coli and B. subtilis lysates were each added to a spectrophotometer cuvette containing 0.380 mL of DI water and 0.03 mL of EtBr from a stock solution with a concentration of 0.4 mg/L.

2.1.7.1 PCR reagents experimental setup.

Furthermore, to validate the DNA released as a result of cell lysis and to ensure that the PPM column did not leach any polymerase chain reaction (PCR) inhibitors, a gene of the DNA present in the cell lysate was amplified by PCR. The PCR reaction was performed in a T100 Thermal Cycler (Bio-RD, Montreal, QC Canada) in a 25 μL volume consisting of 300 nM of forward primer, 300 nM of reverse primer, 200 μM of dNTPs, 3.5 mM of magnesium chloride, 0.625 U of iTaq polymerase, 2.5 μL of 10X PCR buffer, and 5 μL of the crude lysate collected at the outlet of the microfluidic channel [41]. The structure of the E. coli [58] and B. subtilis [59] primers used in the PCR reaction is provided in Table 2.1. The PCR tubes were

first preheated and incubated at 95°C for 3 min., and then the PCR thermal cycler was programed to run for 30 cycles with 95°C for 30 sec., 63°C for 1 min., and 73°C for 1 min.

2.1.7.2 gel electrophoresis

The PCR products were analyzed by gel electrophoresis using Bio-Rad gel electrophoresis apparatus on 1.2% agarose gel using a DC voltage of 85 V and a running time of 30 min. The gel was subsequently detached from the apparatus cavity and was imaged with a Bio-Rad Doc XR imagining system.

Table 2.1: Primers used in PCR experiments

Bacteria	Primer direction	Primer sequence
E. coli	forward	5́-AAAACGGCAAGAAAAAGCAG-3́
	reverse	5́-ACGCGTGGTTACAGTCTTGCG-3́
B. subtilis	forward	5̀-AAGAGTTTGATCATGGCTCAG-3̀
	reverse	5̀-AGGAGGTGATCCAACCGCA-3̀

2.2 Results and discussion

2.2.1 Monolith formation and bonding to the substrate

To form the monoliths, two functional monomers: Boc-AEMA and BuMA, were copolymerized with a third cross-linking monomer in the presence of a porogenic solvent mixture. The functional monomers play a key role in the final product, as they introduce the antibacterial component in the structure. The cross-linking monomer is also necessary to form a network, by contributing to the mechanical stability of the monolith. To form a porous network and also control the pore size, porogenic solvents were used. Since Boc-AEMA was synthesized in the crystallized form, the monomer mixture was sonicated and stirred to form a homogeneous solution prior to polymerization. In order to achieve fast polymerization and complete monomer conversion within approximately 15 min., DMPAP was selected as photoinitiator due to its relatively short half-life time ($t^{1/2}$) or high decomposition rate

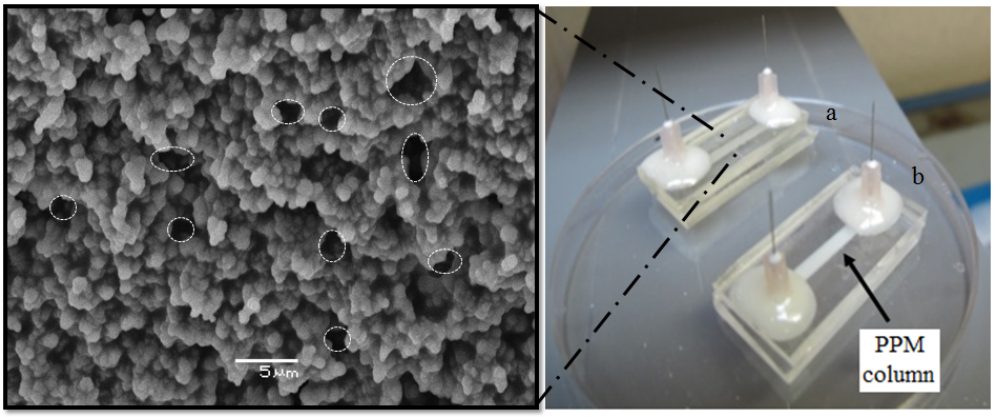

Figure 2.3: Microfluidic chip fabricated by laser micromachining on a 20% X-PMMA substrate filled with a monolith column (right) and SEM image of the PPM column packing (left).

(k_d) [53]. Fig. 2.3 (left) provides a SEM image for the PPM column packing, showing some pores circled and (right) an overall view of the microchip consisting of the microfluidic channel laser-micromachined onto a 20% X-PMMA substrate hosting the monolithic column. To facilitate the tube connections between the microfluidic channel and the bacterial suspension reservoir, a trimmed 30G syringe needles were set over the inlet and outlet of the microfluidic channel and bonded to the surface with a mixture of epoxy glue and fumed silica.

The unreacted double bonds on the surface of the cross-linked PMMA substrate allowed covalent bonding with the monolith material and contributed to the mechanical stability of the PPM column within the microfluidic channel, by decreasing the possibility of debonding leading to the creation of voids along the monolithic column. Surface characterization of the cross-linked PMMA sheets was performed by ATR-FTIR to confirm the presence of unreacted carbon-carbon double bonds upon copolymerization of MMA and EGDMA; the spectra obtained are shown in Fig. 2.4. The absorption band at 1637 cm^{-1} is characteristic for the $C{=}CH_2$ stretching vibration mode vicinal to an ester group [60]. Also visible is the $C{=}CH_2$ out-of-plane bending vibration mode 16 at 949 cm^{-1}. After normalization of the spectra to the C=O stretching band 1722 cm^{-1}, the C=C absorbance was found to increase slowly with the cross-linker content, as illustrated in the inset of

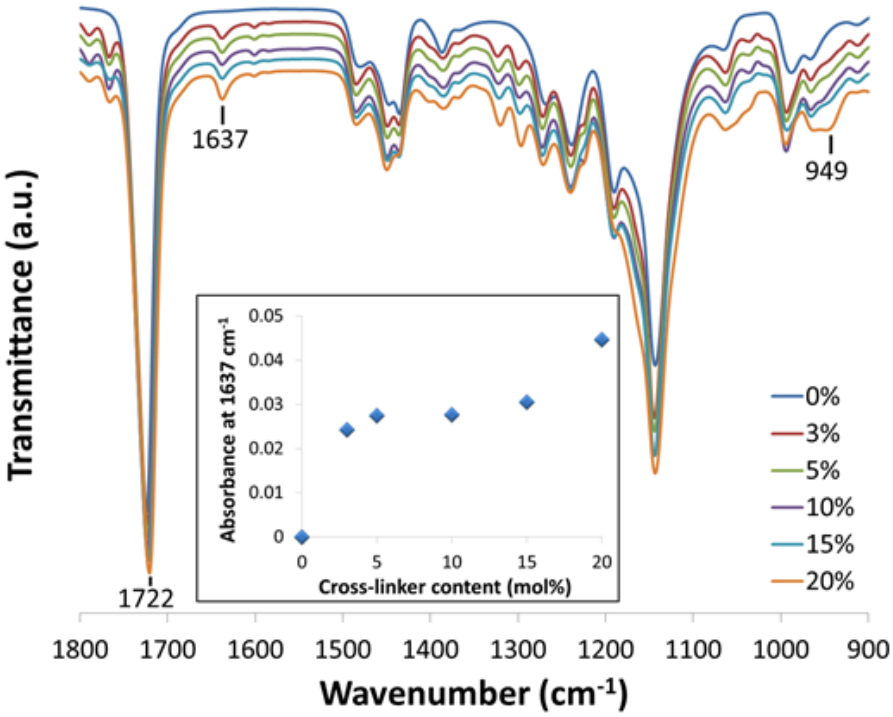

Figure 2.4: ATR-FTIR spectra for native and cross-linked PMMA samples with cross-linker contents ranging from 3 to 20 mol%. The vibrational modes at 1637 and 949 cm^{-1} correspond to CH_2 stretching and out-of-plan bending, respectively. Inset: Absorbance at 1637 cm^{-1} for the different X-PMMA samples.

Fig. 2.4. In contrast to native PMMA, the samples prepared with up to 15 mol% EGDMA presented evidence for unreacted double bonds at the surface, becoming even more obvious for the sample containing 20 mol% of EGDMA. To confirm and quantify bonding between the PPM column and the cross-linked PMMA substrate, a pressure test was conducted. Table 2.2 summarizes the pressure withstood by the column before voids appeared along the channel (i.e. between the monolithic column and the substrate), referred to as 'void pressure', at 3%, 5%, 10%, 15% and 20% cross-linker content. The results in Table 2.2 are consistent with improved bonding or anchoring of the column material as the cross-linking level of the substrate increased.

Table 2.2: Debonding pressure of the column from the substrate for different cross-linking levels.

Cross-linker (mole %)	Void pressure (psi)
3	50
5	60
10	80
15	100
20	150

2.2.2 *t*-Boc group deprotection

Several activation methods were investigated to optimize the antibacterial activity of the PPM column. A mixture of hydrochloric acid and dioxane (1:2 ratio) was first used, but the mixture dissolved the plastic tip of the syringe needle and degraded the connections tubes, which made it unsatisfactory for deprotecting the amine group in the Boc-AEMA monomer. Trifluoroacetic acid (TFA) was also investigated but it was likewise aggressive on the syringe, the needle, and the tubes and it slowly eroded the PPM column; therefore this deprotection method was likewise discarded early on. Phosphoric acid was finally preferred to deprotect the Boc-AEMA units. Deprotection was successfully achieved by flowing 85%phosphoric acid through the monolithic column, as evidenced by FT-IR analysis shown in Fig. A1 of the Appendix A.

2.2.3 Antibacterial activity of the non-porous network

Bacteria viability was monitored by the double staining technique described in Section 2.1.7.2. The green fluorescence is gradually replaced with red fluorescence in these experiments, as shown in Fig. 2.5A and B, providing clear evidence for membrane disintegration. In contrast to the deprotected network, the protected network did not display any lysis ability, as shown in Fig. 2.5C and D. The red and green fluorescence intensities were recorded for up to 300 sec. as shown in Fig. 2.6. For the deprotected network, the green and red intensities decreased and increased with time, respectively, as illustrated in Fig. 2.6, reflecting the fact that the cell membranes slowly became permeable, thus allowing the penetration

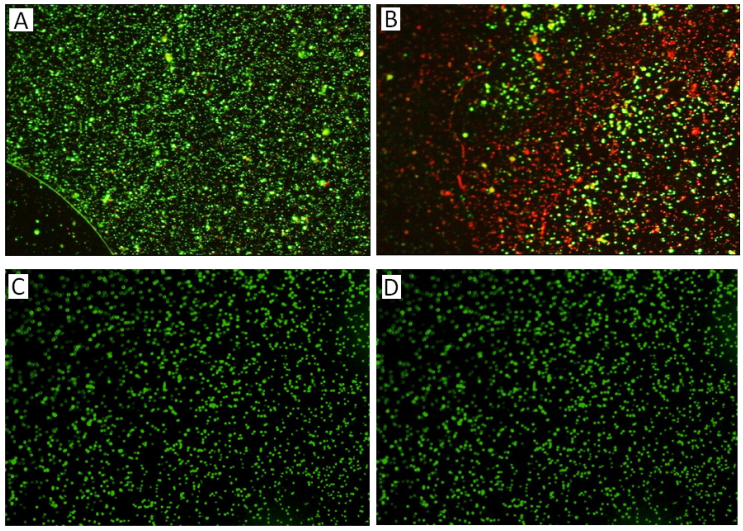

Figure 2.5: Fluorescence intensities for E. coli suspended in PBS buffer and stained with Live/Dead dye in contact with (A) the deprotected antibacterial non-porous network at time zero and (B) after 300 sec, and in contact with (C) the protected non-porous network at time zero and (D) after 300 sec.

of propidium iodide and reducing the fluorescence intensity for SYTO 9. This provides clear evidence that the non-porous network became antibacterial once the t-Boc protecting group was removed. For the protected column, in contrast, the green and red fluorescence intensities remained almost constant as shown in Fig. 2.6, reflecting the fact that protected network does not show any antibacterial activity.

2.2.4 Cell Lysis efficiency of the PPM column

To validate semi-quantitatively the DNA released after lysing the bacterial cells by flowing them through the antibacterial porous medium of the PPM column, ethidium bromide was used as an indicator of DNA presence in the crude cell lysate. Fig. 2.7 illustrates the effect of the released DNA on the EtBr fluorescence intensity after flowing E. coli and B. subtilis bacterial cells through the PPM column before and after deprotection. The figure clearly shows that the fluorescence intensity of EtBr increased when adding the lysate collected after flowing the bacterial cells through the narrow porous channel of the monolithic column, even for the packing

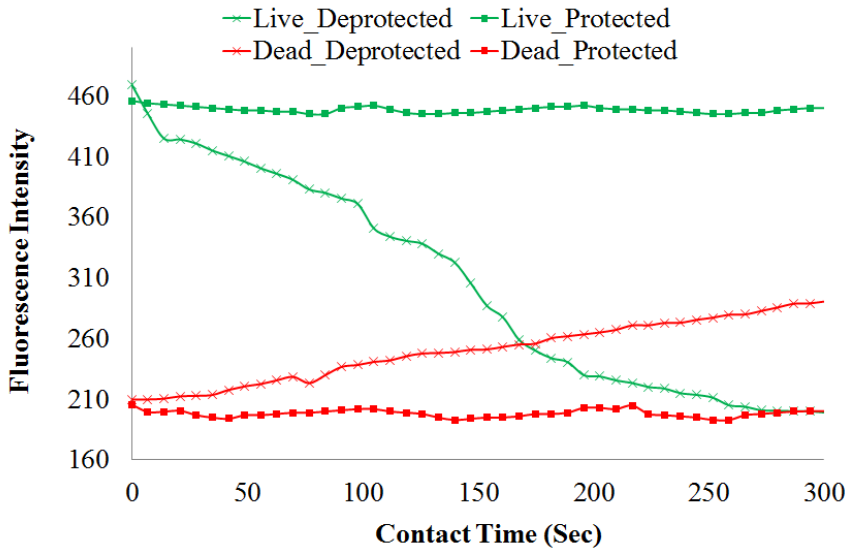

Figure 2.6: Green (Live) and red (Dead) stain intensities with respect to contact time before and after removing the Boc protecting group.

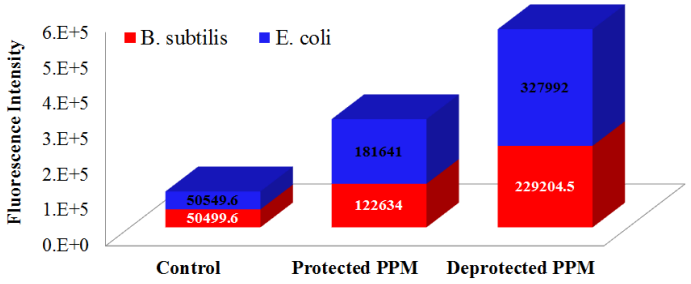

Figure 2.7: Fluorescence intensity of EtBr after adding E. coli (blue) and B. subtilis (red) cells suspended in PBS buffer (control), the lysate of E. coli and B. subtilis suspensions flown through the PPM column before (Protected PPM) and after deprotection (Deprotected PPM).

material in its protected form, confirming that the bacterial cells were partly lysed through shearing and their DNA was released. However it can also be seen that the fluorescence intensity of EtBr further increased for the cell lysate collected after flowing the bacterial cells through the monolithic column in its deprotected form, thus confirming that an incremental amount of cell lysis was achieved by physical contact of the cells with the antibacterial surface, resulting in the release of more DNA.

2.2.5 PCR and gel electrophoresis

Moreover, a gene of the DNA released from both the lysed E. coli and B. subtilis bacterial cells was amplified by PCR and qualitatively validated by gel electrophoresis. Fig. 2.8 shows the gel electrophoresis analysis results for the PCR products of B. subtilis bacterial cells that were not flown through the porous column (column 2), B. subtilis lysate collected at the outlet of the deprotected PPM column (column 3), E. coli lysate collected at the outlet of the deprotected monolithic column before (column 4) and after (column 5) filtration using a 0.2 μm filter, and an E. coli bacterial suspension that was not flown through the porous column (column 6). Fig. 2.8 shows no detectable amount of DNA at the PCR output for the E. coli and B. subtilis samples that were not flown into the monolithic column, which confirms that the bacterial cells had intact cell membranes before passing through the antibacterial monolithic columns. On the other hand, DNA is clearly detected at the PCR output for the E. coli and B. subtilis samples that were flown through the deprotected PPM columns, which confirms that the membranes of bacterial cells were damaged and disintegrated by flowing through the PPM column. It can also be observed that filtration of the cells before running the PCR did not affect the amplification procedure. This shows that the porous column lysed the bacterial cells and filtered the cell debris and any intact cells left in the samples.

2.3 Conclusions

It has been demonstrated that the activated antibacterial porous columns prepared have the ability to effectively lyse E. coli and B. subtilis bacterial cells, and to produce cell lysate that is ready to use in PCR experiments without further cleaning or filtration. The combination of shear degradation and antibacterial properties was clearly beneficial to achieve cell lysis, which was evidenced by the release of DNA. Cell lysis was confirmed by several techniques, namely the LIVE/DEAD Cell Viability Assay that was used to directly monitor cell viability on the nonporous network, the Ethidium Bromide Intercalation Assay utilizing spectrofluorometry,

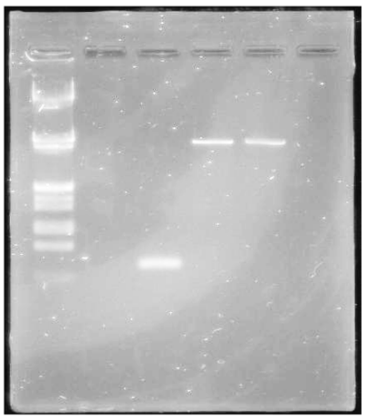

Figure 2.8: Gel electrophoresis analysis of PCR output for unlysed (column 2) and lysed (through PPM) (column 3) B. subtilis cells, filtered (column 4) and non-filtered (column 5) lysed E. coli and unlysed E. coli (column 6). Column 1 is for a 100 bp DNA ladder.

relating the DNA concentration to the increase in fluorescence intensity for EtBr, as well as by gel electrophoresis to analyze and validate the PCR amplification test. The usefulness of X-PMMA as a substrate on which the microfluidic channel could be laser-micromachined without further surface functionalization was also demonstrated in this work. The PPM formed on 20% X-PMMA could withstand 150 psi before voids started to appear across the monolithic column.

Chapter 3

Optimized Boc-Protected Antibacterial PPM

The scope of the work done in Chapter 2 was expanded in this chapter, to enhance the cell lysis efficiency, by tuning the hydrophobic-hydrophilic balance of the PPM columns. The optimal flow rate, at which the bacterial cell walls are sufficiently mechanically sheared through the porous medium of the PPM column to disrupt the cell membrane by physical contact with the antibacterial polymeric biocide covering the pore surface, was also determined at cell concentration of 10^5 CFU/ml. The usefulness of this new technique was also further confirmed in terms of reusability of the monolithic columns, by demonstrating that the PPM columns show no evidence of physical damage, DNA carryover, and suffer from no significant performance loss when used in 20 successive lysis cycles when they were back-flushed between cycles. The biochips efficiently lysed both gram-positive (Enterococcus saccharolyticus and Bacillus subtilis) and gram-negative (Escherichia coli and Pseudomonas fluorescens) bacteria, producing cell lysates containing DNA that was amplified by off-chip PCR without the need for purification, which proves that the monoliths do not leach PCR inhibitors making them unsuitable for sample preparation. The lysis efficiency of the biochips was better than for off-chip chemical, mechanical, and thermal lysis techniques. The biochip also acts as a filter that isolates cell debris and allows PCR-amplifiable DNA to pass through. Contact-killing mechanism showed higher

lysis efficiency than mechanical shearing mechanism. The cell lysis efficiency of the developed antibacterial PPM was verified at different cell concentration ranged from 10^2 to 10^5 CFU/ml.

3.1 Experimental

3.1.1 Materials

The chemical and biological materials used in this chapter are mentioned below:

Methyl methacrylate (MMA, 99 %), butyl methacrylate (BuMA, 99 %), ethylene glycol dimethacrylate (EGDMA, 98 %), and 1,6-hexanediol dimethacrylate (1,6-HDDMA, $\geqslant$90%) were all purchased from Sigma-Aldrich (Oakville, ON Canada), and passed through alumina columns to remove polymerization inhibitors. 1-Dodecanol (98 %, reagent grade), cyclohexanol (99 % Reagent Plus), methanol ($\geqslant$99.9 % Chromasolv), 2,2-dimethoxy-2-phenylacetophenone (DMPAP, 99 %), fumed silica (powder, 0.2-0.3 μm average particle size), phosphoric acid (85%), ethylenediaminetetraacetic acid (EDTA, BioUltra, anhydrous, $\geqslant$99%), and lysozyme (lyophilized powder, protein $\geqslant$90 %) were also purchased from Sigma-Aldrich but were used without further purification. iTaq polymerase, 10X PCR buffer and magnesium chloride were obtained from Bio-Rad.(Montereal, QC Canada). Primers and dNTP mix (dATP, dCTP, dGTP and dTTP) were obtained from Sigma-Aldrich. Ethidium bromide (UltraPure 10 mg/mL, EtBr) and UltraPur Dithiothreitol (DTT, Cleland's reagent) were purchased from Life Technologies Inc. (Burlington, ON Canada). A 1k bp DNA ladder was purchased from BioLabs (Ipswich, MA).

3.1.2 Microchip fabrication

The microfluidic channels were laser-micromachined within 20% X-PMMA substrates with a 10.6 μm CO_2 laser engraving system (Universal Laser Systems, VLS2.30). The synthesis procedure for X-PMMA was described by Aly Saad Aly *et al.* [63]. The channels were 2.5 cm in length, 500 μm wide, and 350 μm deep. To

obtain an enclosed channel another piece of the X-PMMA substrate, with two holes drilled for the inlet and outlet, was chemically bonded with the substrate hosting the microchannel by applying a thin layer of BuMA between the two X-PMMA layers, and placing the top and bottom substrates in a hot press under pressure (130 °C, 10^3 psi) for 30 min. (Heated Press 4386, Carver, Wabash, IN). Two 30G syringe needles were trimmed and placed over the inlet and outlet holes, and set with epoxy glue mixed with fine fumed silica powder to achieve a hard and stable adhesive layer.

3.1.3 Monolith formation and antibacterial activation

Mixtures with compositions as summarized in Table 3.1 were sonicated for 30 min. to help dissolve the crystalline Boc-AEMA, stirred for 30 min under N_2 flow, and then introduced into the microchannel. Polymerization was triggered by irradiation of the substrate for 15 min. with a 365 nm UV source in a cabinet containing a UV lamp (200 mJ/cm^2 intensity, ENF-260C, Spectronics Corp. Westbury, NY). The substrate was then turned over and irradiated with the UV source on the other side

Table 3.1: Composition of the solutions used to form the eleven PPMs (in wt. %).[a]

	Monomer	Monomer	Cross-linker	Cross-linker
PPM	BuMA	Boc-AEMA[b]	EGDMA	1,6-HDDMA
1	1.3	15.6	9.1	-
2	1.3	15.6	8.1	1.0
3	1.3	15.6	7.1	2.0
4	1.3	15.6	6.1	3.0
5	1.3	15.6	5.1	4.0
6	1.3	15.6	4.1	5.0
7	1.3	15.6	3.6	5.5
8	1.3	15.6	3.1	6.0
9	1.0	15.9	3.1	6.0
10	0.5	16.4	3.1	6.0
11	-	16.9	3.1	6.0

[a] All the reactions also included 21.5% cyclohexanol and 52.3% 1-dodecanol as porogenic solvents, and 0.2% DMPAP as photoinitiator.

[b] N-(tert-butyloxycarbonyl)aminoethyl methacrylate (Boc-AEMA) synthesis as described by Aly Saad Aly *et al.* [63].

for 15 min longer. Using a 'Pico Plus Syringe Pump' (Harvard apparatus, Holliston, MA), the microchannel was then flushed with ethanol to remove the porogens and any unreacted monomer.

Activation of the antibacterial monolithic column was achieved through deprotection of the Boc-AEMA units by flowing 250 μL of 85% phosphoric acid through the monolith, before flushing with 250 μL of ethanol and 250 μL of deionized (DI) water to remove acid residues [63]. The deprotection process was validated by acquiring Fourier transform infrared spectroscopy (FT-IR) spectra for the porous column material [63].

Images for the monoliths were obtained with a Hitachi SU-70 scanning electron microscope (SEM) (Hitachi High-Technologies Corporation, Tokyo, Japan) at an acceleration voltage of 10 kV. The SEM samples were prepared by immersing the microchannel hosting the protected PPM column into liquid nitrogen, and then cutting perpendicularly to the monolith-filled X-PMMA channel. To create an electrically conductive layer, gold was sputtered onto the samples prior to SEM imaging. The pore size, surface area and porosity of selected protected PPM were determined by mercury intrusion porosimetry using a Quantachrome Poremaster 60 device (Quantachrome Instruments, Boynton Beach, FL). The PPM were freeze-dried under vacuum and a sample of approximately 1 cm^3 was put into a sample holder cell to force mercury, a non-reactive and non-wetting liquid, into the pores. The relationship between the pressure applied and the diameter of the pores into which the mercury intruded was determined by the Washburn equation [33].

3.1.4 Bacterial culture

E. coli DH5α and P. fluorescens (ATCC 13525) were served as gram-negative test bacterial strains, while B. subtilis 168 and E. saccharolyticus (ATCC 43076) were used as gram-positive strains. E. coli DH5α and B. subtilis 168 were donated by Dr. Michael Palmer (Chemistry Department, University of Waterloo). E. saccharolyticus and P. fluorescens were purchased from American Type Culture Collection (ATCC, Manassas, VA, catalog numbers: ATCC 43076 and ATCC 13525, respec-

tively). Details about bacterial culture and the growth conditions are provided in Appendix B.

3.1.5 Bacterial cell lysis

Samples of 2.5 mL each of the four bacterial cultures at concentration of 1.5 $\times 10^5$, 2 $\times 10^5$, 1.7$\times 10^5$ and 1.9 $\times 10^5$ CFU/ml for E. coli, B. subtilis, P. fluorescens and E. saccharolyticus, respectively, were pelleted at a relative centrifugal force (RCF) of 25513 (13k RPM) for 3 min., washed twice with DI water, and then re-suspended in phosphate-buffered saline (PBS).

3.1.5.1 On-chip cell lysis.

A 110 μL aliquot of the bacterial suspensions was pumped at a flow rate of 1.5 μL/min through each of the monoliths prepared as described in Table 3.1, after deprotection, and the cell lysate was collected at the biochip outlet to investigate the influence of the hydrophobic-hydrophilic balance of the antibacterial monoliths on the cell lysis efficiency. The bacterial suspension was also pumped through monolith (11) before and after deprotection, at flow rates starting at 0.1 μL/min, and then increased in 0.4 μL/min increments after pumping 50 μL at each flow rate, to examine the effect of the flow rate on the cell lysis efficiency of the biochips. In another series of experiments, freshly synthesized PPM were also used at each flow rate to ensure that the PPM started in the same conditions for each flow rate.

To investigate the reusability of the biochips, a biochip containing a deprotected PPM column was reused 35 times and the cell lysis efficiency was evaluated for each cycle. The E. coli bacteria suspended in PBS used in this test were passed through the antibacterial deprotected monolith with the optimal monolith composition and at the optimal flow rate. Two different column washing procedures were compared for their influence on the cell lysis efficiency. In the first procedure (PBS wash), the monolith was back-flushed after each run with 20 μL of PBS buffer; after ten runs it was also washed with 25 μL of 85% phosphoric acid and then with 20 μL

of PBS. In the second procedure (Acid wash), the monolith was back-flushed after each use with 25 μL of 85% phosphoric acid and then with 20 μL of PBS buffer. To investigate possible of DNA carryover, the PBS recovered from the microfluidic channel in the back-flush cycle was mixed with EtBr and any changes in fluorescence intensity were recorded. Two control samples were used in these experiments: a control containing 400 μL of DI water and a second one containing 30 μL of EtBr (from a stock solution with a concentration of 0.4 mg/L), 380 μL of DI water and 20 μL of PBS.

3.1.5.2 Off-chip cell lysis.

Aliquots of the bacterial suspensions (300 μL) were pipetted into three centrifuge tubes. For thermal cell lysis, one tube was immersed in a 90 °C water bath for three min and in a dry ice/acetone bath for three more min to create a thermal shock. This freeze-thaw cycle was repeated three times.

For mechanical cell lysis, the Eppendorf tube was placed in a beaker with cold water and a sonicator probe (Q500 Sonicator, 500 Watt) was introduced into the beaker. The sonicator was operated in the continuous mode and the amplitude was gradually increased from 0 to 9 at 20% power continuously over 1 min. The magnitude was turned back to zero for 30 seconds, the cold water was gently stirred to avoid generating a hot spot, and the amplitude was gradually increased to sonicate again for 1 min. This process was continued for 8 min.

For chemical cell lysis, 15 μL aliquots of FastBreak cell lysis reagent, 10X (V8571, Promega, Madison, WI), and 10 μL of DTT were added to the centrifuge tube (the bacteria had been pelleted and then re-suspended in 75 μL of PBS buffer to compensate the dilution caused by adding FastBreak and DTT, and to consistently use a 100 μL total volume), and then stirred for 15 min at room temperature on a vortex mixer, since adequate mixing was necessary to ensure complete lysis. For gram-positive bacteria the bacterial suspension was pelleted, suspended in 54 μL of EDTA, 6 μL of a 10 mg/mL lysozyme solution were added, and the mixture was incubated at 37 °C for 60 min. Then 15 μL of FastBreak and 10 μL of DTT

were added to the enzymatically treated sample, which was vigorously stirred for 20 min at room temperature on a vortex mixer (15 μL of PBS buffer were then added to obtain a total volume of 100 μL).

3.1.6 Cell lysis efficiency

The bacterial cell lysates collected at the outlet of the biochips described in Table 3.1 were analyzed to study the influence of the hydrophobic-hydrophilic balance and the flow rate on the cell lysis efficiency of the monoliths by the methods described below.

3.1.6.1 DNA detection by fluorometry.

The ethidium bromide (EtBr) intercalation assay was used as an indicator of the presence of DNA in the cell lysate. A 20 μL aliquot of the bacterial cell lysate was added to a spectrofluorometer cuvette containing 380 μL of DI water and 30 μL of EtBr from a stock solution with a concentration of 0.4 mg/L, and the fluorescence intensity of EtBr was measured at a wavelength of 595 nm measured on a Quanta-Master 4 spectrofluorometer (Photon Technology International, London, ON Canada). The control sample did not contain bacterial cell lysate.

3.1.6.2 DNA concentration by UV-Vis spectrophotometry.

A 4 μL aliquot of PBS buffer was pipetted onto the end of a fiber optic cable (receiving fiber) of a UV-Vis Spectrophotometer NanoDrop 2000c (Thermo Scientific, Mississauga, ON Canada) to serve as blank (reference). Another cable was brought into contact with the sample to connect the sample with the fiber optic ends. Then a 4 μL sample of the E. coli DH5α, B. subtilis 168, P. fluorescens (ATCC 13525), or E. saccharolyticus (ATCC 43076) bacterial cell lysate was separately pipetted onto the receiving fiber, to measure the DNA concentration in the cell lysate after flowing the cell suspension through both the protected and deprotected PPMs. Ash *et al.* reported detection limits of 1.0 ng/μL and 0.90 ng/μL for DNA and RNA,

respectively, and a linear dynamic range of 1 - 15,000 ng/μL for DNA when using a NanoDrop 2000/2000c spectrophotometer [65]. The concentrations used in this work are therefore within the linear dynamic range and the limit of detection of that instrument.

3.1.6.3 PCR reagents and experimental setup.

The PCR reaction was performed in a T100 Thermal Cycler (Bio-Rad, Montreal, QC Canada) in a 25 μL volume consisting of 300 nM of forward primer, 300 nM of reverse primer, 200 μM of dNTPs, 3.5 mM of magnesium chloride, 0.625 U of iTaq polymerase, 2.5 μL of 10X PCR buffer, and 200 ng of DNA present in the crude cell lysate collected at the outlet of the biochip. More details about the primers structure (Table B2) and the PCR cycles are provided in the Appendix B.

3.1.6.4 Gel electrophoresis.

A Bio-Rad gel electrophoresis apparatus served to analyze the PCR products on 1.2% agarose gel, using a DC voltage of 85 V and an operating time period of 30 min. The gel was subsequently detached from the apparatus cavity and imaged with a Bio-Rad Doc XR imaging system.

3.2 Results and discussion

An illustration of the lab-on-a-chip experimental setup and the cell lysis evaluation techniques is provided in Fig. B1 of the Appendix B.

3.2.1 Influence of the hydrophobic-hydrophilic balance

It was previously determined that the hydrophobic-hydrophilic balance is a critical parameter controlling the activity of antibacterial polymers (SMAMPs) [75]. Thus the effect of varying the amphipathic nature of the antibacterial monoliths on their cell lysis efficiency was investigated, by changing the proportions of the hydrophobic (BuMA) and the hydrophilic amine-containing (Boc-AEMA) monomers,

as well as the hydrophobic cross-linking (1,6-HDDMA) and hydrophilic (EGDMA) monomers, as outlined in Table 3.1).

To investigate the influence of the hydrophobic-hydrophilic balance variations on selected protected PPM morphology and pore size, SEM images were obtained for different PPM (1, 4, 6 and 11). The pore size, specific surface area and porosity of the PPM selected were determined by mercury intrusion porosimetry. In Fig. 3.1 it can be seen that there is no notable difference between the four PPM in term of morphology and pore size. The quantitative porosimetry analysis results, summarized in Table 3.2 are in agreement with the SEM images. Because the pore size was relatively constant in this study, it is reasonable to assume that the hydrophobic-hydrophilic balance of the PPM is the only factor affecting contact killing lysis. The ethidium bromide (EtBr) intercalation assay served to detect DNA in the cell lysate, as evidence for cell lysis. When ethidium bromide (EtBr) is exposed to UV light at 285 nm it fluoresces with an orange color at 595 nm, which intensifies considerably after its intercalation in DNA. Bonasera *et al.* reported on the linearity

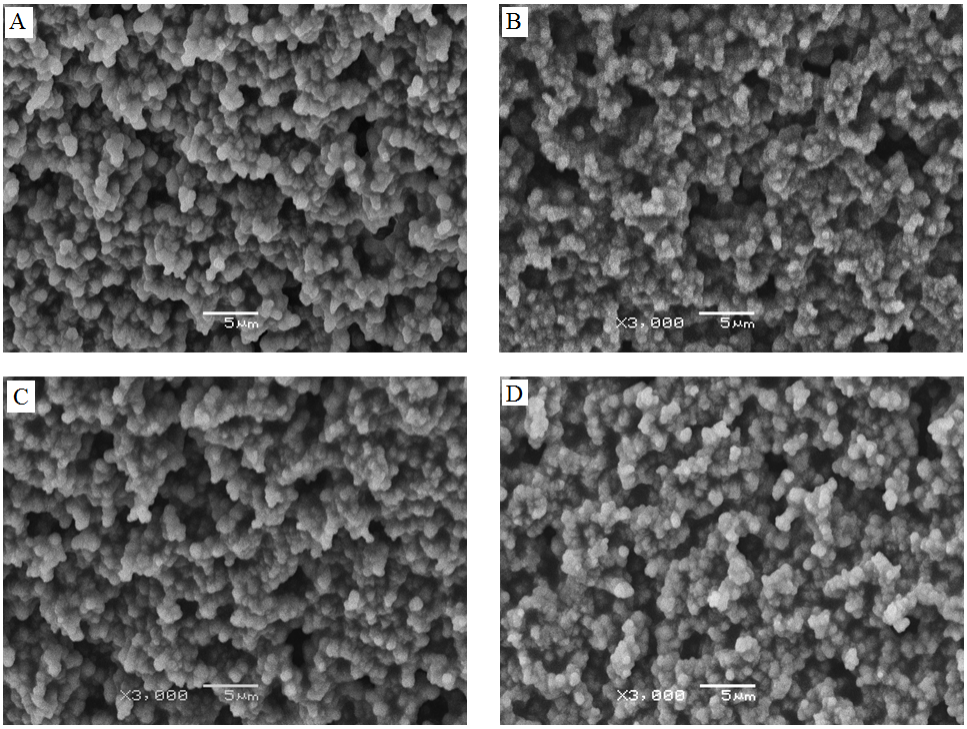

Figure 3.1: SEM images for the protected PPMs (A) 1, (B) 4, (C) 6, and (D) 11.

Table 3.2: Pore size, specific surface area and porosity of the protected PPM 1, 4, 6 and 11, as determined by mercury intrusion porosimetry measurements.

PPM	Median pore diameter (μm)	Surface area (m^2/g)	Porosity (%)
1	2.90	3.54	6.6
4	2.82	3.76	64.6
6	2.85	3.69	64.7
11	3.00	2.11	65.0

and the detection limit for the ethidium bromide (EtBr) intercalation assay [66]. They reported that for DNA concentrations within the range of 20-1250 ng/mL, this relationship is linear. They also reported that this method has a detection limit of 10 ng/mL of DNA at an EtBr concentration of 0.5 μg/mL. This implies that the concentrations used in this experiment are within the linear dynamic range and the limit of detection for the assay method used. The fluorescence intensity for EtBr before and after intercalation in the DNA present in the cell lysate collected at the outlet of the porous antibacterial monoliths (1-11) was quantified on a spectrofluorometer to obtain Fig. 3.2. The experiments performed to obtain Fig. 3.2 were repeated three times and the results shown are the average of these results for each PPM. The standard deviation on the values obtained for each PPM is displayed as error bars on Fig. 3.2.

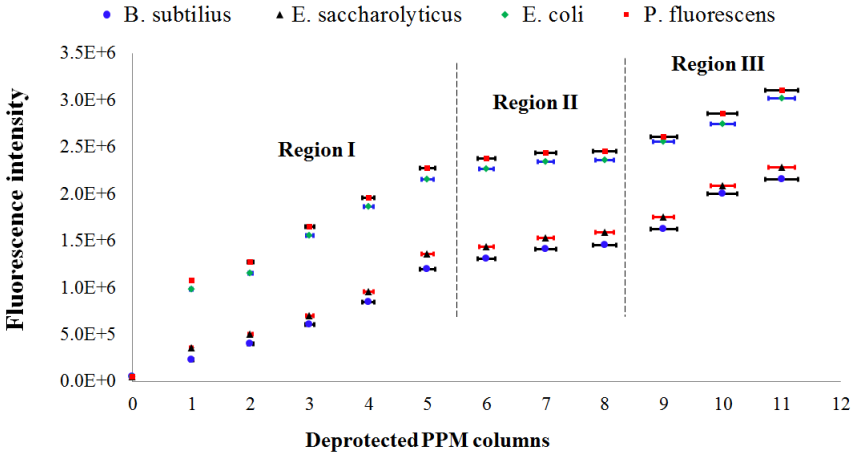

Figure 3.2: Fluorescence intensity for EtBr before (control sample point at 0) and after intercalation into the DNA released from bacterial cells flowing through the eleven deprotected PPMs at flow rate of 1.5 μL/min.

As it can be seen from Fig. 3.2, the fluorescence intensity for the tested monoliths can be divided into three groups: Groups I (columns 1 through 5), II (columns 6 through 8), and III (columns 9 through 11). In Group I, the fluorescence intensity of EtBr gradually increases as the content in the hydrophobic (1,6-HDDMA) and hydrophilic (EGDMA) cross-linking monomers increase and decrease within that series, respectively. This reflects increasing DNA concentrations in the crude lysates collected at the outlet of the microfluidic channels hosting the monoliths, and therefore enhanced lysis as the columns become increasingly hydrophobic. In Group II, the fluorescence intensity of EtBr is relatively insensitive to further variations in hydrophobic and hydrophilic cross-linking monomers (columns 6-8). This saturation shows that further increasing the hydrophobicity of the monoliths does not lead to improved lysis ability for the bacterial species tested in this study. In Group III, the fluorescence intensity of EtBr again increases as the contents of the hydrophobic (BuMA) and hydrophilic, positively charged (AEMA) non-cross-linking monomers decrease and increase, respectively, in the last monoliths. This increase could be contributed to further changes in the hydrophobic-hydrophilic balance, but (on the basis of the trends described above) it is more likely due to increased charge density in the monolith as a result of the higher concentration of the positively charged amine monomer (AEMA).

To validate the cell lysis results obtained by the EtBr assay and to directly quantify the lysis efficiency of the different columns, the DNA concentration in the cell lysates collected at the exit of the microfluidic channels was determined by UV-Vis spectrophotometry as shown in Fig. 3.3. It can be seen that the DNA concentration in the different cell lysates also matches the three regions identified in Fig. 3.2. This further confirms that column (11) had the highest antibacterial activity among the different monolith columns investigated; thus it was used for the subsequent experiments. The experiments to obtain Fig. 3.3 were again repeated three times and the results shown are the average values obtained for each PPM. The standard deviation on the values obtained for each PPM are displayed as error bars on Fig. 3.3.

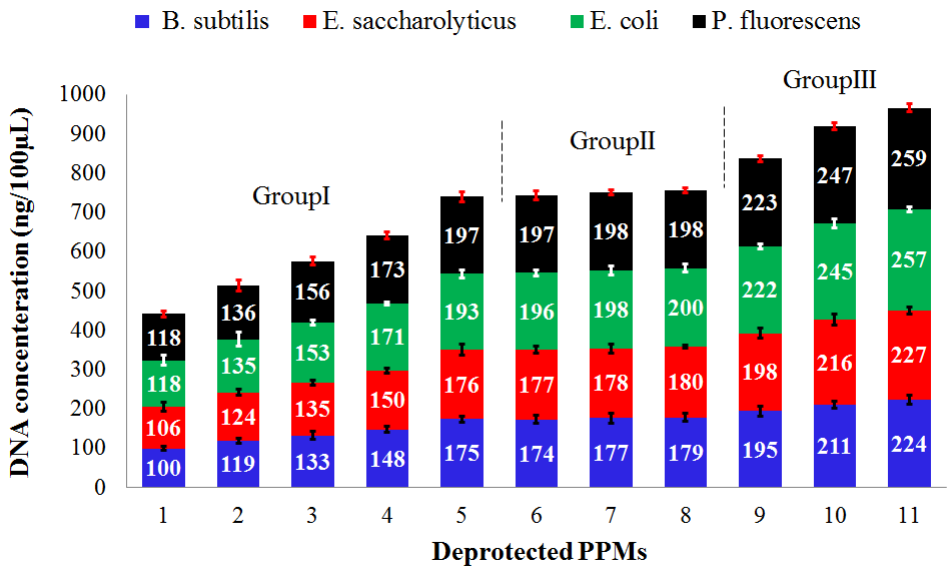

Figure 3.3: Absolute concentration of DNA present in the crude cell lysate collected at the outlet of the different deprotected PPMs.

Fig. 3.2 and Fig. 3.3 both show that the biochips display a comparable lysis efficiency for P. fluorescens and E. coli (the two gram-negative bacteria), as well as for E. saccharolyticus and B. subtilis (the gram-positive bacteria). However it is clear that the lysis efficiency is significantly higher for the gram-negative than for the gram-positive bacteria within the monolith composition range investigated. This is reasonable since gram-positive bacteria have a thicker cell membrane than gram-negative bacteria (as shown in Fig. 1.1), which makes them harder to lyse.

3.2.2 Influence of flow rate

The bacterial cell wall/membrane is mechanically sheared by flowing the cell suspension through the porous medium of the monolith, but it is also damaged and disintegrated by physical of being in contact with the antibacterial polymeric biocide covering the porous surface. Both effects lead to leakage of the intracellular contents. Burke *et al.* thus reported that the flow rate was a critical factor in the mechanical shearing of B lymphocyte cells in porous monolith columns [3]. They demonstrated that B lymphocyte cells could only be mechanically lysed when the cell suspension was pumped at a flow rate of at least 5 μL/min for the specific

system they used. Below this flow rate the cells did not make it to the outlet of the monolith, but they were rather trapped against the inlet side. In this study, the influence of the flow rate on both mechanical shearing and contact killing for bacterial cell lysis was examined. Control samples were prepared for the ethidium bromide intercalation assay containing 20 μL of bacterial cell suspensions that were not flown through the monolith, 380 μL of DI water, and 30 μL of EtBr from a stock solution with a concentration of 0.4 mg/L.

3.2.2.1 Protected PPM.

Before removing the Boc protecting group from the Boc-AEMA monomer, the fluorescence intensity of EtBr after intercalating into the DNA in the cell lysates collected from PPM (11) varied with the flow rate according to four different regimes as shown in Fig. 3.4. At flow rates below 1.2 μL/min (Regime i) the fluorescence intensity for EtBr was similar to the control sample, indicating that no significant lysis took place. This implies that the cells cannot be mechanically lysed through the porous medium of the monolith unless the flow rate exceeds a certain threshold value, in agreement with the findings of Burke *et al.* This is attributed to a back pressure (at these low flow rates) inadequate to force the cells through the pores of the PPM, which leads to filtering and trapping of the cells at the inlet of the PPM, in agreement with the findings of Burke *et al.*

At flow rates between 1.2 and 4.4 μL/min (Regime ii) the fluorescence intensity for EtBr (and the DNA concentration) increased rapidly, as shown in Fig. 3.4 (and Fig. B2 of the Appendix B). However at flow rates between 4.8 and 7.2 μL/min (Regime iii) the fluorescence intensity for EtBr and the DNA concentration gradually leveled off (decreasing slope). In these two regimes, as the flow rate increases, the bacterial cells are forced faster through the porous medium of the monolith, which results in more mechanical lysis of the cells. Finally, at flow rates between 7.6 and 10 μL/min (Regime iv) the fluorescence intensity for EtBr and the DNA concentration saturated which shows that there was no additional influence of the flow rate on cell lysis efficiency beyond 7.2 μL/min. The effect of the flow rate

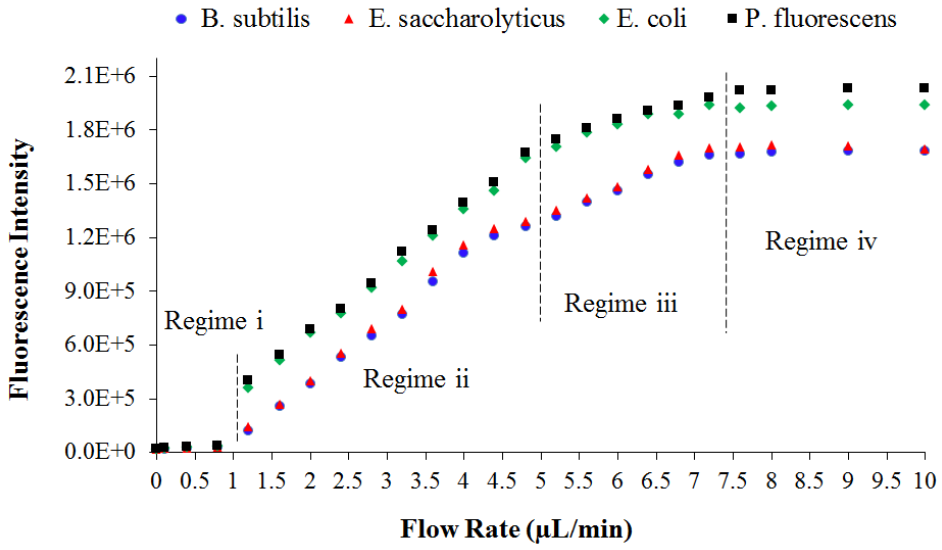

Figure 3.4: Fluorescence intensity for EtBr intercalated into the DNA released from bacterial cells pumped through protected freshly synthesized PPM 11 at each flow rate ranged from 0.1 to 10 μL/min. The point at 0 μL/min is for the control sample.

on lysis efficiency was therefore highest in Regime ii, less significant in Regime iii, and insignificant in Regime iv. The results also reveal that the lysis efficiency was higher for gram-negative than for gram-positive bacteria within the flow rate range investigated. This was again expected, as gram-positive bacteria are harder to lyse due to their thicker cell membranes.

3.2.2.2 Deprotected (antibacterial) PPM.

After deprotecting the amine group of the Boc-AEMA monomer, the fluorescence intensity for EtBr after intercalation into the DNA present in the cell lysates was found to vary with the flow rate in five different regimes, as shown in Fig. 3.5. At flow rates below 1.2 μL/min (Regime i) the fluorescence intensity is similar to the control samples, indicating that no lysis happened. This further confirms the results gathered for the protected PPM.

At flow rates between 1.2 and 3.6 μL/min (Regime ii), fluorescence intensity increased rapidly.The DNA concentration (and the fluorescence intensity for EtBr) at a flow rate of 1.2 μL/min, shown in Fig. 3.5 and Fig. B3 (Appendix B), are

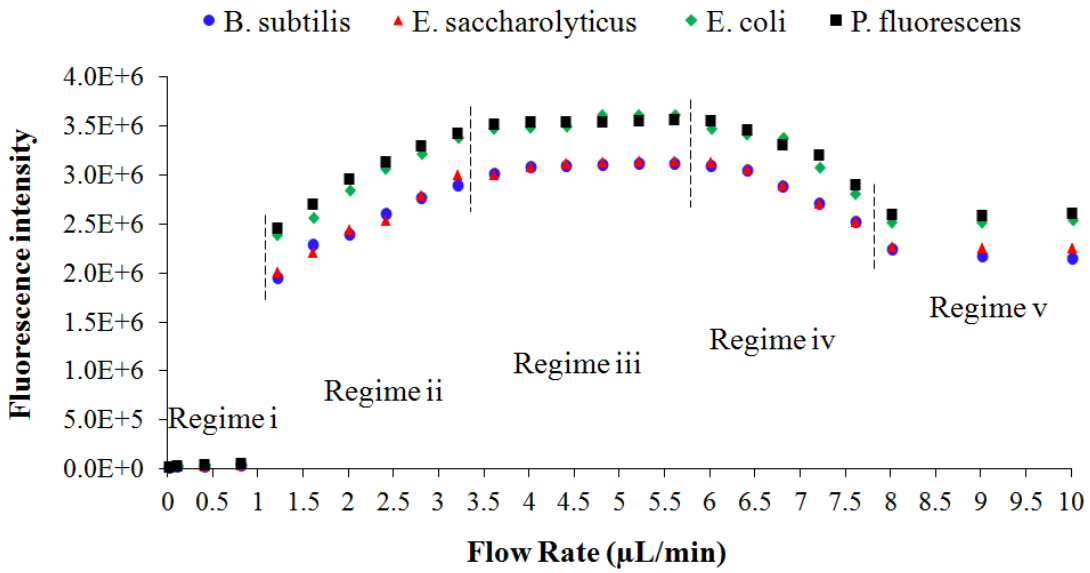

Figure 3.5: Fluorescence intensity for EtBr intercalated into the DNA released from bacterial cells passed through the deprotected PPM (11) at flow rates ranged from 0.1 to 10 μL/min. Point 0 μL/min on the flow rate axis represents the control sample.

6.5 times higher and 2.6 higher, respectively, than the values obtained before deprotection shown in Fig. 3.4 and Fig. B2. This confirms that additional lysis took place after deprotection due to the antibacterial nature of the monolithic surface. At flow rates between 4 and 6 μL/min (Regime iii), the DNA concentration (and fluorescence intensity for EtBr) saturated. This contrasts with the trend observed before deprotection within the same flow rate range, since the fluorescence intensity for EtBr and the DNA concentration continued to increase. At flow rates between 6.4 and 7.6 μL/min (Regime iv) the fluorescence intensity for EtBr and the DNA concentration both decreased rapidly, while the fluorescence intensity for EtBr and DNA concentration continued to increase over the same flow rate range for the columns in the protected state. At flow rates between 8 and 10 μL/min (Regime v) the fluorescence intensity for EtBr and the DNA concentration levelled off again.

These results show that when the flow rate exceeds a critical value the bacterial cells spend insufficient time in contact with the antibacterial surface of the monolith, which leads to less efficient contact killing lysis. Mechanical shearing

lysis is still taking place (4-7.6 μL/min) however, until the flow rate reaches a value (8 μL/min) where further increase has no effect on both lysis mechanisms. The highest overall cell lysis efficiency (highest overall fluorescence intensity and DNA concentration) was therefore achieved at flow rates between 4 and 6 μL/min, as a result of a combination of mechanical shearing and contact killing mechanisms. The fluorescence intensity for EtBr and the DNA concentration at flow rate between 4 and 6.0 μL/min, shown in Fig. 3.5 and Fig. B3 (Appendix B), are on average 2.5 times higher and 3.3 times higher, respectively, than the values obtained before deprotection (Fig. 3.4 and Fig. B2). This implies that contact-killing mechanism causes more lysis than mechanical shearing mechanism at flow rates between 4 and 6 μL/min. It worth mentioning that the time that bacterial cell suspension spend in the PPM at flow rate of 4 μL/min is 43 sec. (Table B1 of the Appendix B), but this interaction or contact time between bacterial cells and the antibacterial sites of the PPM varies with the flow rate.

By looking at Table 3.3, one can observe that the difference in the bacterial cells volume (length and diameter) between the gram-negative bacterial species and between gram-positive bacterial species explain the difference of the cell lysis efficiency between E. coli and P. fluorescens and between B. subtilis and E. saccharolyticus as shown in Fig. 3.4, Fig. B2, Fig. 3.5 and Fig. B3.

3.2.3 Parameters affect the biochip performance

The performance of the developed biochip is determined and controlled by few parameters. These parameters are summarized in Table 3.4.

Table 3.3: The length and diameter of the used bacterial species

Dimension	E. coli [67]	ATCC 13525 [68]	B. subtilis [67]	ATCC 43076 [69]
Length (μm)	1-3	1.4-1.7	2-3	1.2-1.5
Diameter (μm)	0.5	0.5-0.6	0.7-0.8	0.5-0.6

Table 3.4: Parameters affect the biochip performance.

Parameter	Performance
Hydrophobic- Hydrophilic balance	The hydrophobic-hydrophilic balance of the PPM column affects the antibacterial activity of the PPM column as it was observed from Fig. 3.2 and Fig. 3.3. As a result the cell lysis of the PPM column is affected, thus the performance of the biochip is influenced by the hydrophobic-hydrophilic balance of the PPM column.
Flow rate	It could be seen from Fig. 3.4 that flow rate affects the shear mechanical lysis (flow rate between 1.2-7.2 μL/min), as it determines the pressure utilized to force bacterial cells through the porous medium of the protected PPM column. While flow rate affects antibacterial contact-killing cell lysis (as could be observed from Fig. 3.5), because it determines the time where bacterial cells have physical contact with the antibacterial sites of the PPM, contact time. It can be concluded that flow rate affects the cell lysis efficiency of the PPM column , thus affecting the performance of the biochip.
Pore size	The smaller the pore size, the higher the pressure (flow rate) needed to force the bacterial cells through the pore and more mechanical shearing to the bacterial cell membrane. Thus, the pore size of the PPM column influences the mechanical shearing, therefore influences the lysis efficiency of the PPM and as a result affects the performance of the biochip. A set of experiments could be carried to further support this hypothesis.
Mode of action of membrane-disruption	The antibacterial strength of the PPM column determines the strength and efficiency of the antibacterial contact-killing. Mode of action of membrane destruction is a major factor in determining the antibacterial strength of the PPM. A set of detailed micro-biology based experiments should be carried out to further support this hypothesis.
Design and geometry	The microchannel hosting the PPM column serves as a mold for the PPM, thus the shape of the microchannel determines the path shape where bacterial cells go through. Also, the geometry of the microchannel determines the residence time of the bacterial cells into the PPM which in return affect the contact time of the bacterial cells with the antibacterial sites of the PPM column. Thus the design and geometry of the microchannel affect the biochip performance.

3.2.4 Cell lysis efficiency at different cell concentration

The cell lysis efficiency of column (11) at the optimal flow rate, 4 μl/min at four different cell concentrations was determined in term of the fluorescence intensity of EtBr when intercalates with the DNA present in the cell lysate as shown in Fig. 3.6

of the Appendix B. It can be observed from Fig. 3.6, that fluorescence intensity of EtBr is linearly decreasing with the decrease of cell concentration. It is also notable that at cell concentration of 10^2 CFU/ml, there was DNA released from the cells which is a sign of cell lysis at that low cell concentration.

3.2.5 Reusability of the biochip

The change in EtBr fluorescence intensity due to its intercalation in the DNA present in the cell lysate is compared in Fig. 3.7 after each injection and flushing cycle for the two different washing protocols examined. The first two points in Fig. 3.7 are for the two control samples. It can be seen that for the PBS washing protocol the antibacterial efficiency decreased slightly over 10 cycles, but washing of the monolith with 85% phosphoric acid then restores the activity to some extent. This could be due to gradual deprotonation of the amine caused by the successive PBS washes, which is being protonated again by the phosphoric acid wash. The decrease in activity observed for the Acid wash protocol was much more gradual. It is interesting to note that after the twentieth use, the lysis efficiency started degrad-

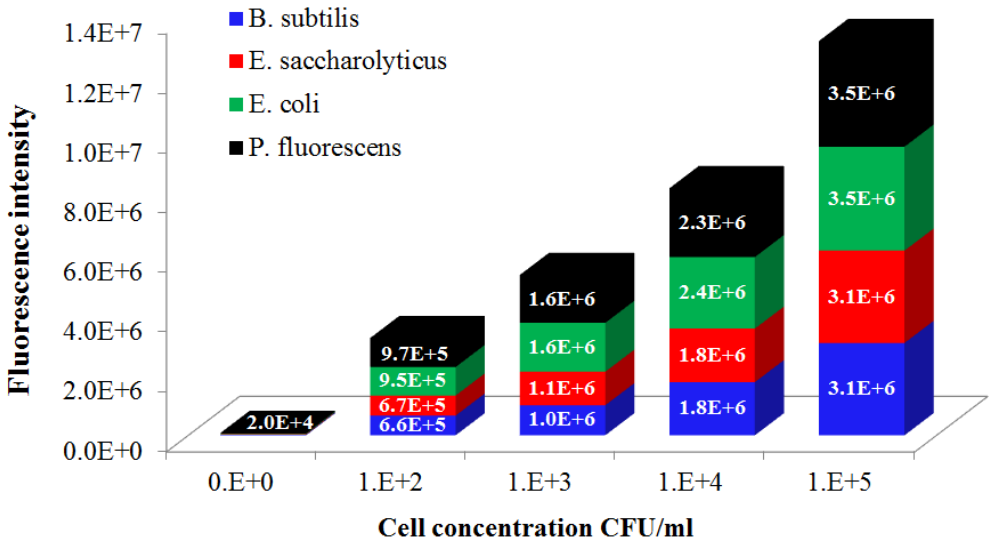

Figure 3.6: Fluorescence intensity for EtBr intercalated into the DNA released from bacterial cells flowing through the deprotected PPM (11) at 4 μL/min at different cell concentration.

ing dramatically regardless of the washing protocol used. The PPM was completely blocked after 30-35 cycles. Gradual blockage of the pores by cell debris, leading to a decrease in the surface area of the porous monolith accessible to the cells, may therefore also explain in part the gradual decrease in cell lysis efficiency observed over multiple cycles. Irrespective of the washing protocol used, the performance of the biochip appears acceptable over multiple cycles since the lysis efficiency only decreased by 10% over 20 cycles. The fluorescence intensity of EtBr mixed with the PBS recovered from the microfluidic channel in the back-flush cycle showed insignificant DNA carry over, reaching only 0.6% of the maximum EtBr intensity reported as shown in Table B3 and plotted with the control sample as shown in Fig. B5 of the Appendix B. It is also worth mentioning that the total cycle time for the biochip was 35 min including both sample lysis and monolith regeneration.

3.2.6 Biochip vs. off-chip cell lysis

A 100 μL aliquot of the bacterial suspension (at the same concentration used in the monolith lysis experiments) was lysed by the off-chip cell lysis methods. The

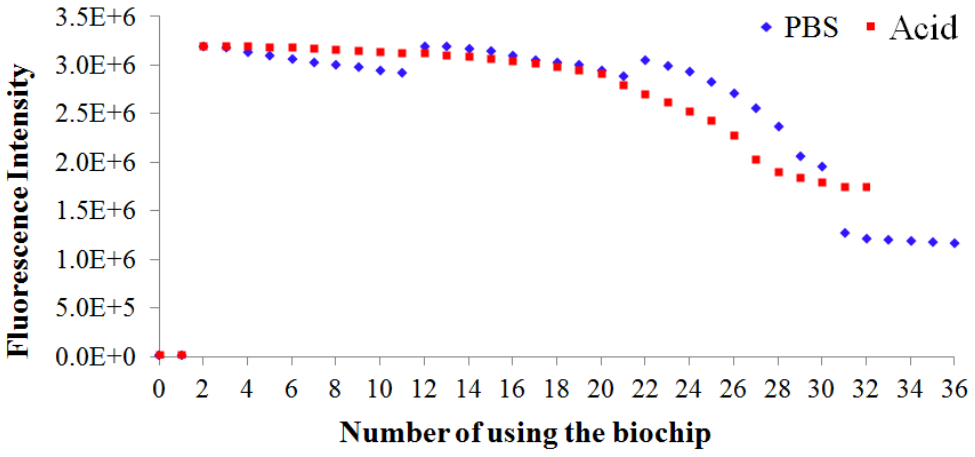

Figure 3.7: Fluorescence intensity for EtBr intercalated into the DNA released from bacterial cells flowing through the deprotected monolith (11) at 4 μL/min over successive runs, for the two different washing protocols (PBS and Acid washes). The first two data points on the horizontal axis (number of uses of the biochip) are for the control samples.

efficiency of the different cell lysis techniques, including the biochip method, is compared in Fig. 3.8 and Fig. B4 (Appendix B). It is clear that the DNA concentration in the cell lysate collected from the biochip was higher than for the off-chip (mechanical, thermal and chemical) methods in terms of the concentration of DNA present in the cell lysate. The experiments performed to obtain Fig. 3.8 and Fig. B4 were repeated three times and the results shown are the average of these results. The standard deviation on the values obtained for each PPM is displayed as error bars on Fig. 3.8 and Fig. B4. It was reported that the masses of DNA and RNA in a single E. coli cell are 5×10^{-12} g/cell [73] and 30×10^{-12} g/cell [74], respectively. If this is considered as a reference, 100 μL of bacterial suspension at cell concentration of 1.5×10^5 CFU/mL, should contain 75×10^{-9} g of DNA and 450×10^{-9} g of RNA. As both DNA and RNA absorb light at 260 nm, it is not possible to distinguish between DNA and RNA by spectrophotometry, consequently, the measurements at 260 nm are for both DNA and RNA combined. In Fig. 3.8, the concentration of DNA and RNA present in E. coli cell lysate collected at the outlet of the antibacterial PPM is 465×10^{-9} g/100μL. This therefore represents 89% of the amount of DNA and RNA contained in the input cells. In other words, this suggests that the lysis efficiency of the antibacterial PPM was around 89 %. Using the same calculations, the efficiency of the mechanical, thermal and chemical lysis methods was 40%, 50%, and 67%, respectively. It is therefore clear that the DNA concentration in the cell lysate collected from the biochip was higher than for the off-chip (mechanical, thermal and chemical) methods. This shows that the biochip approach led to more efficient lysis of the bacterial species tested than the traditional off-chip techniques used in this work. Furthermore, the biochip lysis method does not require power consumption (apart from the pump operation), chemical/enzymatic reagents, the use of centrifugation, sonication, nor a complicated design and fabrication process. As a result, the on-chip cell lysis technique developed appears well-suited for incorporation in an integrated sample preparation system.

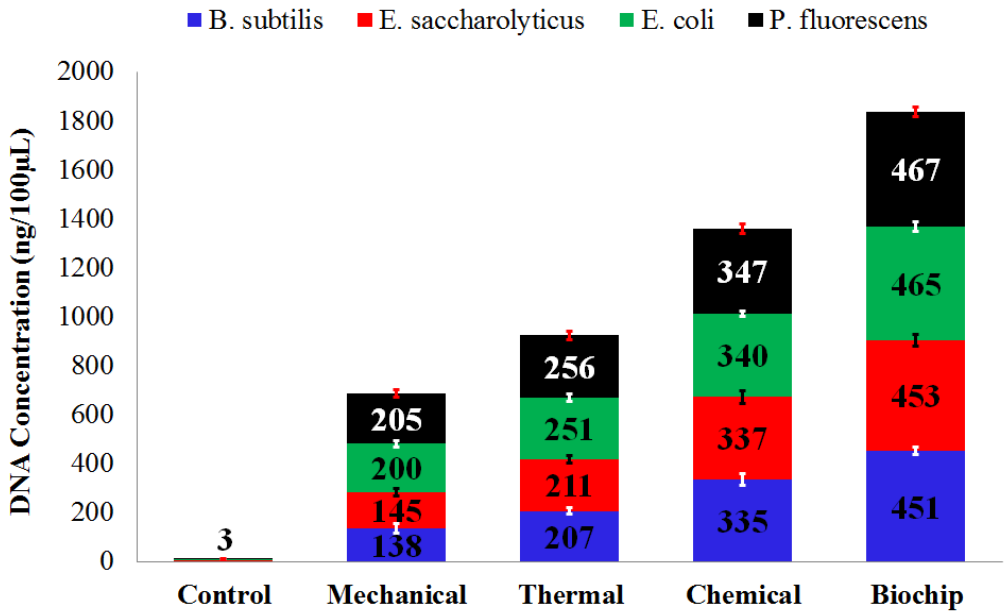

Figure 3.8: Concentration of DNA present in the cell lysate after on-chip cell lysis (deprotected PPM (11) at a flow rate of 4 μL/min) and off-chip mechanical, thermal and chemical cell lysis.

3.2.7 PCR and gel electrophoresis

The genes in the DNA released by lysing the bacterial cells on deprotected PPM (11) were amplified by PCR and qualitatively validated by gel electrophoresis. The analysis results are shown in Figure 8 for the PCR products for the different cell lines investigated. There are no detectable amounts of DNA at the PCR output for the bacteria samples that were not lysed in the deprotected PPM, which shows that the cells had intact membranes before passing through the deprotected PPM. In contrast, DNA is clearly detected at the PCR output for the samples that were passed through the deprotected PPM, which confirms that the membrane of cells was disintegrated. This is a clear sign for lysis, but also demonstrates that the antibacterial PPM did not inhibit PCR.

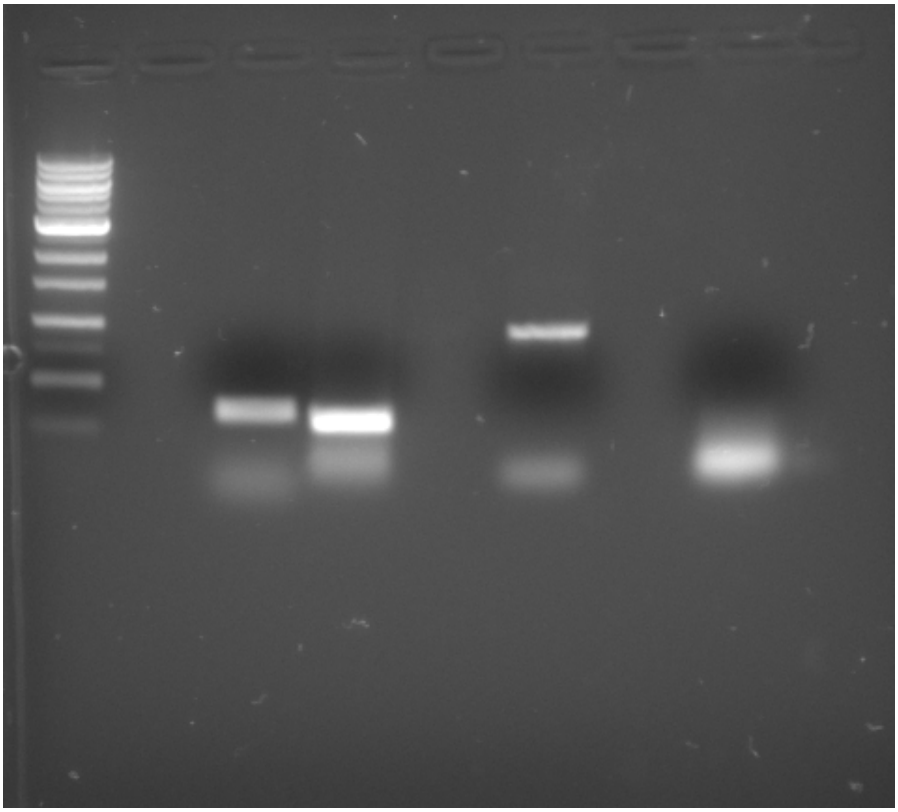

Figure 3.9: Gel electrophoresis analysis of PCR output. Column (1) is for a 100 bp DNA ladder. Columns (2) and (3): unlysed and lysed E. saccharolyticus. Columns (4) and (5): lysed and unlysed B. subtilis. Columns (6) and (7): lysed and unlysed P. fluorescens. Columns (8) and (9): lysed and unlysed E. coli.

3.3 Conclusions

Microfluidic biochips were fabricated that have the ability to efficiently lyse four strains of gram-positive and gram-negative bacterial cells: E. saccharolyticus (ATCC 43076), B. subtilis 168, E. coli DH5α, and P. fluorescens (ATCC 13525). The lysis ability of the biochips was validated with the ethidium bromide intercalation assay, relating the presence of DNA in the cell lysate with an increase in fluorescence intensity for EtBr, and UV-Vis spectrophotometry to directly determine the DNA concentration in the cell lysate. Gel electrophoresis analysis of the PCR products after genes amplification of the DNA present in cell lysate showed that the monoliths did not leach any material interfering with the PCR process. The performance of the microfluidic biochips developed exceeded that of the traditional off-chip me-

chanical, thermal, and chemical cell lysis techniques. SEM images and porosimetry revealed that varying the hydrophobic-hydrophilic balance of the PPM column does not affect the morphology and the pore size of the protected monolithic column. The influence of the hydrophobic-hydrophilic balance on the lysis efficiency was investigated on the deprotected monolith, and the antibacterial monolith with the highest lysis efficiency was used to determine the influence of the flow rate of the bacterial suspension through the protected and deprotected porous monoliths. By comparing the lysis efficiency before and after deprotection, It was shown that the contribution of contact killing to cell lysis was more important than that of mechanical shearing in the PPM. It was also shown that the biochips can be reused for at least twenty times without any evidence of physical damage to the monolith, significant performance degradation or DNA carryover when they are back-flushed between cycles. With further optimization and possibly mass production of the antibacterial PPM column, there would be a great potential for commercially producing cell lysis column, as exists for DNA isolation.

Chapter 4

QAC Based Antibacterial PPM Column

In this chapter, reusable antibacterial non-leaching monolithic columns polymerized in microfluidic channels designed for on-chip cell lysis applications were obtained by the photoinitiated free radical copolymerization of diallyldimethylammonium chloride (DADMAC) and a di(meth)acrylate monomer in the presence of a porogenic solvent. The microfluidic channels were fabricated in cross-linked poly(methyl methacrylate) (X-PMMA) substrates by laser micromachining. The monolithic columns have the ability to inhibit the growth of, kill, and efficiently lyse gram-positive: Micrococcus luteus (Schroeter) (ATCC 4698) and Kocuria rosea (ATCC 186), and gram-negative bacteria: Pseudomonas putida (ATCC 12633) and Escherichia coli (ATCC 35218) by mechanically shearing the bacterial membrane when forcing the cells to pass through the narrow pores of the monolithic column, and simultaneously disintegrating the cell membrane by physical contact with the antibacterial surface of the column.

Cell lysis was confirmed by off-chip PCR without further purification. The influence of the di(meth)acrylate cross-linking monomer on bacterial growth inhibition, leaching, the lysis efficiency of the monolithic column, and its mechanical stability within the microfluidic channel were investigated and analyzed for three different monomers: ethylene glycol diacrylate (EGDA), ethylene glycol dimethacrylate

(EGDMA), and 1,6-hexanediol dimethacrylate (1,6-HDDMA). Furthermore, the bonding efficiency of two X-PMMA substrates with different cross-linking levels was studied. The monolithic columns were shown to be stable, non-leaching, and reusable for over 30 lysis cycles without significant performance degradation or DNA carryover when they were back-flushed between lysis cycles.

4.1 Introduction

Polymers containing quaternary ammonium compounds (QACs) are another class of antibacterial polymers widely used as biocides and disinfectants. In this class materials, no antibacterial units are leaching, thus producing permanent protection against bacterial reproduction [79]. The positive surface charge intrinsically inherited from the quaternary ammonium-functionalized surfaces strongly adhere to negatively charged bacterial membranes, which inhibits bacterial growth, kills, and eventually lyse bacteria by penetrating their membrane and causing an outflow of intracellular material [80]. These polymers have been covalently attached onto various materials by numerous techniques such as 'grafting to' [31], 'grafting from' [81], atom transfer radical polymerization (ATRP) [40], surface initiated ATRP [82] on glass, UV-induced surface graft polymerization to polymer and paper [83], and 'grafting from' mediated radical polymerization on metals [84].

Diallyldimethylammonium chloride (DADMAC) is a quaternary ammonium compound and positively charged monomer potentially useful for that purpose. It possesses a high water solubility, alkenyl double bonds in its molecular structure, and can form hydrophilic homopolymers and copolymers by various polymerization reactions. Poly(diallyldimethylammonium chloride), polyDADMAC, is a polymer with a permanent high cationic charge density (independently of pH), is non-bioaccumulable, non-biodegradable, and adsorbs onto negatively charged surfaces such as bacterial membranes [85]. It was reported that polyDADMAC can inhibit microbial growth [86]. Mei *et al.* reported that polyDADMAC possesses strong bacterial adhesion, and moreover that it has high contact killing activity

against waterborne pathogens (Raoultella terrigena, E. coli, and Brevundimonas diminuta) [87]. Mikhaylova *et al.* developed bacterial barrier dressings treated with polyDADMAC to prevent wound infection, [88] that absorbed wound exudate while not releasing toxic materials into the wound. These dressings were capable of disrupting bacterial membrane, resulting in cell lysis and death.

Lu *et al.* developed antibacterial films by blending konjac glucomannan (KGM) and polyDADMAC in aqueous media [89]. They concluded that the films efficiently inhibited the growth of and lysed gram-positive bacteria (B. subtilis and S. aureus), but was less efficient toward gram-negative bacteria (E. coli and P. aeruginosa). Thome *et al.* added an ultrathin (1-2 nm) antibacterial polyDADMAC film on polymer surfaces by the 'grafting to' technique via radical polymerization [85]. These films reduced the accumulation of bacterial cells including Micrococcus luteus (gram-positive) and E. coli (gram-negative) by a factor of 10^6-10^7.

4.2 Experimental

4.2.1 Materials

The chemical and biological materials used in this chapter are mentioned below:

Methyl methacrylate (MMA, 99 %), ethylene glycol dimethacrylate (EGDMA, 98 %), and 1,6-hexanediol dimethacrylate (1,6-HDDMA, $\geqslant$90 %) were all purchased from Sigma-Aldrich (Oakville, ON Canada), and filtered over alumina to remove inhibitors. Diallyldimethylammonium chloride (DADMAC, 65 wt% in H_2O), 2,2-dimethoxy-2-phenylacetophenone (DMPAP, 99 %), ethylene glycol diacrylate (EGDA, 90 %), methanol ($\geqslant$99.9 % Chromasolv), potassium bromide (ACS reagent, 99.0 % , KBr), and fumed silica (powder, 0.2-0.3 μm average particle size) were purchased from Sigma-Aldrich and were used without further purification. iTaq polymerase, 10X PCR buffer, and magnesium chloride were obtained from Bio-Rad (Montreal, QC Canada). Primers and dNTP mix (dATP, dCTP, dGTP and dTTP) were obtained from Sigma-Aldrich. Ethidium bromide (UltraPure 10 mg/mL,

EtBr) was purchased from Life Technologies Inc. (Burlington, ON Canada). A 100 bp DNA ladder was purchased from BioLabs (Ipswich, MA).

4.2.2 Microchip fabrication

The microfluidic channels were laser-micromachined within X-PMMA substrates with a 10.6 μm CO_2 excimer laser engraving system (Universal Laser Systems, VLS2.30). The synthetic procedure for X-PMMA was adopted from Aly Saad Aly *et al.* [63]. The channels were 2.5 cm in length, 500 μm wide, and 350 μm deep. To obtain an enclosed channel, another piece of the X-PMMA substrate with two holes drilled for the inlet and outlet was thermally bonded with the substrate hosting the microchannel, by placing the top and bottom substrates in a hot press under pressure (115 °C, 10^3 psi) for 15 minutes (Heated Press 4386, Carver, Wabash, IN). To facilitate the tube connections between the microfluidic channel and the bacterial suspension reservoir, two 30G syringe needles were trimmed, set over the inlet and outlet of the microfluidic channel and bonded with a mixture of epoxy glue and fumed silica powder to achieve a hard and stable adhesive layer.

4.2.3 Off-chip non-porous film

The compositions used to prepare the antibacterial networks summarized in Table 4.1, were first investigated off-chip to study their antibacterial activity. To create a thin film of each composition on a X-PMMA substrate, each mixture was spin-coated on the substrate and then exposed to a UV source to initiate the polymerization. The substrates with the grafted film were then gently washed with methanol to remove any unreacted monomer and left to dry for 15 minutes in a fume hood.

Table 4.1: Compositions of the monolith solutions used (in wt%).[a]

	Monomer	Cross-linker	Cross-linker	Cross-linker
Monolith	DADMAC	EGDMA	1,6-HDDMA	EGDA
1	21	9	-	-
2	21	-	9	-
3	21	-	-	9

[a] All the reactions included 70% methanol as porogenic solvent, and 0.2% DMPAP as photoinitiator.

4.2.4 PPM formation, characterization and stability

4.2.4.1 PPM formation.

The mixtures of Table 4.1 were sonicated for 10 minutes to obtain a homogeneous solutions, and were then introduced into the microchannel. Polymerization was triggered by irradiation of the substrate for 10 minutes with a 365 nm UV source in a cabinet containing a UV lamp (200 mJ/cm^2 intensity, ENF-260C, Spectronics Corp. Westbury, NY, USA). The substrate was then turned over and irradiated with the UV source on the other side for 10 minutes longer. Using a Pico Plus Syringe Pump (Harvard apparatus, Holliston, MA), the microchannel was then flushed with methanol followed by deionized (DI) water, to remove unreacted monomers and the porogenic solvent, respectively. Even though allyic monomers are sensitive to allylic chain transfer [64], DADMAC can potentially act as a cross-linker. Thus an attempt of photo-polymerizing DADMAC with no cross-linker to form the PPM within the microfluidic channels was made, but a network was not formed. It is also worth mentioning that the absorbance of the 20 % and 10 % X-PMMA samples at 365 nm was determined to be 0.238 and 0.101, respectively.

4.2.4.2 PPM characterization.

Attenuated total reflectance-Fourier transform infrared (ATR-FTIR) spectra for the DADMAC monomer, poly(DADMAC-*co*-EGDMA), poly(DADMAC-*co*-EGDA), and poly(DADMAC-*co*-1,6-HDDMA) were obtained on Nicolet 4700 FT-IR spectrometer.

Images for the monoliths were obtained with a Hitachi SU-70 scanning electron microscope (SEM, Hitachi High-Technologies Corporation, Tokyo, Japan) at an acceleration voltage of 10 kV. The SEM samples were prepared by immersing the microchannel hosting the PPM column into liquid nitrogen, and then cutting perpendicularly to the monolith-filled X-PMMA channel. To form an electrically conductive layer, gold was sputtered onto the samples prior to SEM imaging.

The pore size and porosity of the PPM columns were determined by mercury intrusion porosimetry using a Quantachrome Poremaster 60 device (Quantachrome Instruments, Boynton Beach, FL). The PPM columns were freeze-dried under vacuum and a sample of approximately 1 cm^3 was put into a sample holder cell to force mercury, a non-reactive and non-wetting liquid, into the pores of the sample. The relationship between the pressure applied and the diameter of the pores into which the mercury intruded was determined by the Washburn equation [33].

4.2.4.3 Mechanical stability of PPM columns.

Pressure tests were conducted to evaluate the mechanical stability of the monolithic columns within the microfluidic channels with diffident cross-linker monomer in the PPM columns and at different cross-linker contents in the X-PMMA substrate. A pressure test was conducted to study the bonding strength by pumping ethanol pressurized by a compressed N_2 cylinder through it. The pressure was increased in 10 psi increments every 5 minutes, to determine the pressure at which the monolithic column started to debond from the substrate (PPM deponding pressure) and a leak started at the interface between the two substrate layers (Substrate deponding pressure).

4.2.5 Bacterial cultures

Pseudomonas putida and Escherichia coli were used as gram-negative test bacterial strains, while Micrococcus luteus (Schroeter) and Kocuria rosea were used as gram-positive strains. These bacterial strains were purchased from American Type

Culture Collection (ATCC, Manassas, VA, catalog numbers: ATCC 12633, ATCC 35218, ATCC4698, and ATCC 186, respectively). Details about the bacterial cultures and the conditions of growth are provided in Appendix C.

4.2.6 Antibacterial, leaching, and growth inhibition tests

The antibacterial activity of the cross-linked films, possible leaching from the PPM columns, and the ability of the PPM column materials to inhibit bacterial growth were studied as follows.

4.2.6.1 Antibacterial activity.

The live/dead viability assay (L7012, Molecular Probe, Burlington, ON Canada) was used to investigate the interactions between the cross-linked films and the bacterial cells. The assay used two fluorescent nucleic acid stains, SYTO 9 (green) and propidium iodide (PI; red). The two stains (0.15 μL of each) were mixed on a vortex mixer, 100 μL of bacterial suspension (Escherichia coli ATCC 35218) was added and mixed, and the stock mixture was incubated for 15 minutes at 37 °C. A 10 μL sample of bacterial suspension-stain mixture was dropped over the cross-linked film and covered with a thin microscope slide. The sandwiched layers were left in contact under the microscope, and images were recorded in the fluorescence mode from zero to 600 seconds of contact time.

The SYTO 9 stain penetrates both healthy bacterial cells (with intact membranes) and non-healthy cells; it therefore dye both live and dead bacteria. Conversely, propidium iodide labels only bacteria with compromised membranes, thus decreasing the SYTO 9 fluorescence intensity. Consequently, live bacteria with intact membranes fluoresce green while dead bacteria (with disintegrated membranes) fluoresce red, while the background remains virtually non-fluorescent. Images were captured on a fluorescence microscope (Nikon Eclipse E600FN upright) with a digital camera (Nikon Photometrics Coolsnap EZ 12-Bit Monochrome Cooled CCD and NIS-ELEMENTS IMAGING Software) through a dual-band filter, so that bacteria

with healthy and disintegrated cell membranes could be visualized simultaneously.

4.2.6.2 Leaching property test.

For each of the three PPM compositions of Table 4.1, two columns were synthesized within microfluidic channels. The microchannels were then flushed with methanol, followed by DI water, to remove unreacted monomers and porogenic solvents. To investigate subsequent leaching from each PPM column, PBS buffer was flown through for one hour in one case, and for 24 hours in the other case. The PPM columns were then opened by cutting vertically through the monolith-filled X-PMMA channel with an electrical saw. The column material was removed by scraping and ground into a fine powder, mixed with KBr in a 1:30 weight ratio, and dried in a vacuum oven at 60 °C overnight. KBr pellets were prepared for analysis by pressing the powder in a dye at 10 kpsi for 3 minutes on a Carver 3851 Press (Thomas Scientific, Swedesboro, NJ). FT-IR spectra for each PPM column were acquired at room temperature on a Bruker Tensor 27 spectrometer, by averaging 64 scans recorded at a rate of 1 scan/sec. The wavenumber region scanned was between 400 and 4000 cm^{-1}.

To confirm leaching detected by FT-IR analysis, 100 μL of Escherichia coli bacterial suspension was pelletized at a relative centrifugal force (RCF) of 25500 (13000 RPM) for 3 minutes and re-suspended in 100 μL of the PBS buffer collected at the outlet of each PPM column after flowing through each column for 24 hours. It is worth mentioning that the PPM columns were first flushed with methanol, followed by DI water, to remove unreacted monomers and porogenic solvents before flowing the PBS buffer to ensure that there was no free monomer present before the leaching test. Using the serial dilution method each 100 μL sample was added, spread on solid agar dishes, and incubated at 37 °C for 24 hours.

4.2.6.3 Bacterial growth inhibition.

To investigate bacterial growth inhibition by the PPM networks, 4 mL of NB media, 10 μL of bacterial suspension (Micrococcus luteus (Schroeter) (ATCC 4698) or

Pseudomonas putida (ATCC 12633)) and a 0.5×1 cm^2 slice of a film corresponding to each of the PPM columns compositions of Table 4.1 were placed in glass test tubes and incubated overnight in a shaker (200 RPM, 37 °C). The positive controls were two tubes containing 4 mL of NB media and 10 μL of gram-negative bacteria (Pseudomonas putida) in one tube, and 10 μL of gram-positive (Micrococcus luteus) bacteria in the other tube. The negative control was a tube containing 4 mL of NB media.

4.2.7 Cell Lysis efficiency

The bacterial cell lysate collected at the microchip outlet after flowing the bacterial suspension through each of the PPM columns described in Table 4.1, at a flow rate of 4 μL/min and at cell concentrations as described in Appendix C, was used to study the cell lysis efficiency of the PPM columns.

4.2.7.1 DNA detection by fluorometry.

The ethidium bromide (EtBr) intercalation assay was used as an indicator of the presence of DNA in the cell lysate. A 20 μL aliquot of bacterial cell lysate was added to a spectrofluorometer cuvette containing 380 μL of DI water and 30 μL of EtBr from a stock solution with a concentration of 0.4 mg/L, and measured on a Quanta-Master 4 spectrofluorometer (Photon Technology International, London, ON Canada).

4.2.7.2 DNA concentration by UV-Vis spectrophotometry.

A 4 μL aliquot of PBS buffer was pipetted onto the end of a fiber optic cable (the receiving fiber) of a UV-Vis Spectrophotometer NanoDrop 2000c (Thermo Scientific, Mississauga, ON) to use as a blank (reference). Another cable was brought into contact with the sample to connect the sample with the fiber optic ends. Then a 4 μL sample of Pseudomonas putida (ATCC 12633), Escherichia coli (ATCC 35218), Micrococcus luteus (Schroeter) (ATCC4698) or Kocuria rosea (ATCC 186)

bacterial cell lysate was separately pipetted onto the receiving fiber to measure the DNA concentration in the lysates after flowing the cell suspensions through each of the PPM columns.

To examine the reusability of the PPM columns, a single microchip was reused 45 times and the cell lysis efficiency was determined each time that it was used. E. coli (ATCC 35218) bacteria were the species used in this test, in which they were suspended in PBS and was passed through the antibacterial monolith at a flow rate of 4 μL/min. The monolith was washed after each run with 25 μL of PBS buffer. To investigate the possibility of DNA carryover, the buffer used to flush the microfluidic channel was mixed with EtBr and the change in fluorescence intensity was recorded. Two control samples were used in these experiments: one containing 400 μL of DI water, and a second one containing 30 μL of EtBr (from a stock solution with a concentration of 0.4 mg/L), 380 μL of DI water, and 20 μL of PBS.

4.2.7.3 PCR reagents and experimental setup.

The PCR reaction was performed in a T100 Thermal Cycler (Bio-RD, Montreal, QC, Canada) in a 25 μL volume consisting of 300 nM of forward primer, 300 nM of reverse primer, 200 μM of dNTPs, 3.5 mM of magnesium chloride, 0.625 U of iTaq polymerase, 2.5 μL of 10X PCR buffer, and 200 ng of DNA present in the crude cell lysate collected at the outlet of the microchip. More details about the structure of the primers (Table C1) and the PCR cycle are provided in Appendix C.

4.2.7.4 Gel electrophoresis.

A Bio-Rad gel electrophoresis apparatus served to analyze the PCR products on 1.2% agarose gel using a DC voltage of 85 V and operating time period of 30 minutes. The gel was subsequently detached from the apparatus cavity and was imaged with a Bio-Rad Doc XR imaging system.

4.3 Results and discussion

4.3.1 Monolith formation, characterization and stability

4.3.1.1 Monolith formation.

The chemical structure of the three PPM columns investigated in this chapter is provided in Fig. C1 of the Appendix C. Also ATR-FTIR spectra for DADMAC (powder), poly(DADMAC-*co*-EDGA), poly(DADMAC-*co*-1,6-HDDMA), and poly(DADMAC-*co*-EGDMA) cross-linked networks is shown in Fig. C2 of the Appendix C. It is noteworthy that none of the functional cross-linking monomer combinations of Table 4.1 could be fully dissolved in commonly used porogenic solvents of cyclohexanol and 1-dodecanol, thus several alternate solvents were investigated. Since it was reported that methanol could serve as porogenic solvent to create a porous network [90, 91], that solvent was investigated and found to be suitable for that purpose. It is also worth mentioning that several compositions (functional, cross-linker and solvent wt%) to form the PPM column were tried, but only with the composition listed in Table 4.1, a homogeneous mixture was formed and a cohesive stable structure for the PPM column was polymerized within the microfluidic channel.

4.3.1.2 Monolith characterization

The SEM images obtained for the PPM columns with different cross-linking monomers are shown in Fig. 4.1. For the images on the right, the microchips were incubated at 45 °C for 20 minutes prior to introducing the PPM mixture in the microfluidic channel and starting the polymerization. Looking at Fig. 4.1, it can be noted that the poly(DADMAC-*co*-EDGA) PPM column is less porous than the poly(DADMAC-*co*-EGDMA) and poly(DADMAC-*co*-1,6-HDDMA) PMM columns. This result implies that the cross-linker structure affects the porosity of the PPM columns, in agreement with the findings reported by Ranjha *et al.* [96]. It can also be seen that the PPM columns on the right are denser than the ones on the left. This effect

is caused by the pre-heating of the microchip prior to polymerization. Nischang *et al.* indeed investigated the influence of temperature on the polymerization kinetics, which directly affected the morphology of monolith surface, and as a result the porosity of the monolith [95]. Thus the variations in PPM morphology and porosity seen in the SEM images on the right are in agreement with the results reported by

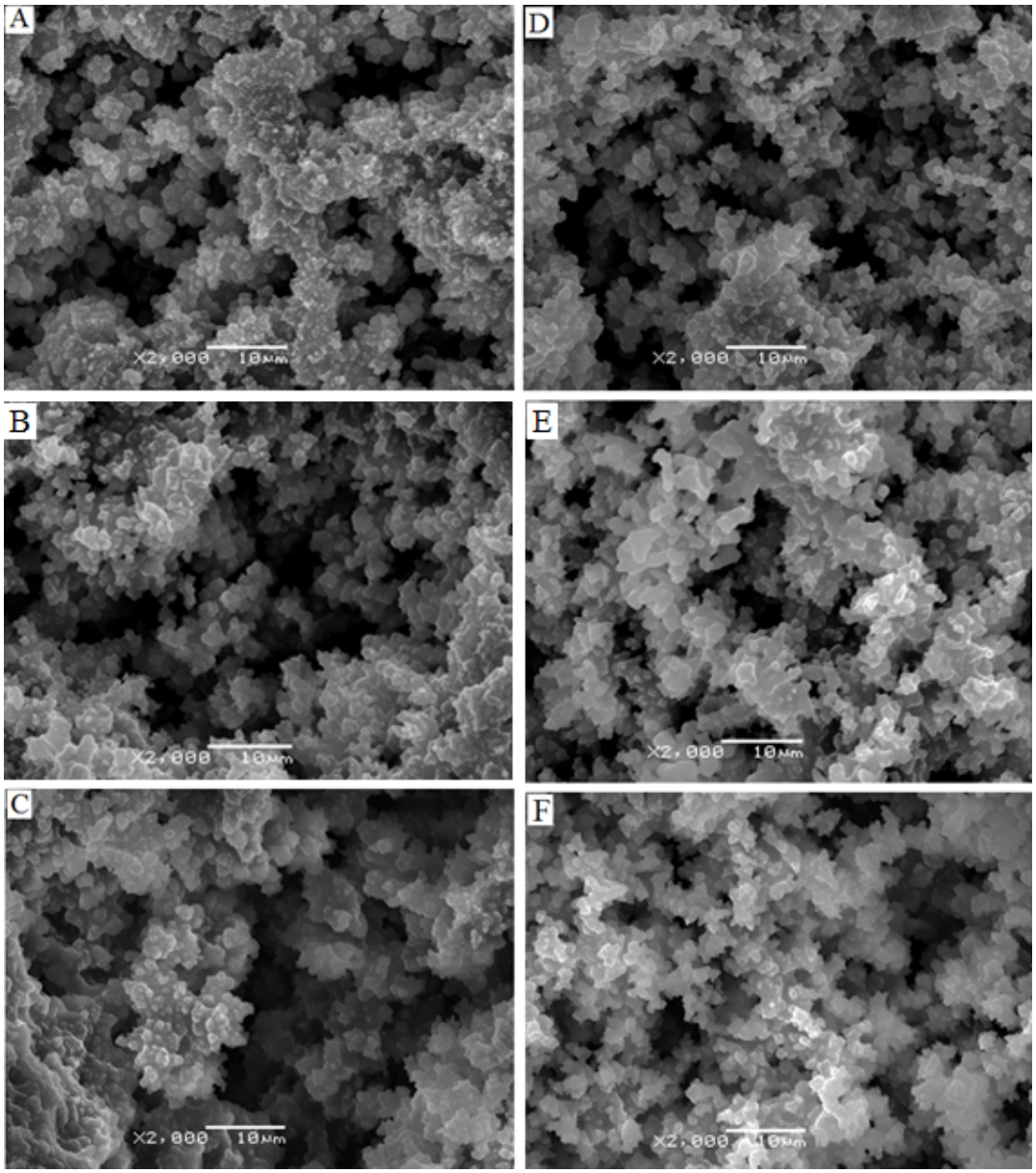

Figure 4.1: SEM images for the monolithic columns: (A), (B) and (C) are EGDMA, 1,6-HDDMA and EGDA-PPM, respectively; (D), (E) and (F) are EGDMA, 1,6-HDDMA and EGDA-PPM formed in the pre-heated microchip, respectively.

Table 4.2: Pore diameter and porosity of the PPM columns determined by Hg intrusion porosimetry.

PPM	Median pore diameter (μm)	Porosity (%)
Poly(DADMAC-*co*-EGDMA)	5.5	75
Poly(DADMAC-*co*-1,6-HDDMA)	4.8	71
Poly(DADMAC-*co*-EGDA)	4.0	66

Nischang *et al.* The pore size and porosity of the PPM columns were determined by mercury intrusion porosimetry to clarify and confirm the SEM results. Porosimetry results for the three PPM columns are provided in Table 4.2. It can be seen that the porosimetry results are in agreement with the visual observations of the SEM images, confirming that the poly(DADMAC-*co*-EDGA) PPM column is less porous than the poly(DADMAC-*co*-EGDMA) and poly(DADMAC-*co*-1,6-HDDMA) PPM columns. A lower porosity may lead to more pronounced mechanical shearing of the cell membranes during their flow through the pores of the PPM column.

4.3.1.3 Monolith stability.

To confirm bonding between the PPM column and the X-PMMA substrate, and to quantify the bonding strength between the two substrate layers, pressure tests were conducted. The pressure withstood by the PPM column before it started to debond from the substrate and to move along the channel (as determined by visual inspection) is provided in Fig. 4.2 for the three PPM compositions studied in combination with X-PMMA substrates having 3, 5, 10, 15 and 20% cross-linker contents. From Fig. 4.2 it can be seen that the three lines have positive slopes, which indicates that bonding or anchoring of the PPM column material to the substrate was improved as the cross-linking level of the substrate increased. Furthermore, the EGDA-cross-linked monolithic columns had stronger bonding to the substrate than the 1,6-HDDMA and EGDMA-cross-linked columns. The experiments performed to obtain Fig. 4.2 were repeated three times and the results shown are the average of these results for each PPM. The standard deviation on the values obtained with each cross-linker are displayed as error bars on Fig. 4.2.

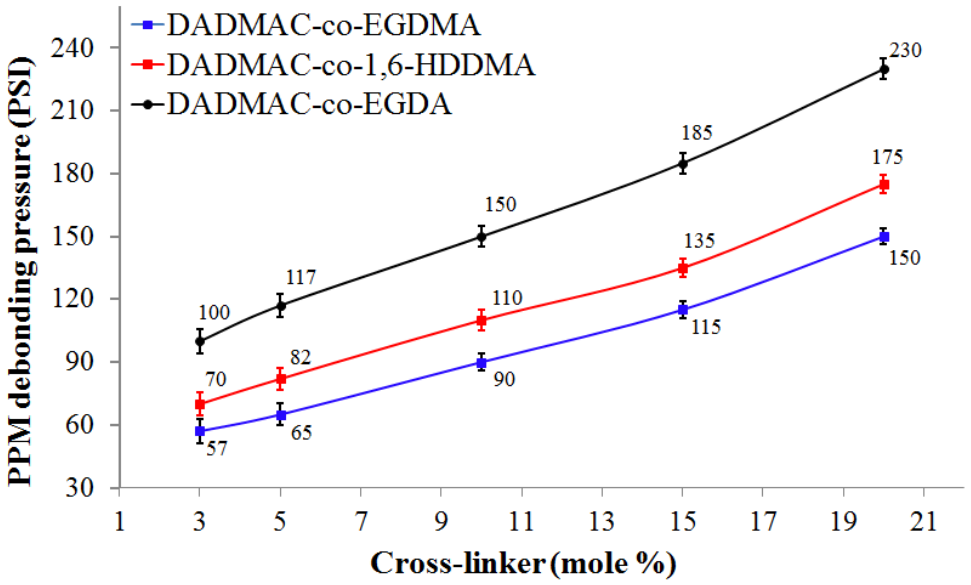

Figure 4.2: Debonding pressure of the monolithic columns from the substrates for different X-PMMA cross-linking levels and different PPM compositions.

The substrate debonding pressure, at which the two substrate layers started to locally debond and leak, was observed at the interface, is provided in Fig. 4.3. It can be seen that the curve has a negative slope, which indicates that bonding between the two substrate layers worsens as the cross-linking level increases. By comparing Fig. 4.2 and Fig. 4.3, it can be concluded that EGDA-cross-linked monolithic columns with either the 10% or 15% X-PMMA substrate offers acceptable bonding between the PPM and the substrate, and between the two substrate layers. The experiments performed to obtain Fig. 4.3 were repeated three times and the results shown are the average of these results for each cross-linker content, and the standard deviation on the values obtained are displayed as error bars.

4.3.2 Antibacterial, Leaching and growth inhibition tests

4.3.2.1 Antibacterial activity.

Bacteria viability was monitored by the double staining technique described in Section 4.2.6.1. The green fluorescence was gradually replaced with red fluorescence in these experiments, as shown in Fig. 4.4 A-D, providing clear evidence for membrane

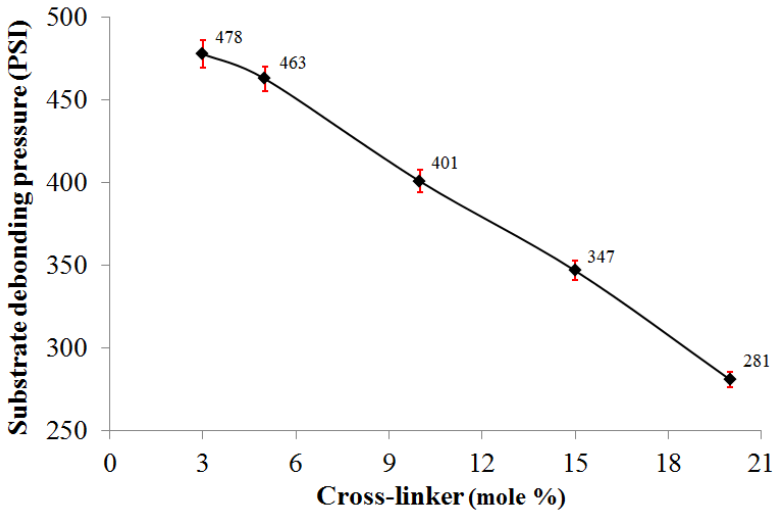

Figure 4.3: Debonding pressure for the two substrate layers at different X-PMMA cross-linking levels.

disintegration. It can be observed that the X-PMMA substrates grafted with the poly(DADMAC-*co*-EGDA) film led to more predominant red fluorescence than the substrates grafted with either poly(DADMAC-*co*-1,6-HDDMA) or poly(DADMAC-*co*-EGDMA) films, respectively. This implies that the poly(DADMAC-*co*-EGDA) film has a higher antibacterial activity than the poly(DADMAC-*co*-1,6-HDDMA) and poly(DADMAC-*co*-EGDMA) films.

The red and green fluorescence intensities were recorded for up to 600 sec., as shown in Fig. 4.5. For the substrates grafted with the antibacterial films the green and red intensities decreased and increased with time, respectively, reflecting the fact that the cell membranes gradually became permeable, thus allowing PI to penetrate the cell membrane and reduce the fluorescence intensity for SYTO 9.

This provides clear evidence that the substrates with the grafted cross-linked films are antibacterial. In contrast to the grafted substrates, the green and red fluorescence intensities for the control sample (pristine X-PMMA film) remained almost constant, reflecting the fact that no antibacterial activity was observed in that case. It can be also observed from Fig. 4.5 that the rate of variation of the green and red fluorescence intensities for the three grafted substrates agree with the visual results of Fig. 4.4.

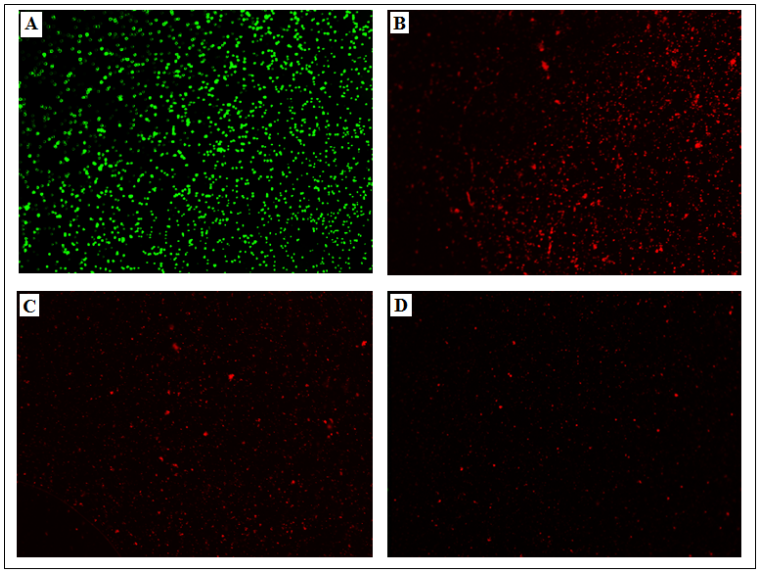

Figure 4.4: Fluorescence intensities for E. coli suspended in PBS buffer and stained with live/dead dye in contact with (A) the three antibacterial networks at time zero, (B) Poly(DADMAC-*co*-EGDA), (C) Poly(DADMAC-*co*-1,6-HDDMA) and (D) Poly(DADMAC-*co*-EGDMA) after 600 second.

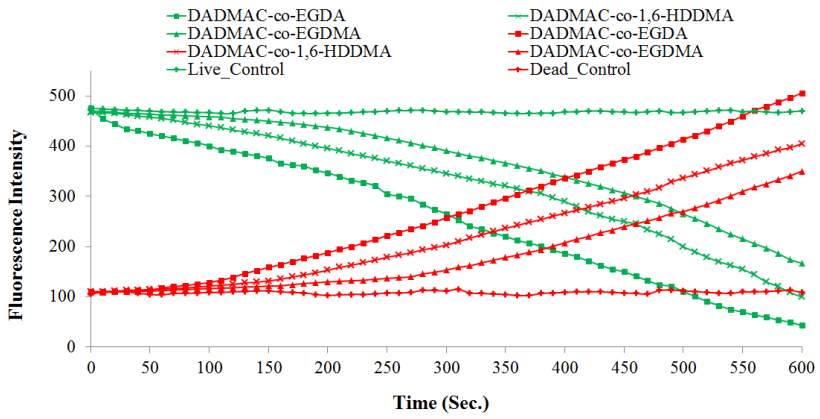

Figure 4.5: Green (live) and red (dead) stain intensity variation with the contact time for poly(DADMAC-*co*-EGDA), poly(DADMAC-*co*-1,6-HDDMA) and poly(DADMAC-*co*-EGDMA) networks.

4.3.2.2 Leaching property test.

Leaching of DADMAC from the poly(DADMAC-*co*-EGDA), poly(DADMAC-*co*-1,6-HDDMA) and poly(DADMAC-*co*-EGDMA) monolithic columns was studied using FT-IR after flushing them with PBS buffer for either one or 24 hours. FT-IR spectra for the poly(DADMAC-*co*-EGDA) PPM column after 24 hours (Fig. 4.6)

shows that the peak for DADMAC in the cross-linked network was essentially unchanged in A and B, indicating that no significant leaching of DADMAC or poly(DADMAC) occurred. In contrast, the FT-IR peak absorption decreased for the poly(DADMAC-*co*-1,6 HDDMA) PPM column, while the effect was even more pronounced for the poly(DADMAC-*co*-EGDMA) PPM column.

To confirm the results obtained in the leaching test, E. coli bacteria were re-suspended in the PBS buffer collected at the outlet of each PPM in the 24 hours leaching test, applied onto solid agar dishes and then incubated at 37 °C. The

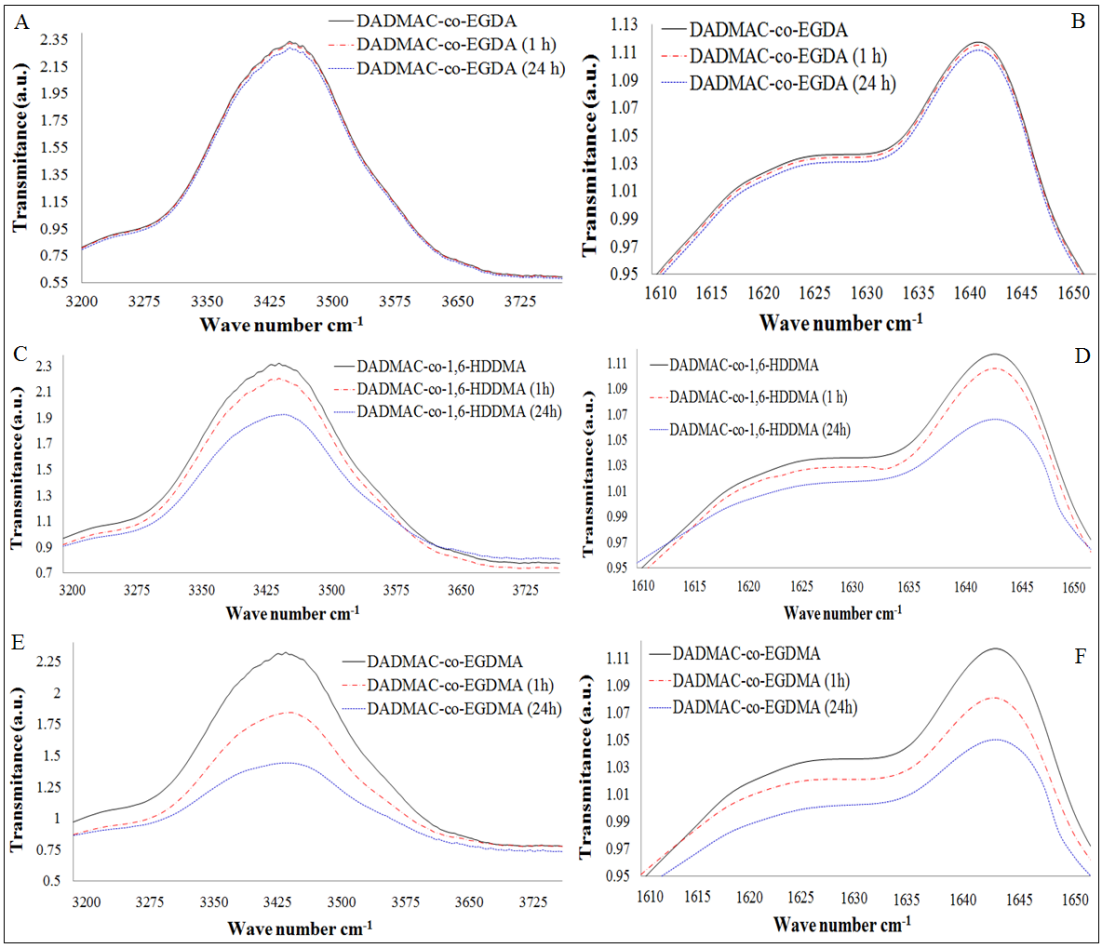

Figure 4.6: FT-IR spectra for the N-H stretching absorbance of the unsaturated primary amine groups (right) and C-N stretching vibration in the secondary amine group followed by NH bend (left) of (A, B) poly(DADMAC-*co*-EGDA), (C, D) poly(DADMAC-*co*-1,6-HDDMA), and (E, F) poly(DADMAC-*co*-EGDMA) before (black line), after 1 hour (red line) and after 24 hours (blue line) of washing with PBS.

colonies obtained on agar after 24 hours of incubation are shown in Fig. 4.7. No colony was produced for the cells suspended in the PBS buffer collected for the poly(DADMAC-*co*-EGDMA) PPM column (as shown in Fig. 4.7C), indicating that extensive leaching took place. In contrast, the plate for cells suspended in the PBS buffer collected in the leaching test for the poly(DADMAC-*co*-EGDA) PPM column has a large number of colonies on it, while the dish for the poly(DMAMS-*co*-1,6 HDDMA) PPM column has fewer colonies on it in comparison to the control dish. These results are in agreement with those obtained in the leaching tests. It is evident that the poly(DADMAC-*co*-EGDMA) PPM column suffered from extensive leaching, while the poly(DADMAC-*co*-EGDA) PPM displayed very moderate

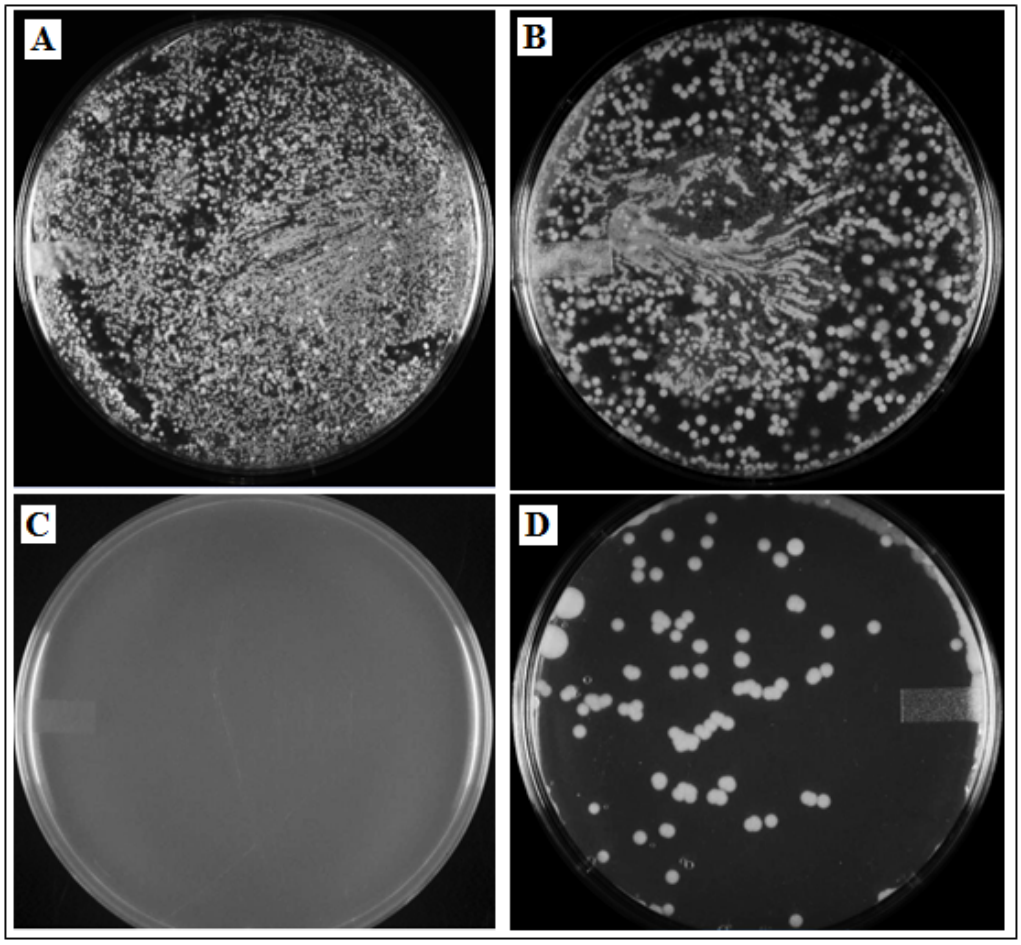

Figure 4.7: Colonies produced on agar after the 24 hours leaching tests for (A) control, (B) poly(DADMAC-*co*-EGDA), (C) poly(DADMAC-*co*-EGDMA), and (D) poly(DADMAC-*co*-1,6-HDDMA).

leaching. The agar leaching experiment was repeated three times to confirm the results shown in Fig. 4.7.

4.3.2.3 Growth inhibition test.

The bacterial growth inhibition ability of the PPM column materials for gram-negative (ATTC 12633) and gram-positive (ATCC 4698) bacteria is illustrated in Fig. 4.8. The gram-negative and gram-positive control samples (Fig. 4.8A and B, respectively) show healthy growth, with optical density values at 600 nm, OD_{600} = 2.38 and 2.012, respectively. In contrast, the same gram-negative and gram-positive bacterial samples exposed to strips of poly(DADMAC-*co*-EGDA), Fig. 4.8C and D, poly(DADMAC-*co*-1,6-HDDMA), Fig. 4.8E and F, or poly(DADMAC-*co*-EGDMA), Fig. 4.8G and H, show major signs of growth inhibition with OD_{600} = 0.013, 0.019, 0.025, 0.030, 0.033, 0.039, respectively. These results further validate the ability of the PPM column materials to inhibit gram-negative and gram-positive bacterial growth.

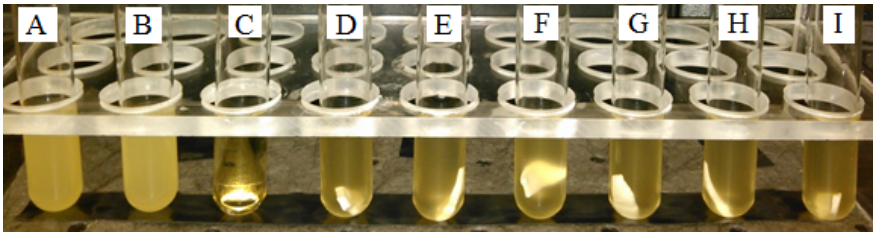

Figure 4.8: Bacterial growth inhibition for (A and B) positive controls (gram-negative, ATTC 12633 and gram-positive, ATCC 4698 bacteria overnight cultured in nutrient broth (NB) and trypticase soy broth (TSB), respectively), (C) negative control (NB media), (D and E), (F and G), and (H and I) gram-positive and gram-negative bacteria overnight cultured in TSB and NB media, respectively, and $0.5 \times 1\ cm^2$ strip of poly(DADMAC-*co*-EGDMA), poly(DADMAC-*co*-EGDA), and poly(DADMAC-*co*-1,6-HDDMA) monolith films, respectively.

4.3.3 Cell Lysis efficiency of the PPM columns

4.3.3.1 DNA detection by fluorometry.

To determine semi-quantitatively the DNA released after lysing the bacterial cells by flowing them through the antibacterial porous medium of the three PPM columns with the different compositions, the EtBr intercalation assay was used to detect DNA in the cell lysate. When EtBr is exposed to UV light at 285 nm it fluoresces with an orange color at 595 nm, but the emission intensifies considerably after its intercalation in DNA. The fluorescence intensity for EtBr before (control) and after intercalation in the DNA present in the cell lysate collected at the outlet of the porous antibacterial monoliths (1-3) was measured on a spectrofluorometer to obtain Fig. 4.9. The figure shows that the fluorescence intensity of EtBr increased dramatically when adding the cell lysate collected from the porous monolith columns, as compared to the control sample. It can be observed from Fig. 4.9 that the fluorescence intensity for EtBr is higher for gram-negative bacteria (ATCC 12633, ATCC 35218) as compared to the gram-positive bacteria (ATCC 4698 and ATCC 186), which implies that more DNA is present in the gram-negative bacterial cell lysate. This is because gram-positive bacteria are harder to lyse than gram-negative bacteria, due to differences in the bacterial cell membrane structure for both bacterial species as shown in Fig. 1.1. The results also show that the fluorescence intensity of EtBr is slightly different among the two different gram-positive and two gram-negative bacterial species, which could be due to size differences among the studied species as it can be seen in Table 4.3. It can be further seen that the poly(DADMAC-*co*-EGDA) PPM column has a higher lysis efficiency than the poly(DADMAC-*co*-1,6-HDDMA) and poly(DADMAC-*co*-EGDMA) PPM columns. By recalling the results observed from Fig. 4.1, Table 4.2, Fig. 4.4 and Fig. 4.5 showing that poly(DADMAC-*co*-EGDA) is less porous and has a higher antibacterial activity than poly(DADMAC-*co*-1,6-HDDMA) and poly(DADMAC-*co*-EGDMA), this confirms that lysis was achieved by a combination of mechanical shearing and antibacterial activity resulting from interactions with the cell mem-

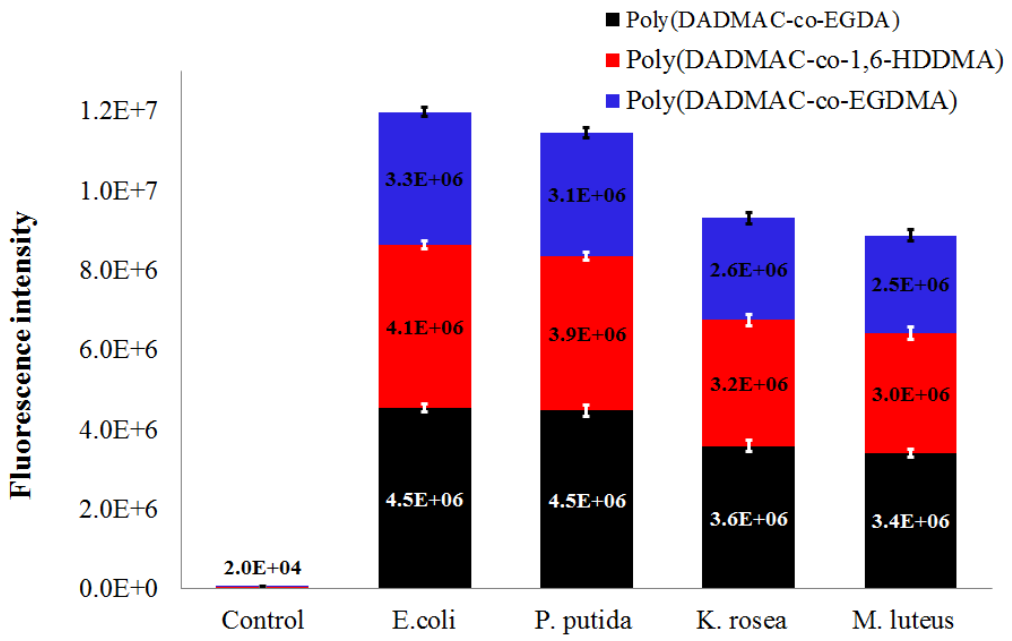

Figure 4.9: Fluorescence intensity for EtBr before (control) and after intercalation into the DNA released after flowing the bacterial cells through the different PPM columns.

Table 4.3: The length and diameter of the used bacterial cells

	K. rosea [70]	M. luteus [71]	P. putida [72]	E. coli [67]
Length μm	-	-	1.5-5	1-3
Diameter μm	1-1.8	0.5-3.5	0.5-1	0.5

brane, as reported previously by Aly Saad Aly *et al.* [63, 97]. The experiments performed to obtain Fig. 4.9 were repeated three times, and the results shown are the average of these experiments for each PPM. The standard deviation on the values obtained for each PPM is displayed as error bars on Fig. 4.9. To this end, it has been shown that poly(DADMAC-*co*-EGDA) PPM column is more mechanically stable, leaching less, inhibit the bacterial growth, and has more lysis efficiency than poly(DADMAC-*co*-1,6-HDDMA) and poly(DADMAC-*co*-EGDMA) PPM columns, thus the PCR followed by gel electrophoresis and reusability test will be run for poly(DADMAC-*co*-EGDA) PPM column. Table C2 summarizes the dimensions of the channel and pore information of the poly(DADMAC-*co*-EGDA) PPM column formed into the microfluidic channel.

To investigate the cell lysis efficiency of the developed antibacterial PPM column at different cell concentrations, cell suspension with four different concentrations (10^2, 10^3, 10^4 and 10^5 CFU/ml) were prepared and flown in the poly(DADMAC-*co*-EGDA). The fluorescence intensity of EtBr before (control) and after intercalating with the DNA present in the cell lysate at the studied four cell concentrations are presented in Fig. 4.10. It is clearly notable that the fluorescence intensity increase linearly with increasing the cell concentration. It is also observable that even at 10^2 CFU/ml, there is measurable DNA released out of the cells as a result of cell lysis. This validates the ability of the developed antibacterial PPM column to lyse bacterial cells at cell concentration as low as 10^2 CFU/ml.

4.3.3.2 DNA concentration by UV-Vis spectrophotometry.

To further validate cell lysis, the concentration of DNA released from the bacterial cells after flowing through the porous medium of the PPM columns was quantified by UV-Vis spectrophotometry as shown in Fig. 4.11. It is evident from these results

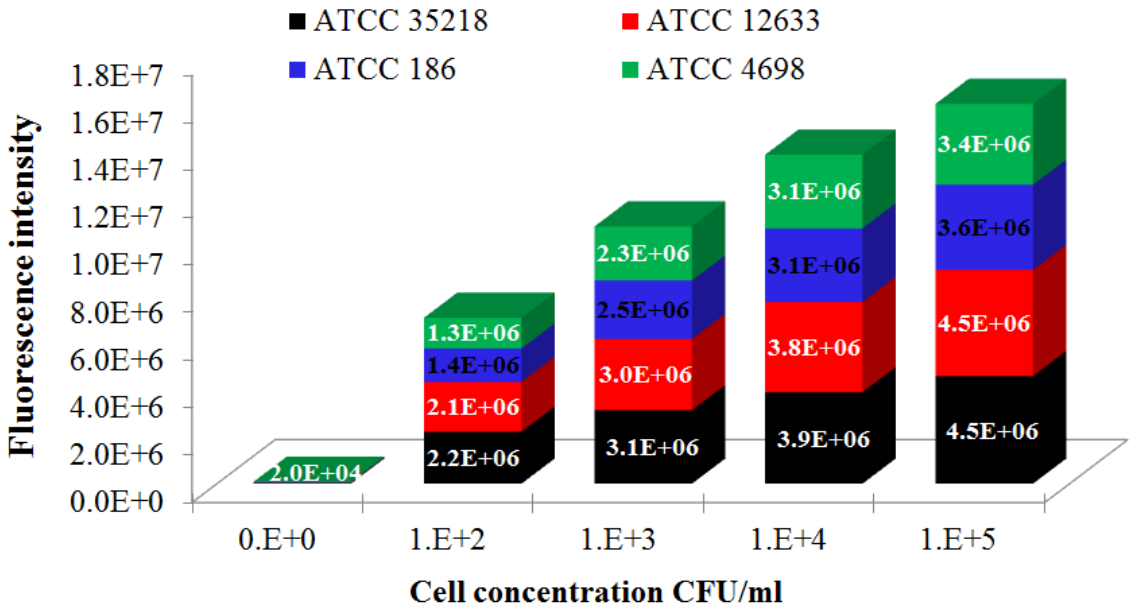

Figure 4.10: Fluorescence intensity of EtBr before (control) and after intercalating into the DNA released from bacterial cells flowing through the microfluidic channels hosting the poly(DADMAC-*co*-EGDA) PPM column at different cell concentrations.

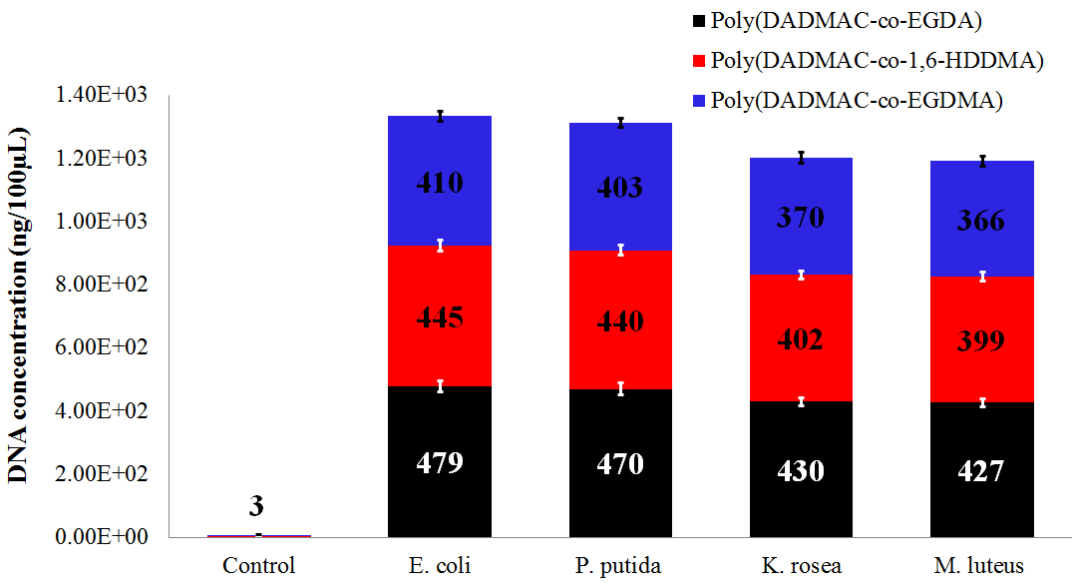

Figure 4.11: Absolute concentration of DNA present in unlysed cells (control) and in the crude cell lysates collected at the outlet of the three PPM columns.

that the DNA concentration in the gram-negative (ATCC 12633 and ATCC 35218) bacterial cell lysates was greater than for the gram-positive (ATCC 4698 and ATCC 186) cell lysates. One can also note again that the DNA concentration varies slightly among both the gram-negative and gram-positive bacterial cell lysates. The results further show that the poly(DADMAC-*co*-EGDA) PPM has a higher lysis efficiency than the poly(DADMAC-*co*-1,6-HDDMA) and poly(DADMAC-*co*-EGDMA) PPM columns. The results presented in Fig. 4.11 are in agreement with those shown in Fig. 4.9. The experiments to obtain Fig. 4.11 were repeated three times and the results shown are the average values obtained for each PPM. The standard deviation on the values obtained for each PPM is displayed as error bars on Fig. 4.11. By looking at Fig. 4.12, one can see that the result presented agree with the results shown in Fig. 4.10, which further confirm the ability of the antibacterial monolithic column to efficiently lyse gram-negative and gram-positive bacterial cells at different cell concentrations.

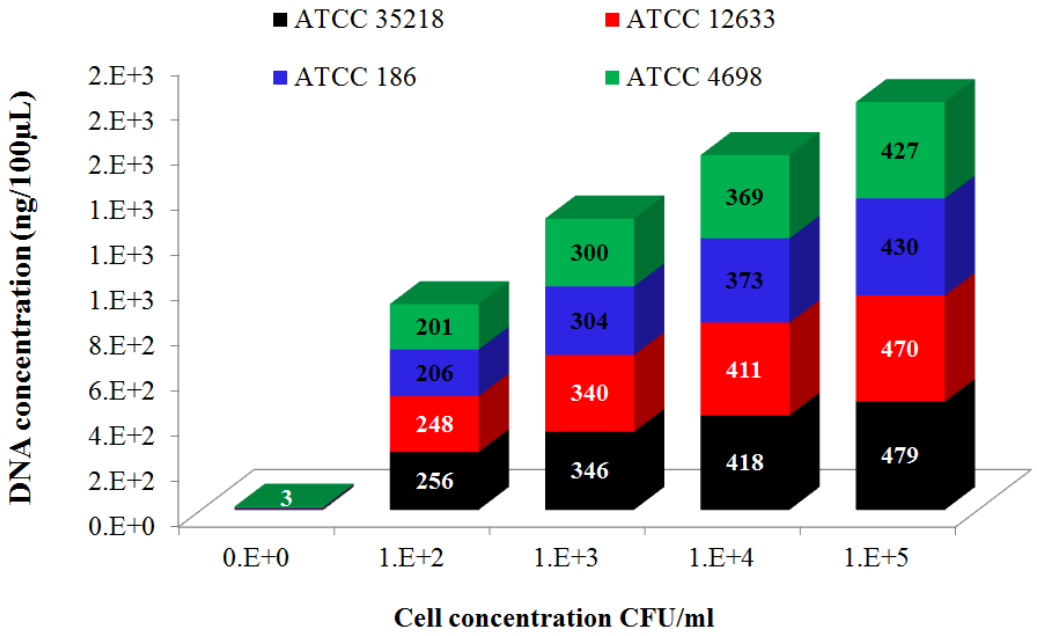

Figure 4.12: Absolute concentration of DNA present in the crude cell lysate collected at the outlet of the outlet of the poly(DADMAC-*co*-EGDA) PPM column at different cell concentrations.

4.3.3.3 PCR and gel electrophoresis

The genes in the DNA released by lysing the bacterial cells on the poly(DADMAC-*co*-EGDA) PPM column were amplified by off-chip PCR and qualitatively validated by gel electrophoresis. The analysis results are shown in Fig. 4.13 for the PCR products of the different bacterial species investigated. There are no detectable amounts of DNA at the PCR output for bacteria samples that were not lysed in poly(DADMAC-*co*-EGDA) PPM column, which shows that the cells had intact membranes before passing through the column. In contrast, DNA is clearly detected at the PCR output for the samples passed through the PPM column, which confirms that the membrane of the bacterial cells was disintegrated. This is a clear sign for lysis, but also demonstrates that the antibacterial PPM did not interfere with the PCR process.

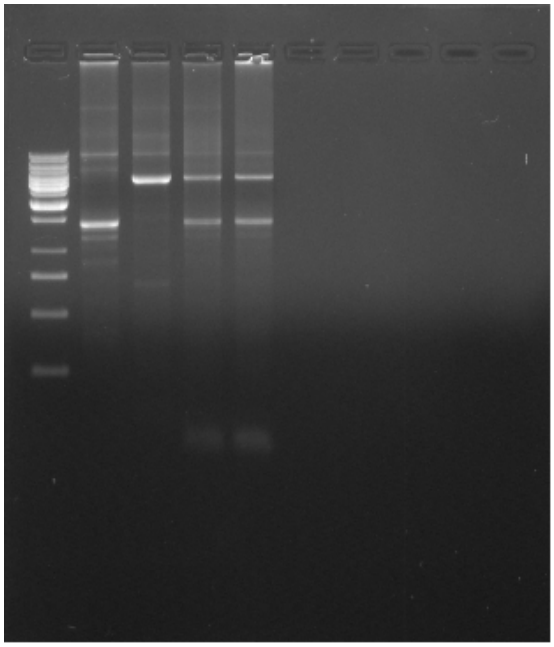

Figure 4.13: Gel electrophoresis analysis of PCR output. Column 1 (from the left) is for a 100 bp DNA ladder. Columns 2 and 6: lysed and unlysed ATCC 35218. Columns 3 and 7: lysed and unlysed ATCC 186. Columns 4 and 8: lysed and unlysed ATCC 12633. Columns 5 and 9: lysed and unlysed ATCC 4698.

4.3.4 Reusability of the biochip

The change in EtBr fluorescence due to its intercalation into DNA in the cell lysate after each use of the microchip, when using a PBS wash between cycles, is shown in Fig. 4.14. It can be seen that the lysis efficiency is reasonably stable, with a slight linear decrease over successive runs. After the thirtieth use, the lysis efficiency degrades dramatically and finally saturates after the fortieth use. It should be mentioned that the monolith was completely blocked and degraded after 45 cycles. The microchip is therefore reusable, with acceptable degradation in the lysis efficiency (9% decrease) for up to 30 cycles. The fluorescence intensity measured for EtBr mixed with the PBS washings recovered from the microfluidic channel in the back-flush cycles showed insignificant DNA carry over, reaching only 0.4% of the maximum EtBr intensity reported, as shown in Table C3 of the Appendix C. It is interesting to note that the PPM column of Fig. 4.14 can be reused for 10 more cycles than the optimized deprotected poly (n-butyl methacrylate-*co*-

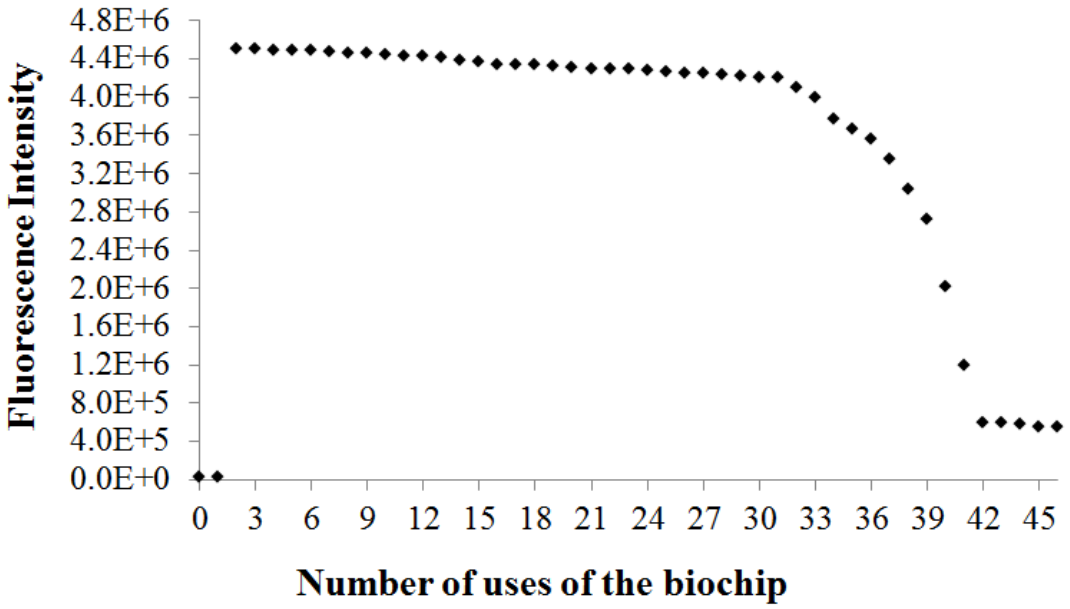

Figure 4.14: Fluorescence intensity for EtBr intercalated into the DNA released from bacterial cells flowing through the antibacterial poly(DADMAC-*co*-EGDA) PPM at a flow rate of 4 L/min over successive runs

N-(tert-butyloxycarbonyl)aminoethyl methacrylate), Boc-PPM, column previously presented in Chapter 3 and with less DNA carryover. The antibacterial PPM column presented in this work also does not require activation or regeneration by flowing phosphoric acid as presented in Chapter 3 thus leading to shorter lysis cycles or increased throughput.

4.4 Conclusions

Microfluidic biochips fabricated with a 10% X-PMMA substrate have the ability to inhibit the growth, kill, and efficiently lyse two species of gram-positive bacteria: Micrococcus luteus (Schroeter) (ATCC 4698) and Kocuria rosea (ATCC 186), and two species of gram-negative bacteria: Pseudomonas putida (ATCC 12633) and Escherichia coli (ATCC 35218). The lysis ability of the microchip was validated using the ethidium bromide intercalation assay, relating the presence of DNA in the cell lysate with an increase in fluorescence intensity for EtBr, and UV-Vis spectrophotometry to directly determine the DNA concentration in the cell lysate. Gel

electrophoresis analysis of the PCR products after DNA gene amplification of the cell lysate showed that poly(DADMAC-*co*-EGDA) PPM columns do not leach any material that inhibits the PCR process. The influence of the cross-linking monomer on bacterial growth inhibition, leaching, the lysis efficiency of the monolithic column and its mechanical stability within the microfluidic channel were investigated using three different cross-linking monomers: ethylene glycol diacrylate (EGDA), ethylene glycol dimethacrylate (EGDMA) and 1,6-hexanediol dimethacrylate (1,6-HDDMA) at different cross-linking levels of the X-PMMA substrate. Furthermore, the bonding efficiency of the X-PMMA substrate layers at different cross-linking levels was studied. It was shown that the microchips can be reused for at least 30 times without significant performance degradation or carryover when they are flushed between cycles. It was concluded that the lysis time is shorter and the number of reuse cycles increased for microchips based on the quaternary ammonium antibacterial PPM developed in this work, in comparison to the microfluidic biochips based on the optimized deprotected antibacterial, poly (n-butyl methacrylate-*co*-N-(tert-butyloxycarbonyl)aminoethyl methacrylate), Boc-PPM columns presented in Chapter 3.

Chapter 5

Conclusion and Future Work

In this chapter, the most significant findings in this thesis are summarized and discussed. In this thesis, a novel reagentless cell lysis technique based on antibacterial porous polymeric monolith (PPM) column is introduced. There are two PPM columns (Boc-protected PPM and QAC PPM) were synthesized, characterized, optimized and tested for their antibacterial activity and cell lysis efficiency. Also, their mechanical stability and their ability to be reused were studied.

5.1 Contributions

The scientific contributions of this dissertation are:

1. The application of PPM columns as an effective tool for bacterial cell lysis within microfluidic chips is demonstrated in this dissertation. By exploiting the expansive surface area and controllable pore size inalienable to PPM, a double mechanism (mechanical-shear/antibacterial contact-killing) cell lysis technique is developed. The bacterial cell wall is mechanically sheared by flowing bacterial suspension through the porous medium of the PPM column (mechanical-shear lysis), but it is also damaged and disintegrated by physical contact with the antibacterial polymeric biocide covering the porous surface (antibacterial contact-killing lysis). This leads to leakage of the intracellular contents.

2. The use of cross-linked poly(methyl methacrylate) as a substrate for microfluidic channel that covalently bonds with the monolithic column through the unreacted C=C double bonds dangling on the surface of poly(methyl methacrylate-*co*-ethylene glycol dimethacrylate), poly(MMA-*co*-EGDMA) is demonstrated in this dissertation. This approach contributes to the mechanical stability of the biochip and eliminates the need of surface functionalization to create a bonding intermediate layer between the substrate and the PPM column.

3. A method of ablating microfluidic channels in poly(MMA-*co*-EGDMA) substrate using a 30W, 1.6 μm CO_2 excimer laser system was presented. Although this technique has poorer resolution compared to the conventional microetching techniques, it is well-controlled, high-throughput, more time and cost effective, safer and easier to handle.

4. The developed cell lysis biochips do not require any chemical and/or enzymatic reagents, power consumption, or complicated design and fabrication processes, which makes it an attractive on-chip lysis device that can be used in sample preparation for bio-genetics and point-of-care diagnostics.

5. PPM columns with antibacterial surfaces polymerized within 20% poly(MMA-*co*-EGDMA) microfluidic chips were prepared to form antibacterial amphiphilic porous cationic structures that belong to the SMAMPs antibacterial polymer family. The antibacterial PPM columns are fabricated by *in situ* photo-initiated free radical copolymerization of n-butyl methacrylate (BuMA) and N-(tert-butyloxycarbonyl) aminoethyl methacrylate (Boc-AEMA), cross-linked with ethylene glycol dimethacrylate (EGDMA) in the presence of porogenic solvents, 1-dodecanol and cyclohexanol, and photoinitiator, 2,2-dimethoxy-2-phenylacetophenone (DMPAP).

The lysis efficiency of the Boc-protected PPM based bio-chip was optimized by investigating and analyzing the influence of the flow-rate when pumping the bacterial suspension through the monolith. Furthermore, the effect of the hydrophobicity of the monoliths on the antibacterial property of the monolithic column was studied by comparing the results of eleven different compositions of the monolith mixture

at a cell concentration of 10^5 CFU/ml. The lysis efficiency of the biochips was shown to be better when compared to traditional off-chip chemical, mechanical, and thermal lysis techniques. The cell lysis efficiency of the developed antibacterial PPM column was verified at different cell concentration ranged from 10^2 to 10^5 CFU/ml.

The antibacterial PPM column synthesized within microfluidic channel was used for 20 successive cycles without any evidence of physical damage to the monolith, significant performance degradation or DNA carryover when they were back-flushed between cycles. The PPM also acts as a filter that isolates cell debris and allows PCR-amplifiable DNA to pass through. The biochips efficiently lysed two gram-positive: Enterococcus saccharolyticus (ATCC 43076) and Bacillus subtilis and two gram-negative: Escherichia coli and Pseudomonas fluorescens (ATCC 13525) bacteria.

6. PPM columns with antibacterial surfaces formed within 10% poly(MMA-*co*-EGDMA) microfluidic chips were prepared. The antibacterial PPM columns were fabricated by *in situ* photo-initiated free radical copolymerization of quaternary ammonium compound, diallyldimethylammonium chloride (DADMAC), and ethylene glycol diacrylate (EGDA) in the presence of photo-initiator, 2,2-dimethoxy-2-phenylacetophenone (DMPAP), and porogenic solvent, methanol.

The influence of the cross-linker monomer on bacterial growth inhibition, leaching property, lysis efficiency of the monolithic column and its mechanical stability within the microfluidic channel were investigated and analyzed by trying three different cross-linker monomers: ethylene glycol dimethacrylate (EGDMA), ethylene glycol acrylate (EGDA) and 1,6-hexanediol dimethacrylate (1,6-HDDMA). Furthermore, the bonding efficiency of the two X-PMMA substrate layers at different cross-linking percentage of the poly(MMA-*co*-EGDMA) was studied.

The QAC monolithic columns are shown to be stable, non-leaching and can be reused for over 30 lysis-cycles without any evidence of physical damage to the monolith, significant performance degradation or DNA carryover when they are

back-flushed between cycles.

The QAC monolithic columns possess the ability to inhibit the growth, kill and efficiently lysis two gram-positive: Micrococcus luteus (Schroeter) (ATCC 4698) and Kocuria rosea (ATCC 186) and two gram-negative: Pseudomonas putida (ATCC 12633) and Escherichia coli (ATCC 35218) bacterial cells at cell concentration ranged from 10^2 to 10^5 CFU/ml.

5.2 Advantage, disadvantage and constraints

Table 5.1 summarizes the advantage, disadvantage and constraints of the work presented in this thesis.

5.3 Conclusion

A novel, reagentless, reusable, stable microchip based on antibacterial non-leaching monolithic columns polymerized in poly(MMA-*co*-EGDMA) microfluidic channels for on-chip cell lysis applications was developed in this dissertation. The lysis efficiency of the biochips was shown to be better when compared to traditional off-chip chemical, mechanical, and thermal lysis techniques. The biochips do not require chemical and/or enzymatic reagents, power consumption, or complicated design and fabrication processes. The DNA present in the cell lysate produced by lysing bacterial cell with the developed cell lysis technique is ready to be used in PCR with no further purification and/or filtration. These facts make the developed biochip an attractive on-chip lysis device that can be integrated in sample preparation lab-on-chip for bio-genetics and point-of-care diagnostics. The developed biochips are shown to be stable, non-leaching and can be reused for 20-30 lysis cycles without any evidence of physical damage to the PPM, significant performance degradation or DNA carryover when they are back-flushed between cycles. Two antibacterial PPM columns were formed in microfluidic channels to lyse bacterial cells via continuous microfluidic flow: antibacterial PPM column based on optimized Boc-

Table 5.1: The advantage, disadvantage and constraints of the work presented in this thesis.

Advantage	1. The substrate surface (cross-linked PMMA) intrinsically has dangling C=C double bonds, thus further surface modification prior to form the PPM in order to establish good anchoring with the PPM surface is not required. 2. The microchip was fabricated by well-controlled, time and cost efficient, and high-throughput laser micromachining. 3. The lysis technique does not require chemical/enzymatic reagents, power consumption, or complicated design and fabrication processes, which makes it an attractive onchip lysis process that can be used in sample preparation for bio-genetics and point-of-care diagnostics. 4. The stable and non-leaching antibacterial PPMs introduced in this work alleviates the need for chemical or enzymatic lysins and their potential release of polymerase chain reaction (PCR) inhibitors. Therefore the cell lysate is ready to be used in PCR without further filtering or purification. 5. The developed biochips were reused for 20-30 lysis cycles without any evidence of physical damage to the monolith, significant performance degradation or DNA carryover when they were back-flushed between cycles.
Disadvantage and constraints	1. Laser micromachining has low resolution in feature size smaller than 250 μm, thus it is limited to features sized equal or bigger than 250 μm which consider be a fabrication constraint. 2. PPM columns should be stored in water otherwise it will dry out, crack and will not be reusable. 3. The cell lysis efficiency was shown to be flow-rate dependent within the studied range (0.2-10 μL/min). 4. The procedure used to synthesize X-PMMA is low-throughput method that need to be optimized or replaced.

antibacterial polymer belongs to the SMAMPs antibacterial polymer family and antibacterial PPM column based on an antibacterial polymer that contains quaternary ammonium compound. The QAC-PPM based microchips were stored by immersing in a beaker filled with water to avoid shrinkage and drying. However Boc-PPM based micro-chip does not suffer from shrinkage and drying if left over the bench. The mass-production of the developed on-chip cell lysis would give it a commercial value to be used as a disposable on-chip bacterial cell lysis (when different bacterial strains are used) or to be reusable for lysing the same bacterial strains.

5.4 Publications

The academic accomplishments achieved during the PhD program are mentioned below. The first three publications are related to the work presented in this thesis, while the last three present side projects that were done during the PHD program.

[1] **Aly Saad Aly M.**, Nguon O., Gauthier, M. and Yeow J. T. "Antibacterial porous polymeric monolith columns with amphiphilic and polycationic character on cross-linked PMMA substrates for cell lysis applications", RSC Advances, Vol. 3, 24177-24184, 2013.

[2] **Aly Saad Aly M.**, Gauthier, M. and Yeow J. T. "Lysis of Gram-positive and Gram-negative Bacteria by Antibacterial Porous Polymeric Monolith Formed in Microfluidic Biochips for Sample Preparation", Analytical and Bioanalytical Chemistry, Vol. 406, 5977-5987, 2014.

[3] **Aly Saad Aly M.**, Gauthier, M. and Yeow J. T. "On-Chip Cell Lysis by Antibacterial Non-Leaching Reusable Quaternary Ammonium Monolithic Column", Biomedical Microdevices, Vol. 406, No. 1, DOI: 10.1007/s10544-015-0025-z, 2016.

[4] **Aly Saad Aly M.** and Wang J. "Design and Simulation of Mechanically-Coupled Filters Based on ZnO Piezoelectrically Transduced Contour Mode Ring Resonators" Proceeding of International Conference On Nanotechnology: Fundamentals and Applications (ICNFA2010). P.P (5041-5048). 4-6 Aug. 2010, Ottawa, Canada.

[5] Pallapa M., **Aly Saad Aly M.**, Chen A. I. H., Wong L., Wong K. W., Abdel-Rahman E. and Yeow Tze-Wei J. "Modeling and Simulation of a Piezoelectric Micro-power Generator", Proceedings of COMSOL Users Conference. P.P (1-7). 7-9 Oct. 2010, Boston, MA USA. ISBN: 978-0-9825697-4-0.

[6] **Aly Saad Aly M.**, Lopez N., Weyers D., Rasheed S., Abdel-Rahman E. and Hajian A. "Investigating Carbon Nanotubes for MRI Receiver Coils" Proceedings of the ISMRM Annual Meeting Montreal, 6-13 May 2011.

5.5 Cost breakdown

The developed antibacterial PPM column has a commercial value, thus a cost breakdown is necessary to evaluate its commercial visibility. An initial cost breakdown for the developed biochip is first demonstrated including, the cost of materials, one time purchased items, labor wages and charges for using facilities. Secondly, a commercial estimate of manufacturing the bio-chip provided by a professional microfluidic company is provided. Table 5.2 summarize the cost breakdown of the developed biochip in an academic environment, and a commercial estimate cost provided by a microfluidic manufacture company.

5.6 Future work

The following are the recommended/proposed future work to the introduced on-chip cell lysis technique:

1. Testing the developed lab-on-chip against fungus, yeasts, mammalian cells and viruses to investigate its efficiency to lyse these species.

2. Developing an antimicrobial PPM column that lyse bacteria, fungus, yeasts, mammalian cells and viruses cells and extract DNA to have a single column that lyse bacterial cells and isolate DNA.

3. Consider commercializing the two developed antibacterial porous polymeric monolith column to lyse gram positive and gram negative bacteria.

4. Consider commercializing the single PPM column to lyse and extract DNA of bacteria, fungus, yeasts, mammalian cells and viruses cells.

5. Integrate the developed cell lysis technique with DNA isolation, PCR and detection mechanism into one integrated lab-on-chip.

Table 5.2: Cost breakdown of the developed two antibacterial PPM columns.

Item	Cost	Total
One time purchased items		
UV cross-linker	\$650	
Universal laser system, VLS2.30	\$10 K	
Laboratory usage fees	\$1200	
		\$12650
Materials		
1. Substrate		
Methyl methacrylate (MMA) 1 Kg	\$75	
Ethylene glycol dimethacrylate (EGDMA) 500 ML	\$160	
Benzoyl peroxide (BPO) 50 g	\$45	
Aluminum oxide: 1Kg	\$55	
		\$335
2. Boc-PPM column		
Butyl methacrylate (BuMA) 100 ML	\$40	
Di-tert-butyl dicarbonate (BOC_2O) 25 g	\$165	
Ammonium chloride (NH_4Cl) 25g	\$40	
N,N-diisopropylethylamine (DIPEA) 100 ML	\$40	
1-dodecanol 500 g	\$40	
Cyclohexanol: 1L	\$45	
2,2-dimethoxy-2-phenylacetophenone (DMPAP) 50 g	\$65	
Phosphoric acid (85%) 1Kg	\$75	
Triethylamine (TEA) 100 ML	\$30	
2-aminoethanol (ETA) 100 ML	\$80	
Dichloromethane (DCM) 1L	\$75	
Sodium sulfate (Na_2SO_4) 500 g	\$60	
Methacryloyl chloride (MACl)50 ML	\$100	
1,6-hexanediol dimethacrylate (1,6-HDDMA) 100 ML	\$100	
		\$955
3. QAC PPM column		
Diallyldimethylammonium chloride (DADMAC) 1L	\$110	
Ethylene glycol diacrylate (EGDA) 5ML	\$175	
Methanol 1L	\$55	
		\$340
4. Microchip		
30 G Syringe Needles pack of 100	\$40	
Fumed Silica 500 G	\$70	
Epoxy glue pack of 10	\$50	
		\$160
Labour		
25 hours × \$20/h		\$500
Commercial estimate		
16 parallel channels chip		\$2500

References

[1] Manz A., Graber N. and Widmer H.M. "Miniaturized total chemical analysis systems: A novel concept for chemical sensing", *Sensors and Actuators B: Chemical*, Vol. 1, pp. 244-248, 1990.

[2] Carlo D. D., Jeong K.-H. and Lee L. P. "Reagentless mechanical cell lysis by nanoscale barbs in microchannels for sample preparation", *Lab on Chip*, Vol. 3, pp. 287-291, 2003.

[3] Burke J. M. and Smela E. "A novel surface modification technique for forming porous polymer monoliths in poly(dimethylsiloxane)", *Biomicrofluidics*, Vol. 6, pp. 016506-1-016506-10, 2012.

[4] Mahalanabis M., Al-Muayad H., Dominika Kulinski M.,Altman D. and Klapperich C. M. "Cell lysis and DNA extraction of Gram-positive and Gram-negative bacteria from whole blood in a disposable microfluidic chip", *Lab on chip*, Vol. 124, pp. 84-89, 2009.

[5] Sambrook J. and Russel D. W. *Molecular Cloning: A Laboratory Manual*, Cold Spring Harbor: New York, 2001.

[6] Lee C.-Y., Lee G.-B., Lin J.-L., Huang F.-C. and Liap C.-S. "Integrated microuidic systems for cell lysis, mixing/pumping and DNA amplification", *Journal of Micromechanics and Microengineering*, Vol. 15, pp. 1215-12233, 2005.

[7] Lee D. W., Cho and Y.-H. "A continuous electrical cell lysis deviceusing a

low dc voltage for a cell transport and rupture", *Sensors and Actuators B: Chemical*, Vol. 124, pp.84-89, 2007.

[8] Chang D. C., Chassy B. M., Saunders J. A. and Sowers A. E. *Guide to Electroporation and Electrofusion*, Academic Press: San Diego, 1992.

[9] Shahini M. and Yeow J. T. W. "Cell electroporation by CNT-featured microfluidic chip", *Lab on Chip* Vol. 13, pp. 2585-2590, 2013.

[10] Irimia D., Tompkins R. G. and Toner M. "Single-Cell Chemical Lysis in Picoliter-Scale Closed Volumes Using a Microfabricated Device", *Analytical Chemistry*, Vol. 76, pp. 6137-6143, 2004.

[11] Cichova M., Proksova M., Tothova L., Santha H. and Mayer, V. "On-line cell lysis of bacteria and its spores using a microfluidic biochip", *Central European Journal of Biology*, Vol. 7, pp. 230-240, 2012.

[12] Sethu P., Anahtar M., Moldawe L. L.; Tompkins R. G. and Tone, M. "Continuous Flow Microfluidic Device for Rapid Erythrocyte Lysis", *Analytical Chemistry*, Vol. 76, pp. 6247-6253, 2001.

[13] El-Ali J., Gaudet S., Gunther A., Sorger P. K. and Jensen K. F. "Cell Stimulus and Lysis in a Microfluidic Device with Segmented Gas-Liquid Flow", *Anal. Chem.*, Vol. 77, pp. 3629-3636, 2005.

[14] Schilling E. A., Kamholz A. E., Yager P. "Cell Lysis and Protein Extraction in a Microfluidic Device with Detection by a Fluorogenic Enzyme Assay", *Anal. Chem.*, Vol. 74, pp. 1798-1804, 2002.

[15] Kim Y.-B., Park J.-H., Chang W.-J., Koo Y.-M., Kim E. K. and Kim J.-H. "Statistical optimization of the lysis agents for Gram-negative bacterial cells in a microuidic device" *Biotechnology and Bioprocess Engineering*, Vol. 11, pp. 288-292, 2006.

[16] Hall J., Felnagle E., Fries M., Spearing S., Monaco L. and Steele A. "Evaluation of cell lysis procedures and use of a microfluidic system for an automated DNA-based cell identificationin interplanetary missions", *Planetary and Space Science*, Vol. 54, pp. 1600-1611, 2006.

[17] Radoslaw K., Maciej S., Karina Z., Elzbieta J., Michal C., Artur D., Zbigniew B., "A microfluidic device with fluorimetric detection for intracellular components analysis", *Biomedical Microdevices*, Vol. 13, pp. 431-440, 2011.

[18] Yasuhiro Sasuga, Tomoyuki Iwasawa, Kayoko Terada, Yoshihiro Oe, Hiroyuki Sorimachi,Osamu Ohara, and Yoshie Harada, "Single-cell chemical Lysis Method for Analyses of Intracellular Molecules Using an Array of Picoliter-Scale Microwells", *Analytical Chemistry*, Vol. 80, pp. 9141-9149, 2008.

[19] Kenawy E., Worley S. D. and Broughton R. "The Chemistry and Applications of Antimicrobial Polymers: A State of the Art Review", *Biomacromolecules*, Vol. 8, pp. 1359-1384, April 2008.

[20] Santillo M. F., Heien M. L. and Ewing A. G. "Temporal analysis of protozoan lysis in a microfluidic device", *Lab Chip*, Vol. 9, pp. 2796-2802, 2009.

[21] Lienkamp K., Madkour A. E., Musante A., Nelson C. F., Nusslein K. and Tew G. N. "Antimicrobial polymers prepared by ROMP with unprecedented selectivity: a molecular construction kit approach", *Journal of the American Chemical Society*, Vol. 130, pp. 9836-9843, 2008.

[22] Timofeeva L. and Kleshcheva N. "Antimicrobial polymers: mechanism of action, factors of activity, and applications", *Applied Microbiology and Biotechnology*, Vol. 89, pp. 475-492, 2011.

[23] Cornell R. J. And L. Donaruma G. "2-Methacryloxytropones. Intermediates for the Synthesis of Biologically Active Polymers", *Journal of Medicinal Chemistry*, Vol. 8, pp. 388-390, 1965.

[24] Sledenbiedel F. and Tiller J. C. "Antimicrobial Polymers in Solution and on Surfaces: Overview and Functional Principles", *Polymers*, Vol. 4, pp. 46-71, 2012.

[25] Kawabata N. and Nishiguchi M. "Antibacterial activity of soluble pyridinium-type polymers", *Applied and Environmental Microbiology*, Vol. 54, pp. 2532-2535, 1988.

[26] Zuo H., Wu D. and Fu R. "Synthesis of antibacterial polymers from 2-dimethylamino ethyl methacrylate quaternized by dimethyl sulfate", *Polymer Journal*, Vol. 42, pp. 766-771, 2010.

[27] Vogl O. and Tirrell D. "Functional Polymers with Biologically Active Groups", *Journal of Macromolecular Science: Part A-Chemistry*, Vol. 13, pp. 415-439, 1979.

[28] Stasko N. A. and Schoenfisch M. H. "Dendrimers as a Scaffold for Nitric Oxide Release", *Journal of the American Chemical Society*, Vol. 128, pp. 8265-8271, 2006.

[29] Charville G. W., Hetrick E. M., Geer C. B. and Schoenfisch M. H. "Reduced bacterial adhesion to fibrinogen-coated substrates via nitric oxide release", *Biomaterials*, Vol. 29, pp. 4039-4044, 2008.

[30] Coneski P. N. , Rao K. S. and Schoenfisch M. H. "Degradable Nitric Oxide-Releasing Biomaterials via Post-Polymerization Functionalization of Cross-Linked Polyesters", *Biomacromolecules*, Vol. 11, pp. 3208-3215, 2010.

[31] Tiller J. C., Liao C., Lewis K. and Klibanov A. M. "Designing Surfaces That Kill Bacteria on Contact", *Journal of the American Chemical Society*, Vol. 98, pp. 5981-5985, 2001.

[32] Advincula R. "Polymer Brushes by Anionic and Cationic Surface-Initiated Polymerization (SIP): Surface-Initiated Polymerization I", Springer: Berlin Heidelberg, 2006.

[33] Skudas R., Thommes M. and Unger Klaus K. "Monolithic Silicas in Separation Science: Characterization of the Pore Structure of Monolithic Silicas", Wiley-VCH Verlag GmbH and Co. KGaA: Weinheim, Germany, 2011.

[34] Edmondson S., Osborne V. L. and Huck W. T. S. "Polymer brushes via surface-initiated polymerizations", *Chemical Society Reviews*, Vol. 33, pp. 14-22, 2003.

[35] Hammond P. T. "Engineering materials layer-by-layer: Challenges and opportunities in multilayer assembly", *American Institute of Chemical Engineers*, Vol. 57, pp. 2928-2940, 2011.

[36] Lyklema J. and Deschenes L. "The first in layer-by-layer depostioion: Electrostatics and/or non-electrostatics?", *Advances in Colloid and Interface Science*, Vol. 168, pp. 1547-5905, 2011.

[37] Friedrich J. "Mechanisms of Plasma Polymerization:Reviewed from a Chemical Point of View", *Plasma Processes and Polymers*, Vol. 8, pp. 783-802, 2011.

[38] Madkour A. E., Dabkowski J. M., Nusslein K. and Tew G. N. "Fast Disinfecting Antimicrobial Surfaces", *Langmuir*, Vol. 25, pp. 1060-1067, 2008.

[39] Li Y., Leung W. K., Yeung K. L., Lau P. S. and Kwan J. K. C. "A Multilevel Antimicrobial Coating Based on Polymer-Encapsulated ClO_2", *Langmuir*, Vol. 25, pp. 13472-13480, 2009.

[40] Lee S. B., Koepsel R. R., Morley S. W., Matyjaszewski K., Sun Y. and Russell A. J. "Permanent, Nonleaching Antibacterial Surfaces. 1. Synthesis by Atom Transfer Radical Polymerization", *Biomacromolecules*, Vol. 5, pp. 877-882, 2004.

[41] Wan W. and Yeow J. "Integration of nanoparticle cell lysis and microchip PCR for one-step rapid detection of bacteria", *Biomedical Microdevices*, Vol. 14, pp. 4128-4129, 2012.

[42] Weyant R. S., Edmonds P. and Swaminathan B."Effect of ionic and nonionic detergents on the Taq polymerase, *BioTechniques*, Vol. 9, pp. 308-309, 1990.

[43] Yeow J. and Wan W. "The effects of nanoparticles on polymerase chain reaction", *Nano/Micro Engineered and Molecular Systems (NEMS), 2010 5th IEEE International Conference on*, pp. 855-859, Jan. 2009.

[44] Arrua R. D., Strumia M. C. and Igarzabal C. I. A. "Macroporous Monolithic Polymers: Preparation and Applications", *Materials*, Vol. 2, pp. 2429-2466, 2009.

[45] Oberacher H. and Huber C. G. "Capillary monoliths for the analysis of nucleic acids by high-performance liquid chromatography-electrospray ionization mass spectrometry", *TrAC Trends in Analytical Chemistry*, Vol. 21, pp. 166-174, 2002.

[46] Stachowiak T. B., Rohr T., Hilder E. F., Peterson D. S., Yi M., Svec F. and Frechet J. M. J., "Fabrication of porous polymer monoliths covalently attached to the walls of channels in plastic microdevices", *ELECTROPHORESIS*, Vol. 24, pp. 1522-2683, 2003.

[47] XIE S., Svec F. and Frechet J. M. J. "Preparation of porous hydrophilic monoliths: Effect of the polymerization conditions on the porous properties of poly (acrylamide-co-N,N′-methylenebisacrylamide) monolithic rods", *Journal of Polymer Science Part A: Polymer Chemistry*, Vol. 35, pp. 1099-0518, 1997.

[48] Odian G. "Radical Chain Polymerization: Principles of Polymerization", John Wiley and Sons, Inc.: Hoboken, New Jersey, US, 2004.

[49] Yu C. Davey M. H., Svec F., and Frechet J. M. J. "Monolithic Porous Polymer for On-Chip Solid-Phase Extraction and Preconcentration Prepared by Photoinitiated in Situ Polymerization within a Microfluidic Device", *Analytical Chemistry*, Vol. 73, pp. 5088-5096, 2001.

[50] Huaa Y. , Jemereb A. B., Harrison D. J. "On-chip solid phase extraction and enzyme digestion using cationic PolyE-323 coatings and porous polymer monoliths coupled to electrospray mass spectrometry", *Journal of Chromatography A*, Vol. 1218, pp. 4039-4044, 2011.

[51] Aimin Tan, Salete Benetton, and Jack D. Henion , "Chip-Based Solid-Phase Extraction Pretreatment for Direct Electrospray Mass Spectrometry Analysis Using an Array of Monolithic Columns in a Polymeric Substrate", *Analytical Chemistry*, Vol. 75, No. 20, pp. 5504-5511, Sep. 2003.

[52] Kulinski M. D., Mahalanabis M., Gillers S., Zhang J. Y., Singh S. and Klapperich C. M., "Sample preparation module for bacterial lysis and isolation of DNA from human urine", *Biomedical Microdevices*, Vol. 11, pp. 671-678, Jan. 2009.

[53] Arpita Bhattacharyya and Catherine M. Klapperich , "Thermoplastic Microfluidic Device for On-Chip Purification of Nucleic Acids for Disposable Diagnostics", *Analytical Chemistry*, Vol. 78, No. 3, pp. 788-792, Dec. 2006.

[54] Bhattacharyya A., Kulinski D. and Klapperich C. "Fabrication of the Thermoplastic Microfluidic Channels", *Journal of Visualized Experiments*, Issue 12, e664, DOI:10.3791/664, 2008, http://www.jove.com/video/664/.

[55] Klapperich C. M., Kaufman J. D., Kulinski M. D., Altman D., Singh S. "Method For Bacterial Lysis", U.S. Patent 20100203521, April 02, 2008.

[56] Fedotenko I. A., Zaffalon P., Favarger F. and Zumbuehl A. "The synthesis of 1,3-diamidophospholipids", *Tetrahedron Letters*, Vol. 51, pp. 5382-5384, 2010.

[57] Kuroda K. and DeGrado W. F. "Amphiphilic Polymethacrylate Derivatives as Antimicrobial Agents", *Journal of the American Chemical Society*, Vol. 127, pp. 4128-4129, 2005.

[58] BEJ A. K., DiCESARE J. L., HAFF L. and ATLAS R. M. "Detection of

Escherichia coli and Shigella spp. In water by using PCR and gene probes for uid", *Applied and Environmental Microbiology*, Vol. 57, pp. 1013-1017, 1991.

[59] Abushady H. M., Bashandy Aziz A. S., N.H. and Ibrahim H.M.M. "Molecular Characterization of Bacillus subtilis Surfactin Producing Strain and the Factors Affecting its Production", *International Journal of Agriculture and Biology*, Vol. 7, pp. 337-344, 2005.

[60] Pretsch E., Clerc T., Seibl J. and Simon W. *Tables of spectral data for structure determination of organic compounds*, Springer, Berlin, 1989.

[61] Pretsch E., Buhlmann P. and Badertscher M. *Structure Determination of Organic Compounds*, Springer, Berlin, 2009.

[62] Roy S. G., Acharya R., Chatterji U. and De P. "RAFT Polymerization of Methacrylates Containing Tryptophan Moiety: Controlled Synthesis of Biocompatible Fluorescent Cationic Chiral Polymers with Smart pH-Responsiveness", *Polymer Chemistry*, Vol. 4, pp. 1141-1152, 2013.

[63] Aly Saad Aly M., Nguon O., Gauthier, M. and Yeow J. T. "Antibacterial porous polymeric monolith columns with amphiphilic and polycationic character on cross-linked PMMA substrates for cell lysis applications", *RSC Advances*, Vol. 3, pp. 24177-24184, 2013.

[64] Zimmerman J. "Radiation grafting of allylic monomers to solid polymeric substrates", *Journal of Polymer Science*, Vol. 49, pp. 247-252, 1961.

[65] Ash D. L., Page A. F. "Microvolume Quantification of Nucleic Acids in Molecular Diagnostics", Poster presented at 26th Clinical Virology Symposium M78, Daytona Beach, FL.

[66] Bonasera V., Alberti S. and Sacchetti A. "Protocol for high-sensitivity/long linear-range spectrofluorimetric DNA quantification using ethidium bromide", *BioTechniques*, Vol. 43, pp. 173-176, 2007.

[67] http://www.filterair.info/literature/Files%2FBacteriaFungusVirusChart.pdf

[68] Holt J. G., Krieg N. R., Sneath P. H. A, Staley J.T. and Williams S.T. *Bergey's manual of determinative bacteriology: Characteristics differentiating the species of Micrococcus*, 9th ed. Baltimore (MD): Williams and Wilkins, Table 17.11, p.542, 1994.

[69] Kokkinosa A. , Fasseas C. , Eliopoulos E. and Kalantzopoulos G. "Cell size of various lactic acid bacteria as determined by scanning electron microscope and image analysis" , Vol. 78, pp.491-500, 1998.

[70] Tvrzova L., Schumann P., Sedlacek I., Pacova Z., Sproer C., Verbarg S., Kroppenstedt R. M. "Reclassification of strain CCM 123, previously classified as Kocuria carniphila sp. nov.", *International Journal of Systematic and Evoluationary*, Vol. 55, pp. 139-142, 2005.

[71] Smith N. and Yeager S. "Micrococcus folliculitis", *British Journal of Dermatology*, Vol. 141, pp. 1365-2133, 1999.

[72] Careli R. T., Andrade N. J., Soares N. F., Ribeiro J. I., Rosado M. S., Bernardes P. C. "The adherence of Pseudomonas fluorescens to marble, granite, synthetic polymers, and stainless steel", *Food Science and Technology Campinas*, Vol. 29, pp. 171-142, 2009.

[73] Kubitschek, H. E. and Freedman, M. L. "Chromosome Replication and the Division Cycle of Escherichia coli B/r", *Journal of Bacteriology*, Vol. 107, pp. 95-99, 1971.

[74] Cox, Robert A. "Quantitative relationships for specific growth rates and macromolecular compositions of Mycobacterium tuberculosis, Streptomyces coelicolor A3(2) and Escherichia coli B/r: an integrative theoretical approach", *Microbiology*, Vol. 150, pp. 1413-1426, 2004.

[75] Rao A. "Conformation and Antimicrobial Activity of Linear Derivatives of Tachyplesin Lacking Disulfide Bonds", *Archives of Biochemistry and Biophysics*, Vol. 361, pp. 127-134, 1999.

[76] Lee C. and Kim J., Shin S. G. and Hwang S. "Absolute and relative QPCR quantification of plasmid copy number in Escherichia coli", *Journal of Biotechnology*, Vol. 123, pp. 273-280, 2006.

[77] Marchand S., Vandriesche G., Coorevits A., Coudijzer K., De Jonghe V., Dewettinck K., De Vos P., Devreese B., Heyndrickx M., De Block J. "Heterogeneity of heat-resistant proteases from milk Pseudomonas species", *International Journal of Food Microbiology*, Vol. 133, pp. 68-77, 2009.

[78] Jackson C. R., Fedorka-Cray P. J. and Barrett J. B. "Use of a Genus- and Species-Specific Multiplex PCR for Identification of Enterococci", *Journal of Clinical Microbiology*, Vol. 42, pp. 3558-3565, 2004.

[79] Dizman B., Elasri M. O., and Mathias L. J. "Synthesis and Antibacterial Activities of Water-Soluble Methacrylate Polymers Containing Quaternary Ammonium Compounds", *Journal of Polymer Since Part A: Polymer Chmmistry*, Vol. 44, pp. 5965-5973, 2006.

[80] Harkes G., Dankert J. and Feijen J. "Growth of uropathogenic Escherichia coli strains at solid surfaces", *Journal of Biomaterials Science, Polymer Edition*, Vol. 3, pp. 403-418, 1992.

[81] Biesalski M. and Ruhe J. "Preparation and Characterization of a Polyelectrolyte Monolayer Covalently Attached to a Planar Solid Surface", *Macromolecules*, Vol. 32, pp. 2309-2316, 1999.

[82] Murata H., Koepsel R. R., Matyjaszewski K. and Russell A. J. "Permanent, non-leaching antibacterial surfaces2: How high density cationic surfaces kill bacterial cells", *Biomaterials*, Vol. 32, pp. 4870-4879, 2007.

[83] Cen L., Neoh K. G., Kang E. T. "Antibacterial activity of cloth functionalized with N-alkylated poly(4-vinylpyridine)", *Journal of Biomedical Materials Research Part A*, Vol. 71A, pp. 70-80, 2004.

[84] Ignatova M., Voccia S., Gilbert B., Markova N., Mercuri P. S. and Galleni M., Sciannamea V., Lenoir S., Cossement D., Gouttebaron R., Jerome R. and Jerome C. "Synthesis of Copolymer Brushes Endowed with Adhesion to Stainless Steel Surfaces and Antibacterial Properties by Controlled Nitroxide-Mediated Radical Polymerization", *Langmuir*, Vol. 20, pp. 10718-10726, 2004.

[85] Thome J., Hollander A., Jaeger W., Trick I. and Oehr C. "Ultrathin antibacterial polyammonium coatings on polymer surfaces", *Surface and Coatings Technology*, Vol. 174, pp. 584-587, 2003.

[86] Koslow, E.E. "Structures that inhibit microbial growth", U.S. Patent 7287650 B2, Oct. 30, 2007.

[87] Van der Mei H. C., Rustema-Abbing M., Langworthy D. E., Collias D. I., Mitchell M. D., Bjorkquist D. W. and Busscher H. J. "Adhesion and viability of waterborne pathogens on p-DADMAC coatings", *Biotechnology and Bioengineering*, Vol. 99, pp. 1097-0290, 2008.

[88] Mikhaylova A., Liesenfeld B., Moore D., Toreki W. and Vella J., Batich C. and Schultz G. "Preclinical evaluation of antimicrobial efficacy and biocompatibility of a novel bacterial barrier dressing", *Wounds: A Compendium of Clinical Research and Practice*, Vol. 23, pp. 24-31, 2011.

[89] Lu J., Wang X., Xiao C. "Preparation and characterization of konjac glucomannan/poly(diallydimethylammonium chloride) antibacterial blend films", *Carbohydrate Polymers*, Vol. 73, pp. 427-437, 2008.

[90] Yu S., Ng F. L., Ma K. C. C., Mon A. A., Ng F. L. and Ng Y. Y. "Effect of porogenic solvent on the porous properties of polymer monoliths", *Journal of Applied Polymer Science*, Vol. 127, pp. 1097-4628, 203.

[91] Yu S., Ng F. L., Ma K. C. C. Ng F. L., Zhao J. and Tong S. K. K. "Development of porous polymer monolith by photoinitiated polymerization", *Journal of Applied Polymer Science*, Vol. 120, pp. 1097-4628, 2011.

[92] Mwangi I., Ngila J. C., Ndungu P. and Msagati T. A. M. "Method Development for the Determination of Diallyldimethylammonium Chloride at Trace Levels by Epoxidation Process", *Water, Air, and Soil Pollution* Vol. 224, pp. 1-9, 2013.

[93] Ye Y., Song Q. and Mao Y. "Single-step fabrication of non-leaching antibacterial surfaces using vapor crosslinking", *Journal of Materials Chemistry*, Vol. 21, pp. 257-262, 2011.

[94] Xamena F. X. L., Arean C. O. and Spera S., Merlo E. and Zecchina A. "Formaldehyde Oligomerization on Silicalite: An FTIR and NMR Study", *Catalysis Letters*, Vol. 95, pp. 51-55, 2004.

[95] Nischang I., Svec F. and Frechet J. M. J. "Downscaling Limits and Confinement Effects in the Miniaturization of Porous Polymer Monoliths in Narrow Bore Capillaries", *Analytical Chemistry*, Vol. 81, pp. 7390-7396, 2009.

[96] Ranjha N. M. and Qureshi U. F. "Preperation and Characterization of Crosslinked Acrylic Acid/Hydroxypropyl Methyl Cellulouse Hydrogels For Drug Delivery", *International Journal of Pharmacy and Pharmaceutical Sciences*, Vol. 6, pp. 400-410, 2014.

[97] Aly Saad Aly M., Gauthier, M. and Yeow J. T. "Lysis of gram-positive and gram-negative bacteria by antibacterial porous polymeric monolith formed in microfluidic biochips for sample preparation", *Analytical and Bioanalytical Chemistry*, Vol. 406, pp. 5977-5987, 2014.

Appendices

Appendix A

Synthesis of cross-linked PMMA

The synthetic procedure of X-PMMA substrate is chemically illustrated in Sch. A1. MMA and EGDMA were filtered over a thin layer of basic aluminum oxide (alumina, AL_2O_3) and added to a dry Erlenmeyer flask. The total reaction volume was set at 150 mL, and the amount of EGDMA was adjusted to either 3, 5, 10, 15, or 20 mole % as shown in Table A1. After the addition of BPO (2.30 g, 9.5 mmol, 0.75 mol %) the mixture was degassed for 1 h under N_2 flow. The solution was transferred with a canula to a dry soap-washed crystallizing dish (190 $\times$ 100 cm^2) covered with aluminum foil and kept under nitrogen atmosphere. The dish was immersed in a water bath at 35°C and leveled to insure a uniform substrate thickness. The solution was kept for 1.5 h under nitrogen before turning off the water bath heater. As the polymerization reaction was exothermic, cold water was added to the water bath to avoid overheating, and then the dish was kept under nitrogen at room temperature for 11 h. The transparent cross-linked PMMA substrate was washed by soaking in methanol for 30 min, and dried under air flow. The polymer was easily removed from the dish with a spatula. The X-PMMA substrate was then cut into 40 $\times$ 20 mm^2 slices with 1 mm thickness using a laser ablation machine. Using a spectrophotometer, the absorbance of the X-PMMA samples at 365 nm wavelength was determined to be 0.238.

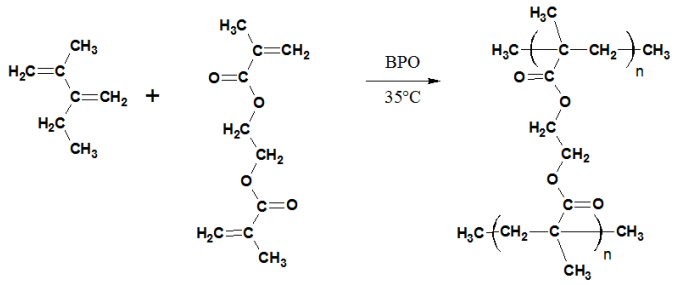

Scheme A1: Synthesis of X-PMMA.

Table A1: MMA and EGDMA volumes used in the preparation of the different cross-linked PMMA (X-PMMA) substrates.

Cross-linker (mole %)	MMA (mL)	EGDMA (mL)
3	145.6	4.4
5	142.9	7.1
10	136.4	13.6
15	130.4	19.6
20	125.0	25.0

Boc-EA synthesis

The synthetic procedure shown in Sch. A2 was adapted from Fedotenko *et al* [56]. Briefly, distilled triethylamine (TEA, 19.2 mL, 138 mmol) was added to a solution of 2-aminoethanol (5.42 mL, 89.7 mmol) in 200 mL of dry dichloromethane (DCM) and stirred at room temperature for 30 min. before cooling to 0°C. A solution of di-*tert*-butyl dicarbonate (BOC_2O, 20 g, 89.7 mmol) in 50 mL of dry DCM was then added drop-wise. The reaction mixture was stirred at room temperature for 10 h, and quenched with a saturated aqueous solution of ammonium chloride (NH_4Cl). Liquid extraction with 100 mL of DCM was repeated 3 times, and the combined organic fractions were washed with brine. After drying over Na_2SO_4, the solvent was vaporized in vacuum conditions. The crude product was purified on a silica gel column (2% methanol/DCM) and yielded a clear liquid (9 g, 55.8 mol, 62%). Rf: 0.29. ^{1}H NMR (300 MHz, $CDCl_3$): δ 5.268 (br s, 1H), 3.647 (s, 2H), 3.238 (s, 2H), 3.007 (br s, 1H), 1.409 (s, 9H). ^{13}C NMR (300 MHz, $CDCl_3$): δ 167.166, δ 155.629, δ 135.920, δ 126.776, δ 79.447, δ 63.823, δ 39.573, δ 28.230, δ 18.160.

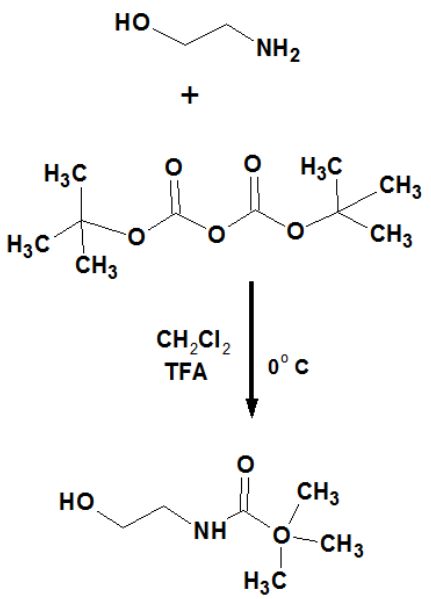

Scheme A2: Synthesis of Boc-EA.

Boc-EAMA synthesis

The synthetic procedure shown in Sch. A3 was adapted from Kuroda *et al* [57]. Boc-EA, DCM and DIPEA were added to an oven-dried round-bottom flask, and the solution was degassed with nitrogen flow for 20 min. The flask was then cooled in a dry ice/acetone bath and MACl was added drop-wise with vigorous stirring under nitrogen atmosphere. After 15 min., the solution was brought to room temperature and allowed to react overnight. The light purple solution was washed successively with water, 10% (w/v) citric acid, 10% (w/v) K_2CO_3, 9% (w/v) $NaHCO_3$, and saturated NaCl aqueous solutions. The bottom organic layer was dried over Na_2SO_4, and the solvent was evaporated under reduced pressure. Recrystallization from DCM/hexanes yielded clear crystals (22.4 g, 61% yield). ^{1}H NMR (300 MHz, CDCl3): δ 6.090 (s, 1H), 5.552 (s, 1H), 4.768 (br s, 1H), 4.170 (t, 2H), 3.405 (br, 2H), 1.915 (s, 3H), 1.410 (s, 9H). 13C NMR (300 MHz, CDCl3): δ 167.166, δ 155.629, δ 135.920, δ 126.776, δ 79.447, δ 63.823, δ 39.573, δ 28.230, δ 18.160.

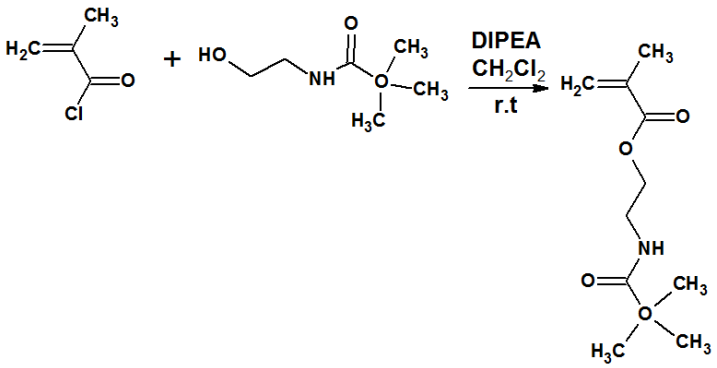

Scheme A3: Synthesis of Boc-EAMA.

t-Boc group deprotection

The deprotection of the t-Boc group was successfully achieved by flowing 85%phosphoric acid through the PPM, as evidenced by FT-IR analysis shown in Fig. A1. The absorption bands characteristic for the carbamate functional group at 1518 cm^{-1}, corresponding to the -N-H bending vibrational mode, decreased significantly in the spectrum after the deprotection reaction and a small broad peak visible at 1541 cm^{-1} appeared, corresponding to the -NH_2 bending mode. A weaker absorbance associated with the N-CO-O symmetrical stretching mode at 872 cm^{-1} was also observed [61, 62]. Additionally, the peak for the CH_3 bending mode of the tert-butyl group at 1367 cm^{-1} decreased in intensity [62].

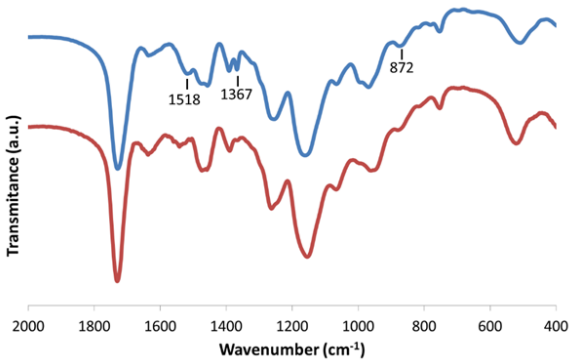

Figure A1: FT-IR spectra for the PPM before (blue) and after (red) deprotection of the t-Boc group. Vibrational band assignments: N-CO-O symmetrical stretching at 1518 cm^{-1}, CH_3 bending at 1367 cm^{-1}, and N-CO-O symmetrical stretching at 872 cm^{-1}.

Appendix B

Bacterial culture

E. coli DH5α and B. subtilis 168 were cultured in lysogeny broth (LB), while P. fluorescens (ATCC 13525) and E. saccharolyticus (ATCC 43076) cells were cultured in nutrient broth (NB) and brain-heart infusion broth (BHIB), respectively. The cells in the cultured media were placed in a shaking incubator at 37 °C (26 °C for ATCC 13525) and were shaken at 180 rpm for 24 hours. The concentration of the bacterial cultures was quantified by performing the solid agar plate-count technique (LB agar for E. coli and B. subtilis, BHI agar for ATCC 43076 and nutrient agar for ATCC 13525) and incubation overnight at 37 °C (26 °C for ATCC 43076). The E. coli, B. subtilis, ATCC 13525, and ATCC 43076 counts were 1.5 10^5, 2×10^5, 1.7×10^5 and 1.9×10^5 colony forming units (CFUs) per mL of culture.

Contact time

By using Table B1 and the below calculation, the contact time is calculated:

- Channel volume = $2.5\times10^{-2}\times$ $500\times10^{-6}\times350\times$ 10^{-6} = $0.004375\mu m^3$ = 4.375 μL
- Volume of the voids (pores) = $(65\times4.375\times$ $10^{-6})\div100$ = 2.84375μL
- Contact time is the time which bacterial suspension spends into the entire PPM.
- At 1.2, 4, 7.2 and 10 μL/min the contact time, T_c, is equal to:
    - 2.9μL$\div$1.2 μL/min=2.4 min.$\times$60 = 143 sec.
    - 2.84375μL$\div$4 μL/min=0.7 min.$\times$60 = 43 sec
    - 2.84375μL$\div$7.2 μL/min=0.4 min.$\times$60 = 24 sec.
    - 2.84375μL$\div$10 μL/min=0.3 min.$\times$ 60 = 17 sec.

Experimental setup

An illustration of the lab-on-chip experimental setup and the cell lysis evaluation techniques is provided in Fig. B1.

Table B1: Channel dimensions and pore information of the optimized PPM column

Channel width (m)	Channel length (m)	Channel depth (m)	Channel vol. (μL)
500 $\times 10^{-6}$	2.5 $\times 10^{-2}$	350 $\times 10^{-6}$	4.375
	Pore diameter (μm)	Porosity (%)	Void vol. (μL)
	3	65	2.844

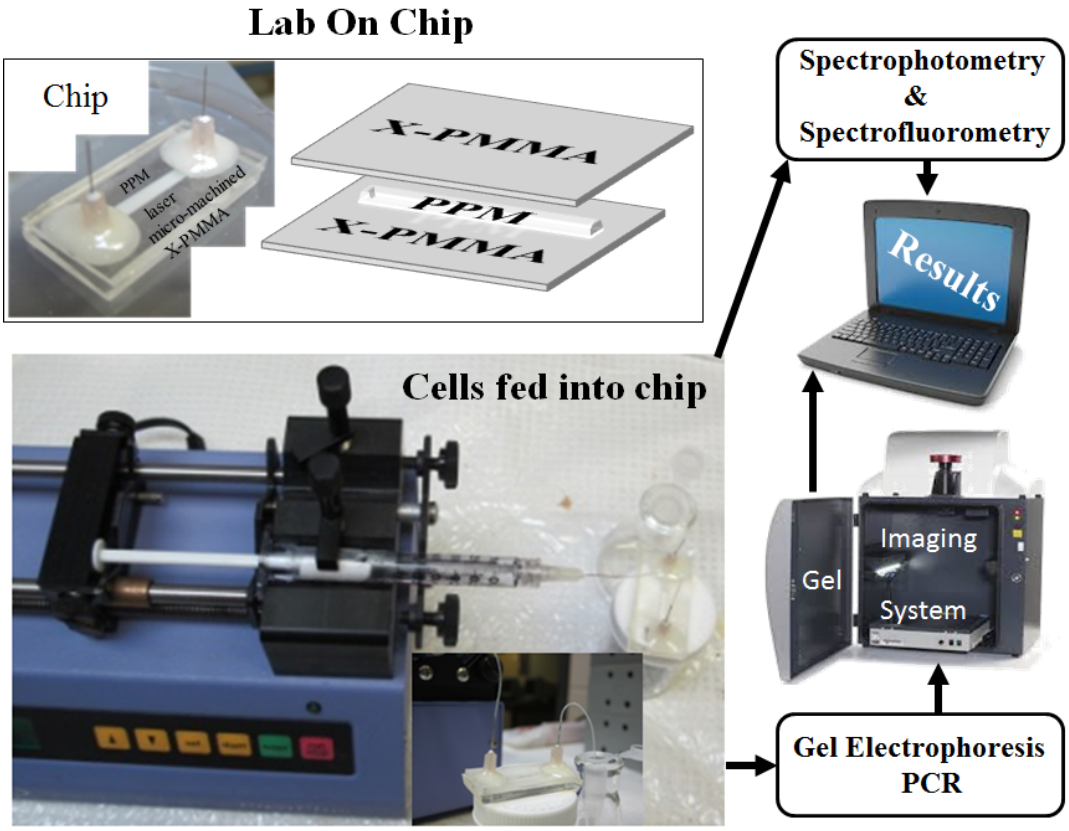

Figure B1: PPM column polymerized into cross-linked PMMA microfluidic channel (shown on top left), experimental set up (shown on bottom left) and cell lysis evaluation techniques (shown on right).

PCR reagents and experimental setup

The structure of the E. coli [76], B. subtilis [4], ATCC 13525 [77], and ATCC 43076 [78] primers used in the PCR reaction is provided in Table B2. The PCR tubes were first preheated and incubated at 95°C for 3 min for initial denaturation, and then the PCR thermal cycler was programed to run for 30 cycles at 95°C for 30 sec., 55°C for 70 sec., 72°C for 70 sec., and 72°C for 10 min. for the extension step.

Table B2: Primers used in PCR experiments

Bacteria	Direction	Sequence	Gene
E. coli DH5α	Forward	AAAACGGCAAGAAAAAGCAG	Dxs
	Reverse	ACGCGTGGTTACAGTCTTGCG	
ATCC 13525	Forward	AAATCGATAGCTTCAGCCAT	aprX
	Reverse	TTGAGGTTGATCTTCTGGTT	
B. subtilis 168	Forward	CCTACGGGAGGCAGCAG	16S rRNA
	Reverse	CCAGTTTCCAATGACCCTCCCC	
ATCC 43076	Forward	AAACACCATAACACTTATGTG	sodA
	Reverse	GTAGAAGTCACTTCTAATAAC	

Influence of flow rate

Fig. B2 and Fig. B3 show the absolute concentration of DNA in the crude bacterial cell lysate collected at the outlet of the protected and deprotected PPM 11, respectively, at flow rates ranged from 0.1 to 10 μL/min.

Biochip vs. off-chip cell lysis efficiency

Fig. B4 shows the florescence intensity of EtBr after intercalating into DNA released from cells flowing through the PPM (11) and resulted from mechanical, thermal, and chemical cell lysis.

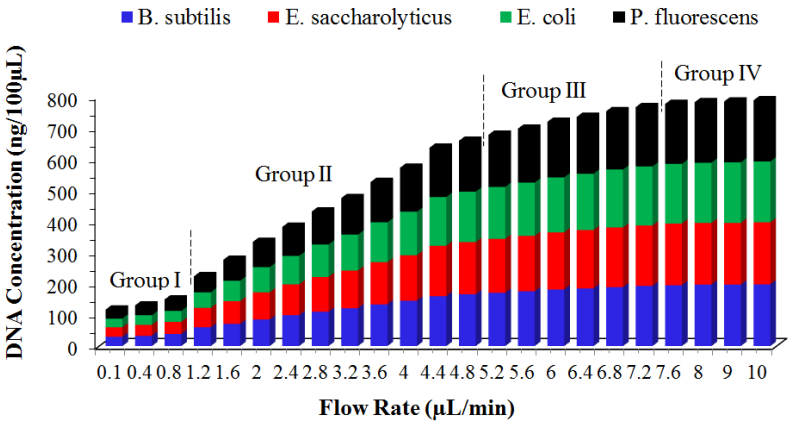

Figure B2: Absolute concentration of DNA in the crude cell lysate collected at the outlet of protected PPM 11 at flow rates ranged from 0.1 to 10 μL/min.

DNA carryover

The florescence intensity of EtBr mixed with the PBS recovered from the microfluidic channel in the back-flush cycle showed insignificant DNA carry over, reaching

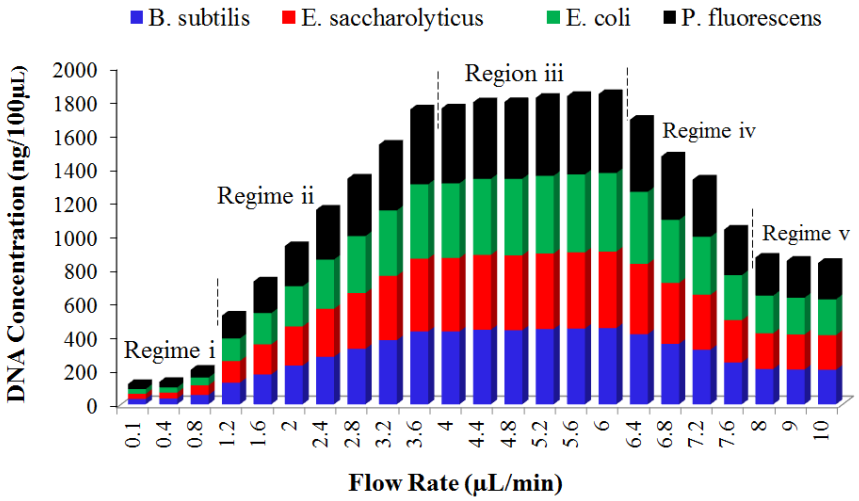

Figure B3: Concentration of the DNA present in the crude cell lysate collected at the outlet of the microfluidic channels hosting deprotected PPM (11) flown at flow rates ranged from 0.1 to 10 μL/min.

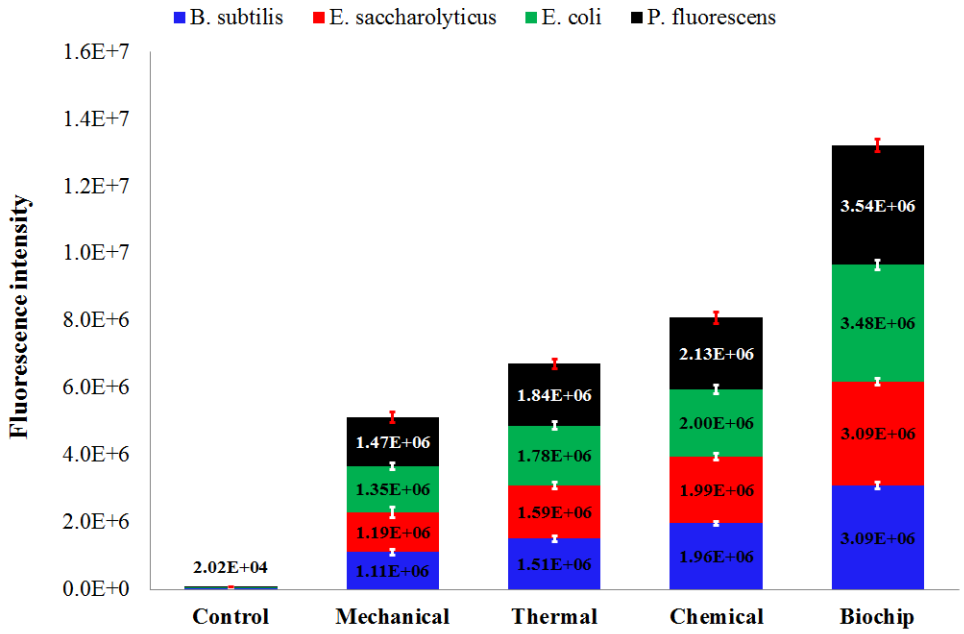

Figure B4: Florescence intensity of EtBr after intercalating into the DNA released from bacterial cells flowing through the PPM (11) at flow rate of 4μL/min and resulted from mechanical, thermal, and chemical cell lysis.

only 0.6% of the maximum EtBr intensity reported as shown in Table B3 and plotted with the control sample as shown in Fig. B5.

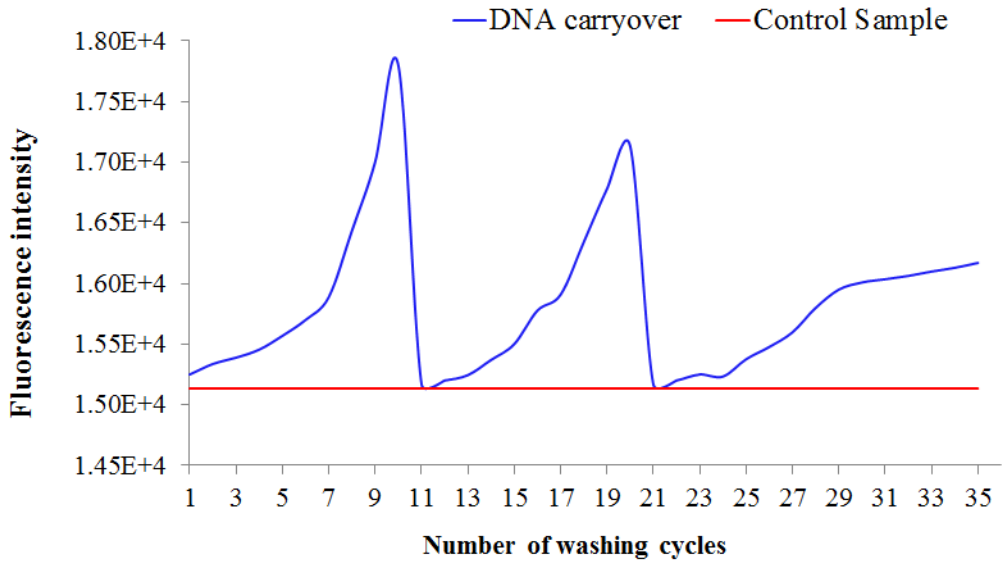

Figure B5: DNA carryover collected in wash cycles after each PPM use.

Table B3: DNA carryover after each backwash cycle

Cycle number	Fluorescence intensity	Cycle number	Fluorescence intensity
1	15250	19	16779
2	15337	20	17133
3	15389	21	15170
4	15455	22	15201
5	15569	23	15250
6	15700	24	15233
7	15888	25	15376
8	16436	26	15477
9	17001	27	15598
10	17798	28	15799
11	15169	29	15950
12	15201	30	16009
13	15245	31	16035
14	15370	32	16063
15	15500	33	16099
16	15777	34	16130
17	15908	35	16170
18	16342		

Appendix C

Bacterial culture

Kocuria rosea (ATCC 186), Pseudomonas putida (ATCC 12633), and Escherichia coli (ATCC 35218) were cultured in nutrient broth (NB), while Micrococcus luteus (Schroeter) (ATCC 4698) cells were cultured in trypticase soy broth. The Kocuria rosea (ATCC 186) and Pseudomonas putida (ATCC 12633) cells in the cultured media were placed in a shaking incubator at 26 °C (37 and 30 °C for Escherichia coli (ATCC 35218) and Micrococcus luteus (Schroeter) (ATCC 4698), respectively) and were shaken at 180 rpm for 18-36 hours. The concentration of the bacterial cultures was quantified by the plate-count technique, by performing agar media plating (NB agar ATCC 186, ATCC 12633 and ATCC 35218, and trypticase soy agar for ATCC 4698) and incubation overnight at 26 °C for ATCC 186 and ATCC 12633 (37 and 30 °C for ATCC 35218 and ATCC 4698, respectively). The Pseudomonas putida (ATCC 12633) and Escherichia coli (ATCC 35218), Micrococcus luteus (Schroeter) (ATCC 4698) and Kocuria rosea (ATCC 186) counts were on average 1.6 10^5, 1.5×10^5, 1.8×10^5 and 1.9×10^5 CFU/mL of culture. These concentrations were used in all the experiments done in this work unless other wise mentioned.

PCR reagents and experimental setup

The structure of Micrococcus luteus (ATCC 4698), Kocuria rosea (ATCC 186), Pseudomonas putida (ATCC 12633), and Escherichia coli (ATCC 35218) primers used in the PCR reaction is provided in Table C1. The PCR tubes were first preheated and incubated at 95°C for 3 min. for initial denaturation, and then the PCR thermal cycler was programed to run for 30 cycles at 95°C for 30 sec., 55°C (6°C gradient) for 70 sec., 72°C for 70 sec., and 72°C for 10 min. for the final extension step.

Table C1: Primers used in PCR experiments

Bacterial strain	Direction	Sequence
ATCC 12633	Forward	GTTGCCAATGACGAAACCTAC
	Reverse	CGTAGCCGTGTCTACTGATTTA
ATCC 35218	Forward	CTTATGGCGGCGTGTTATCT
	Reverse	CTCCGGTACGTGCGTAATTT
ATCC 4698	Forward	GTCAGAGAGTTCTGGCGTAATC
	Reverse	CAGTTGATGCCAGACGAGATAG
ATCC 186	Forward	ACGATCGTCGAGATGGAGAA
	Reverse	GTGGTTGGTGTTGTCGTAGA

PPM characterization

The chemical structure of the three PPM columns investigated in Chapter 4 is provided in Fig. C1. It can be seen that the cross-linked PPM networks have positive charges scattered along the polymer structure, due to the presence of DADMAC. Attenuated total reflectance-Fourier transform infrared spectra for the DADMAC monomer (in powder form), poly(DADMAC-*co*-EDGA), poly(DADMAC-*co*-1,6-HDDMA), and poly(DADMAC-*co*-EGDMA) were obtained on a Nicolet 4700 FTIR spectrometer as shown in Fig. C2. The band at 3470 cm^{-1} is attributed to the N-H stretching in the unsaturated primary amine groups of DADMAC [92]. The peak at 1741 cm^{-1}, corresponding to the C=O stretching from EGDA, EGDMA and 1,6-HDDMA [93] is absent in the DADMAC spectrum. The absorption at 1644 cm^{-1} represents the C-N stretching vibration in secondary amine group, followed by the NH bend. The band at 1482.5 cm^{-1} indicates the presence of a long carbon chain with a high degree of regularity for the backbone structure [94].

EGDA-PPM column

Table C2 summarize the channel dimensions and the pore information of the poly(DADMAC-*co*-EGDA) PPM formed into the channel.

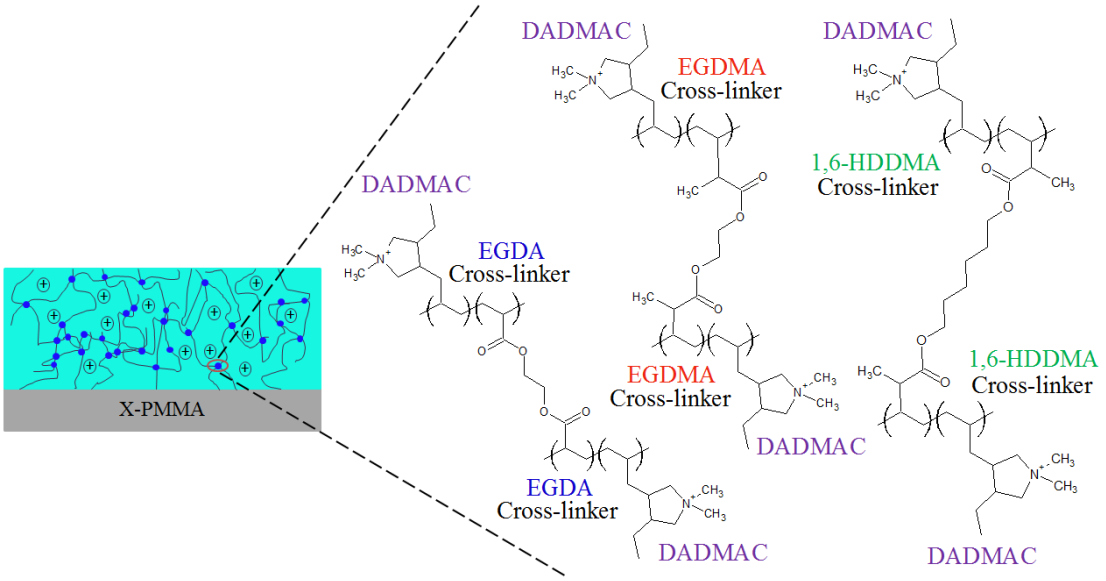

Figure C1: Structure of the cross-linked Poly(DADMAC-*co*-EDGA), Poly(DADMAC-*co*-1,6-HDDMA), and Poly(DADMAC-*co*-EGDMA) networks.

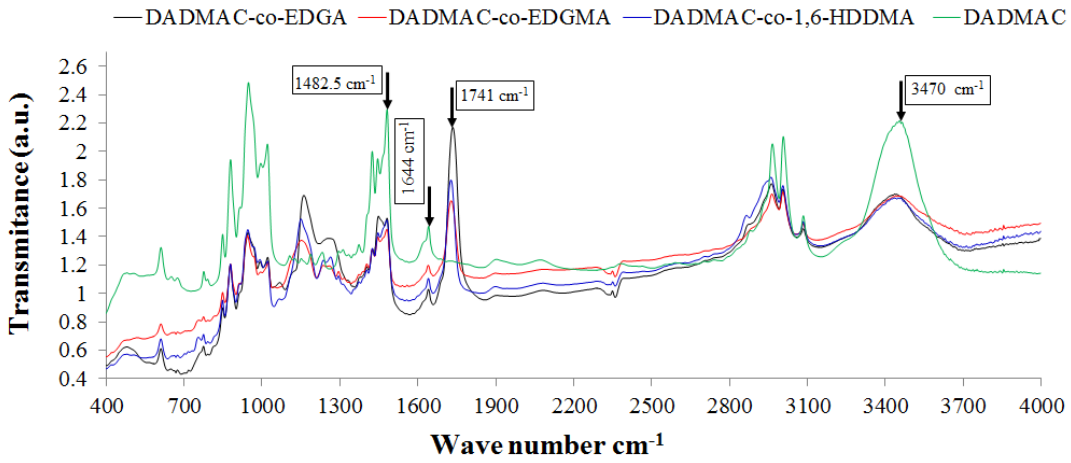

Figure C2: ATR-FTIR spectra for DADMAC (powder), poly(DADMAC-*co*-EDGA), poly(DADMAC-*co*-1,6-HDDMA), and poly(DADMAC-*co*-EGDMA) cross-linked networks.

Table C2: Dimensions of the channel and pore information of the poly(DADMAC-*co*-EGDA) PPM formed in the channel

Channel width (m)	Channel length (m)	Channel depth (m)	Channel vol. (μL)
500×10^{-6}	2.5×10^{-2}	350×10^{-6}	4.375
	Pore diameter (μm)	Porosity (%)	Void vol. (μL)
	4	66	2.9

DNA carryover

The florescence intensity of EtBr mixed with the PBS recovered from the channel in the back-flush cycle showed insignificant DNA carryover, reaching 0.6% of the maximum EtBr intensity reported as summarized in Table C3 and shown in Fig. C3

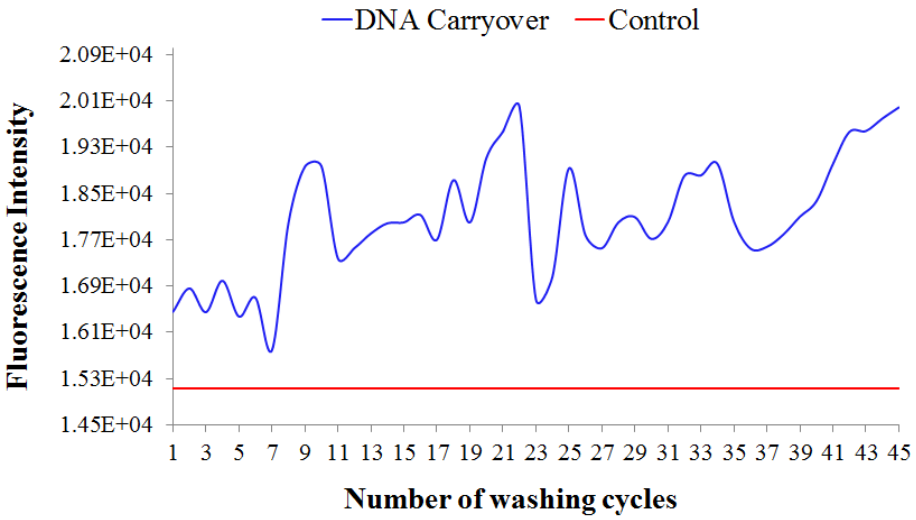

Figure C3: DNA carryover collected after each PPM use and control sample.

Table C3: DNA carryover after each backwash cycle

Cycle number	Fluorescence intensity	Cycle number	Fluorescence intensity	Cycle number	Fluorescence intensity
1	16457	16	18129	31	18003
2	16860	17	17701	32	18804
3	16451	18	18730	33	18811
4	16993	19	18000	34	19012
5	16375	20	19113	35	18020
6	16700	21	19567	36	17549
7	15793	22	19996	37	17578
8	17991	23	16672	38	17791
9	18964	24	17061	39	18099
10	18970	25	18933	40	18365
11	17378	26	17781	41	18807
12	17556	27	17554	42	19262
13	17809	28	17999	43	19578
14	17985	29	18091	44	19793
15	18001	30	17715	45	19985